63-3-1

Final Summary Report

on

RESEARCH & DEVELOPMENT OF HIGH TEMPERATURE SEMICONDUCTOR DEVICES

1 March 1959 through 31 July 1962

DEPARTMENT OF THE NAVY
BUREAU OF SHIPS

CONTRACT NUMBER NObsr-77536
&
CONTRACT NUMBER NObsr-85224

TEXAS INSTRUMENTS
INCORPORATED

Final Summary Report

1 March 1959 through 31 July 1962

RESEARCH AND DEVELOPMENT

OF

HIGH TEMPERATURE SEMICONDUCTOR DEVICES

Prepared by: E. C. Wurst

Texas Instruments Incorporated

March 1963

DEPARTMENT OF THE NAVY

BUREAU OF SHIPS

CONTRACT NUMBER NObsr-77532

AND

CONTRACT NUMBER NObsr-85424

TEXAS INSTRUMENTS
INCORPORATED

TABLE OF CONTENTS
(Continued)

Part		Page
IV	SILICON DIOXIDE MASKING ON GALLIUM ARSENIDE	81
	A. General	81
	B. Magnesium Diffusion Through SiO_2 Film into GaAs	86
	C. Zinc Diffusion Through SiO_2 Film into GaAs	89
V	MISCELLANEOUS TECHNOLOGY STUDIES ON GaAs	94
	A. Chemotaxial Polished Surfaces	94
	B. Delineation of Junctions	94
	C. Post-Alloy Diffusion	96
	D. Surface "Passivation" of GaAs Transistors	98
VI	TUNNEL DIODES	100
	A. General	100
	B. Fabrication Technology and Characteristics	100
	C. Anomalous Characteristics	104
	D. Temperature Behavior of Characteristics	107
VII	TRANSISTORS	111
	A. General	111
	B. Fabrication Techniques	112
	C. Transistor Characterization	114
	D. "h" Parameters vs Frequency Characterization	119
	E. Switching Time Characterization	127
	F. High Temperature Characterization	133
	G. Reliability	136
VIII	CONCLUSION	144
	REFERENCES	146

APPENDIXES

A. Estimating Statistical Errors in Determining Nuclear Disintegration Rate

B. Mg Diffusion Through SiO_2 Film - Analytic Solution

TABLE OF CONTENTS
(Continued)

List of Figures

Figure		Page
1	Gallium Arsenide Crystal III Growth Direction	2
2	Dependence of the Segregation Coefficient of Manganese in Gallium Arsenide on the Concentration in the Melt	6
3	Dependence of the Segregation Coefficient of Manganese in Gallium Arsenide on Solid Concentration	7
4	DC Power Supply for Contact Resistance Studies.	10
5	Power Amplifier for Contact Resistance Studies.	11
6	Photograph of the Probe and Carriage for Contact Studies. . .	13
7	Measurement Selector for Contact Resistance Studies	14
8	Detector Circuit for Contact Resistance Studies	16
9	Potential vs Distance from a Contact made by Alloying an Evaporated Film of 95% Au - 5% Sb into N-Type Gallium Arsenide and Nickel Plating Surfaces	18
10	Zinc Diffusion in GaAs at 1000°C where the Solid Line Demonstrates the Poor Fit with Allen's Theory.	27
11	Zinc Diffusion Profiles in GaAs at 900°C.	36
12	Iso-Concentration Run. Surface Concentration with Tracer Zinc Maintained at Same Concentration as Non-Tracer Bulk. . .	37
13	Zinc Diffusion Profiles in GaAs at 750°C.	38
14	Zinc Diffusion Profile in Gallium Arsenide at 692°C Showing Absence of Orientation Effects.	39
15	Zinc Diffusion in GaAs at 900°C	41
16	Resistivity-Carrier Concentration Data for GaAs at 27°C Used for Diffusion Calculations.	43
17	Effect of Heat Treatment at 220°C on Heavily Zinc Doped GaAs Demonstrating Precipitation	45
18	Zinc Diffusion in GaAs at 750°C	46
19	P-N Junction Depth for Zinc Diffusion in GaAs for a Normalized Time of 10^4 Seconds and $10^{17} cm^{-3}$ Bulk Donors.	49
20	Effect of Zinc Partial Pressure on Surface Concentration with Theoretical Curves Assuming Zinc Ionization Energy of .08 eV.	55
21	Zinc Surface Concentration Using a Zinc-Gallium Alloy Diffusion Source	56
22	Temperature Variation of the Equilibrium Constant for the Zinc in GaAs Vapor-Solid Equilibria	58
23	Solid Solubility of Zinc in GaAs.	63

TABLE OF CONTENTS
(Continued)

List of Figures
(Continued)

Figure		Page
24	10 Hours at 1100°C with 0.2 atm. Cadmium^{115} Showing Transient Effects due to Indium^{115}	65
25	53 Hours at 1000°C with 0.15 atm. of Cadmium^{115}	66
26	Dependence of the Diffusion Constant of Manganese on Gallium Arsenide on Temperature	68
27	Surface Concentration, C_o, of Manganese in Gallium Arsenide as a Function of Diffusion Temperature	69
28	Diffusion of Sulfur in GaAs	70
29	Diffusion of Magnesium in GaAs (N-Type). Source, 60 Atomic % Mg	72
30	Diffusion of Magnesium in GaAs (N-Type). Source, 60 Atomic % Mg	73
31	Concentration as a Function of Diffusion Depth. Source, 60 Atomic % Mg	74
32	Concentration as a Function of Diffusion Depth. Source, 60 Atomic % Mg	75
33	Concentration as a Function of Diffusion Depth. Source, 60 Atomic % Mg	76
34	Hg^{203} Diffusion in GaAs	78
35	Zinc Diffusion with 1% Zn-Ga Alloy in Sealed Ampoule at 800°C for 5 Hours	82
36	Mg Diffusion with 60% Mg-Ga Alloy in Sealed Ampoule at 1000°C for One Hour	83
37	Two-Zone Open Tube Diffusion at 800°C, Zn Source at 360°C in He Flow (1CHF) for 1 Hour 12,000°A Film Blocked Diffusion	85
38	Diffusion of Magnesium in GaAs - N-Type for 6 Hours at 1000°C (Source Diluted with 40% Gallium)	87
39	Effect of SiO_2 Film Against Mg Diffusion in Gallium Arsenide.	88
40	Zinc Diffusion in GaAs.	90
41	Zinc Diffusion in GaAs.	91
42	Zinc Diffusion in GaAs.	92
43	Chemotaxial Polishing System.	95
44	Cross Section of the Active Region of a Diffused Base-Alloyed Emitter Gallium Arsenide Transistor	97
45	Common Emitter Output Characteristics Before and After NaOH, H_2O_2 Etch	99

TABLE OF CONTENTS
(Continued)

List of Figures
(Continued)

Figure		Page
46	V-I Characteristics of a Gallium Arsenide Tunnel Diode. . . .	102
47	V-I Characteristics of a Gallium Arsenide Tunnel Diode Showing Anomalous Hump in the Curve	105
48	V-I Characteristics of a Gallium Arsenide Tunnel Diode Made from Oxygen Containing Material Showing Anomalous Hump in the Valley Region	106
49	Temperature Behavior of the V-I Characteristics of a Gallium Arsenide Tunnel Diode	108
50	GaAs Tunnel Diode - Peak and Valley Current Temperature Dependence.	109
51	Structural View of Gallium Arsenide NPN Mesa Transistor . . .	113
52	Common Base Output Characteristics of a GaAs Transistor I_E = ma/step	115
53	Common Emitter Output Characteristics of a GaAs Transistor I_B = 0.02 ma/step.	116
54	Frequency Dependence of Grounded Emitter Input Impedance for an Experimental Gallium Arsenide Transistor V_{ce} = 3V, I_c 5 ma	120
55	Frequency Dependence of Grounded Emitter Input Impedance for an Experimental Gallium Arsenide Transistor V_{ce} = 3V, I_c 5 ma	121
56	Frequency Dependence of Common Emitter Current Gain for an Experimental Gallium Arsenide Transistor. V_{CB} = 3V, I_E = 5 ma	123
57	Test Circuit for Switching Transistors in the Saturated Mode.	129
58	Circuit for Determining GaAs Common Emitter Saturated Switching Times	131
59	Block Diagram of the Test Equipment Used to Observe GaAs Transistor Switching Characteristics.	132
60	A Gallium Arsenide Transistor Collector Current Turn On Response, t_{on} = 6.5 nsec.	134
61	A Gallium Arsenide Transistor Collector Current Turn Off Response, t_{off} = 3.8 nsec	135
62	Temperature Effects on Common Emitter Output Characteristics of a GaAs Transistor.	137
63	DC Beta vs Temperature.	138

TABLE OF CONTENTS
(Continued)

List of Tables

Table		Page
I	Degenerate P-Type Zn Doped GaAs Crystals.	4
II	Data on Tin-Doped Gallium Arsenide Crystals	5
III	Results of Contact Specific Resistance Measurements	17
IV	Zinc Diffusion in GaAs.	35
V	Experimental Results on Thermal Conversion of Gallium Arsenide.	80
VI	Results of Controlled Electrolytic Etching of Gallium Arsenide Tunnel Diodes.	103
VII	h Parameters and Power Gain of Several Gallium Arsenide Transistors at V_{CB} = 5V & I_E = -1ma	117
VIII	Parameter Measurements on a Gallium Arsenide Transistor . . .	118
IX	Gain Bandwidth Product for Some Gallium Arsenide Transistors.	124
X	Switching Characteristics of Some Experimental Gallium Arsenide and Silicon (2N706) Transistors.	128
XI	Switching Characteristics of Some Experimental Gallium Arsenide Transistors Under Optimized Conditions	130
XII	150°C Life Storage Effect on I_{CBO}	140
XIII	150°C Life Storage Effect on Beta	141
XIV	150°C Life Storage Effect on BV_{CBO}.	142
XV	150°C Life Storage Effect on BV_{EBO}.	143

Final Summary Report
on
RESEARCH AND DEVELOPMENT OF HIGH TEMPERATURE SEMICONDUCTOR DEVICES

FOREWORD

The principal objectives of the programs conducted under Contracts NObsr 77532 and NObsr 85424 were to carry out studies and to investigate methods and techniques which would lead to the development of gallium arsenide transistors. This work was to include the following:

(a) Investigation of contact materials, etching and surface preparations, junction forming processes, and encapsulation techniques.

(b) Fabricate feasibility samples of a high-temperature low-power gallium arsenide transistor.

(c) Fabricate feasibility samples of a high temperature medium power gallium arsenide transistor.

Final Summary Report

on

RESEARCH AND DEVELOPMENT OF HIGH TEMPERATURE SEMICONDUCTOR DEVICES

ABSTRACT

This Final Summary Report on Department of the Navy, Bureau of Ships, Contracts NObsr 77532 and NObsr 85424, titled Research and Development of High Temperature Semiconductor Devices, covers the period 1 March 1959 through July 1962.

Much improvement was achieved in GaAs single crystals used for device studies. Single crystal GaAs was grown by the Teal-Little method from ingots compounded by the gradient freeze technique. Tunnel diodes were prepared from Zn doped degenerate p-type GaAs. Transistors were generally fabricated from 1×10^{17} atoms/cm^3 Sn doped n-type material, with typical mobilities in the range of 3000 to 4000 cm^2/volt-sec. Improved crystal growing techniques yielded material with dislocation densities as low as 3000-4000/cm^2, an order of magnitude better than generally obtained. Successful attempts were made to make a grown diffused GaAs transistor with current gains, $\beta \approx 0.2$.

Initially alloyed contact studies were made to obtain both ohmic and rectifying contacts on GaAs. Ultimately, studies were made to find a high efficiency, high temperature emitter alloy for the transistor. Au-Sn and Au-Se were satisfactory as ohmic contacts on p- and n-type GaAs, respectively. Only Sn and Au-Sn, of several alloys investigated as rectifying contacts, exhibited satisfactory injection efficiency; neither had the necessary high temperature capability (up to 400°C) for the transistor. Both ohmic and rectifying contacts were incorporated and alloyed successfully on the transistor, with the upper temperature limitation of the unit being restricted to 300°C or less.

Zn, Cd, Mn, S, Mg, and Hg diffusion in GaAs for forming p-n junctions was studied. Zn diffusion was investigated in some detail because Zn behaves in an anomalous manner. The diffusion coefficient of Zn varies by about 4 to 5 orders of magnitude over a relatively small concentration range. Cd diffusion was also quite interesting because of its apparent diffusion in a direction opposite to its concentration gradient. We have shown this is primarily because of the independent diffusion of the decay daughter of the radioactive Cd used. Cd like Zn seemed to be sharply concentration dependent. Mn diffusion data utilizing electrical methods are reported. The diffusion coefficients of Mn are considerably higher than those of Zn at equivalent concentrations and appear to obey a co-error function distribution. Sulphur diffusion data using both electrical and radioactive tracer results are shown. Surface compound formation in this experiment was greatly reduced. Diffusion coefficients were considerably higher than reported in other published data. Mg results as obtained from electrical measurements are presented. No concentration dependence of the diffusion coefficients was observed, but Mg obeyed an error function distribution. Hg diffusion data were obtained by tracer techniques and diffusion was found extremely slow and obeyed a complementary error function.

Zn and Mg diffusion in the presence of sputtered SiO_2 film on GaAs was carried out. The SiO_2 was found to be a diffusion mask, depending on film thickness, diffusion time and diffusion temperature. It also prevents decomposition of the GaAs surface during the diffusion cycle. This film may lead to ultimate planarization of GaAs transistors.

Thermal conversion of GaAs during diffusion cycles was definitely attributed to Cu diffusion and means of controlling the degree of thermal conversion was found.

Because mechanical polishing damaged GaAs surfaces and caused adverse effects to device characteristics, a chemotaxial polishing technique was

developed. An etch consisting of 80:10:10 parts of H_2SO_4, H_2O_2 and H_2O respectively was found to optically polish the As surfaces.

Several stains and etches that delineated both diffused and alloyed junctions in GaAs were discovered; e. g., 5HCl and $1HNO_3$ in a 3 to 2 ratio with H_2O.

A token effort of post-alloy diffusion on GaAs with a Au-Sn-Zn alloy yielded transistors with a β's $\approx$ 1.

A surface "passivation" etch of 5NaOH to $1H_2O_2$ was observed to improve current gains, β, by as much as an order of magnitude. Devices maintained this value of β when exposed to ambients.

Tunnel diodes were fabricated from Zn doped p-type degenerate GaAs. Peak current-to-valley current ratios as high as 70/1 were realized with voltage swings of 0.4 volts. An electrolytic etch was evolved that allowed tailoring the diodes to desirable peak currents. Peak current densities of 500-5000 amperes/cm^2 were observed, with capacitances of typically 2-4 picofarads. High temperature characterization of the diodes, up to 350°C, was successfully carried out, and I_p and I_v values vs temperature presented. Anomalous humps or inflections observed in the I-V curves of some units were attributed to deep-lying impurity levels in the energy gap into which a second tunneling phenomena could have been taking place.

GaAs transistors were proved feasible. N-P-N mesa units that exhibited current gains as high as 3000, with typical β's of 5-20, were fabricated. Other typical dc parameters were $I_{CBO} = 10^{-10} - 10^{-8}$ amps; BV_{CBO} = 15 volts; BV_{CEO} = 15 volts; and V_{CE} = 0.5 to 1.0 volt.

Measurement of "h" parameters at 1000 cps yielded calculated matched power gain values as high as 43.6 db in the common emitter case. Typical h_{ib} = 50 ohms with h_{ob} = 0.5 micromhos were measured.

"h" parameter measurements vs frequency were made for h_{ie} and h_{fe}. The h_{ie} vs frequency curves yielded values of $r_b' C_c$ measurements. h_{fe} vs frequency yielded values for the gain bandwidth product f_T, with the highest observed being 800 Mc. Minority carrier lifetime, τ_n, in the base, was calculated from the f_T and β values and found to be in the range of 10^{-9} - 10^{-8} sec.

Saturated switching time measurements were performed on a number of units. The best transistor switched 10 ma of current in a total time of 10 nsec, with less than a nanosecond being realized in the storage time.

Beta vs temperature, up to 350°C, was observed on several units. On a particular unit the β changed from 14 to 11 over the temperature range of 25°C to 350°C. No permanent degradation in the unit resulted upon returning to room temperature.

Twenty-one state-of-the-art transistors were placed on storage test at 150°C for 1000 hours. Again no serious degradation problem was observed in any of the units.

Final Summary Report

On

RESEARCH AND DEVELOPMENT OF HIGH TEMPERATURE SEMICONDUCTOR DEVICES

I. GALLIUM ARSENIDE MATERIALS RESEARCH

During the period of these contracts, considerable improvement was achieved in the gallium arsenide single crystals used for device studies. Although this materials work was not directly supported by contract funds, some of the results of the research are reported here to give a better understanding of the progress gained in transistor performance.

Primarily, the gallium arsenide material was routinely compounded by the gradient freeze technique, which in many cases yielded large single crystal areas. Degenerate n- and p-type ingots were prepared for tunnel diode studies. Some single crystal areas of the non-degenerate n-type ingots were used in technology and transistor fabrication studies. In these cases, the material was off the <111> orientation and needed orientation. In general, these regions were of relatively high purity, $\approx 10^{15}$-10^{16} atoms/cc, with mobilities in excess of 5000 cm^2/volt sec at room temperatures.

Mostly, the technology and device fabrication studies were performed on crystals grown by the Teal-Little method. They were pulled from material first compounded in the gradient freeze furnace. Generally, these crystals were grown in the <111> growth direction. See Fig. 1 for a picture of such a crystal. These crystals were grown both non-degenerate and degenerate and in intentionally doped and undoped states.

Fig. 1 Gallium Arsenide Crystal, III Growth Direction

Table I shows the results of pulled crystals grown from melts doped heavily with zinc when we attempted to obtain degenerate p-type GaAs for tunnel diodes. Despite heavy doping, no difficulty was encountered in obtaining single crystals. The values shown in Table I were obtained from Hall measurements.

Crystals were grown to study the effective distribution coefficient of tin in gallium arsenide; (tin is an n-type dope and used almost exclusively in crystals for transistor fabrication).

The Hall coefficients near the tops of the crystals were measured and used to compute the donor concentrations in the solid. Table II shows the measured values and the resulting segregation coefficients. An average value of $k = 3.2 \times 10^{-3}$ was obtained. The crystal resulting from the most heavily doped melt showed tin inclusions which indicated that the solubility limit was reached at a value of about 7×10^{18} atoms/cc. Experiments on tunnel diodes indicate that considerably higher tin concentrations are obtained by alloying at lower temperatures. This is probably because retrograde solubility is usually more pronounced for impurities having a low segregation coefficient. Mobility values most generally realized on 10^{17} atoms/cc tin doped crystals ranged from 3000 to 4000 cm^2/volt-sec.

Experiments similar to those described for tin were performed to determine the segregation coefficient of manganese (found to be a p-type impurity) at the melting point of gallium arsenide. Figure 2 shows the dependence of the segregation coefficient, k, on the total manganese concentration added to the liquid. Figure 3 shows k as a function of solid concentration. The curves show that k varies inversely as the square root of the solid concentration over a wide range of concentrations.

Table I

Degenerate p-Type Zn Doped GaAs Crystals

Crystal Number	Carrier Concentration (Cm^{-3})	Mobility (cm^2/volt-sec)	Resistivity (ohm-cm)
1	2.6×10^{19}	79	0.0058
2	8.2×10^{19}	58	0.0025
3	1.2×10^{20}	53	0.0018

Table II

Data on Tin-doped Gallium Arsenide Crystals

Melt Composition (% tin)	Excess Donor Concentration (cm^{-3})	$k = \frac{C_s}{C_L}$
1.98	2.12×10^{18}	3.9×10^{-3}
7.85	6.9×10^{18}	3.0
0.250	1.97×10^{17}	3.5
0.113	8.87×10^{16}	3.0
0.145	7.27×10^{16}	1.9
0.107	8.9×10^{16}	3.4×10^{-3}

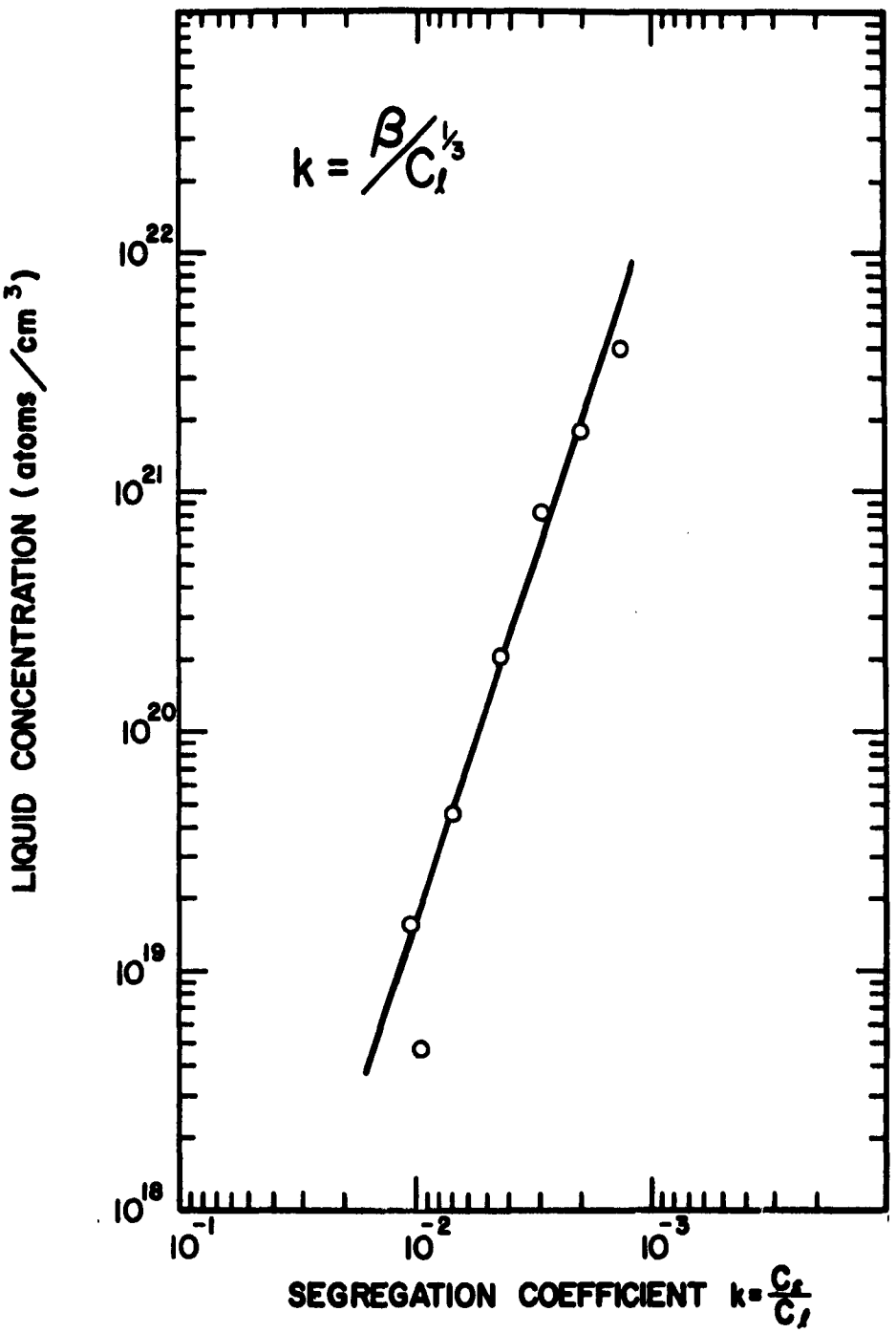

Fig. 2 Dependence of the segregation coefficient of manganese in gallium arsenide on the concentration in the melt

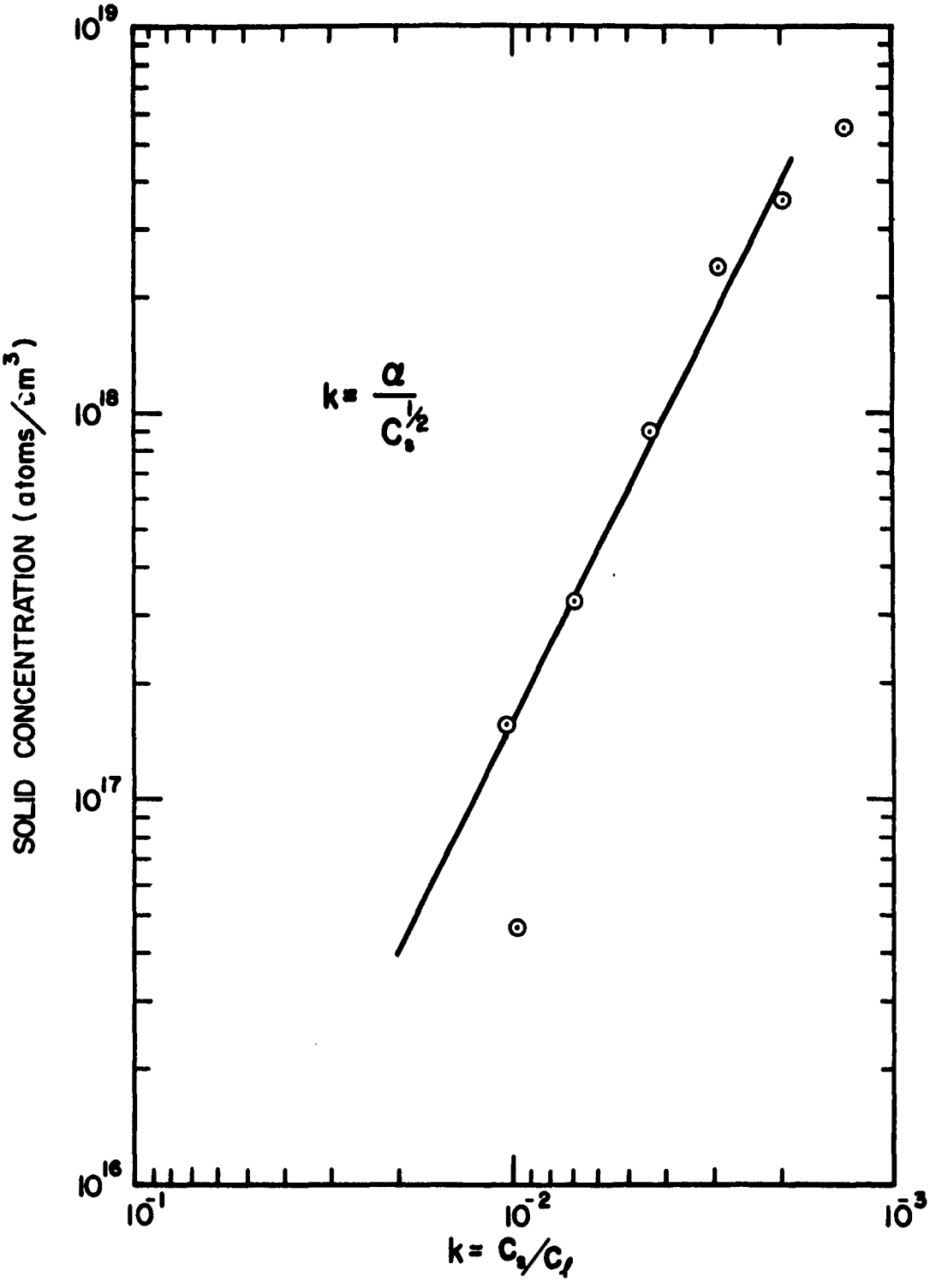

Fig. 3 Dependence of the segregation coefficient of manganese in gallium arsenide on solid concentration

Crystal growing techniques were also studied for their effect on dislocation density and homogeneity of impurity distribution. Variation of the growth parameters - pull-rate, spin-rate, doping and crystal diameter - resulted in improved crystals for transistor fabrication. Some crystals showed dislocation densities as low as 3000 - 4000/cm^2, an order of magnitude lower than generally obtained. Impurity homogeneity was so significantly improved that flat diffused junctions were obtained in the transistors.

Attempts were also made to apply the grown diffused technique to gallium arsenide for transistor fabrication with tin and manganese as impurities. The general procedure was first to grow approximately half the crystal from a charge doped with a small amount of tin, yielding n-type gallium arsenide with properties appropriate for the transistor collector. The remainder of the charge was re-etched and the impurities added. Amounts calculated to give solid concentrations of 5×10^{17} and 6×10^{18} atoms/cc of manganese and tin, respectively, were used. The doped charge was remelted, and the initial crystal used as the seed from which growth was continued for an additional 2-10 minutes. Since diffusion studies show that manganese diffuses much faster than tin, manganese should form a p-type base region ahead of the heavily doped n-type emitter. In a few cases, an n-p-n structure was actually formed and fabricated into transistors with current gains, α, as high as 0.2. Primarily, this technique appeared to offer difficulty in obtaining a thin base region. It was discontinued because of later successes with the n-p-n mesa structure.

II. ALLOYED CONTACT STUDIES

The alloyed contact studies were initially concerned with obtaining both ohmic and rectifying contacts on gallium arsenide. The ultimate objective was to find a high efficiency, high temperature emitter alloy for the transistor.

A. Ohmic Contacts

Initially, the studies were to find low resistance ohmic contacts on n- and p-type gallium arsenide. Equipment was designed and constructed to accurately measure the specific resistance of these contacts. Basic electrical circuitry and apparatus are shown in Figs. 4 through 8 and are described in the following paragraphs. This equipment allowed both square-wave ac and dc measurements.

Direct Current Supply (Fig. 4)-- A set of cascaded rheostats permits continuous adjustment of the current between 9 ma and 3 a (when a 1 ohm sample is in the sample holder). A switch allows the source polarity to be reversed.

Square-wave Alternating Current Supply (Fig. 5)-- A 150 cps square-wave was available from a Heathkit S-3 electronic switch. This wave has less than 0.1μsec rise time with negligible tilt, but the output is a high impedance voltage source. Therefore, we designed and constructed a three-stage transistor current amplifier to act as a current source. The first stage serves as a limiter and clamper. The input square-wave drives the transistor between I_{cbo} and the saturation current. The second stage matches the impedance between the limiter and the output stage and prevents the latter from reaching saturation. Charge storage is prevented and distortion reduced; base current is limited by a 470 ohm resistor, which is bypassed by a 100μf capacitor to prevent excessive signal transient times. The output stage is operated between

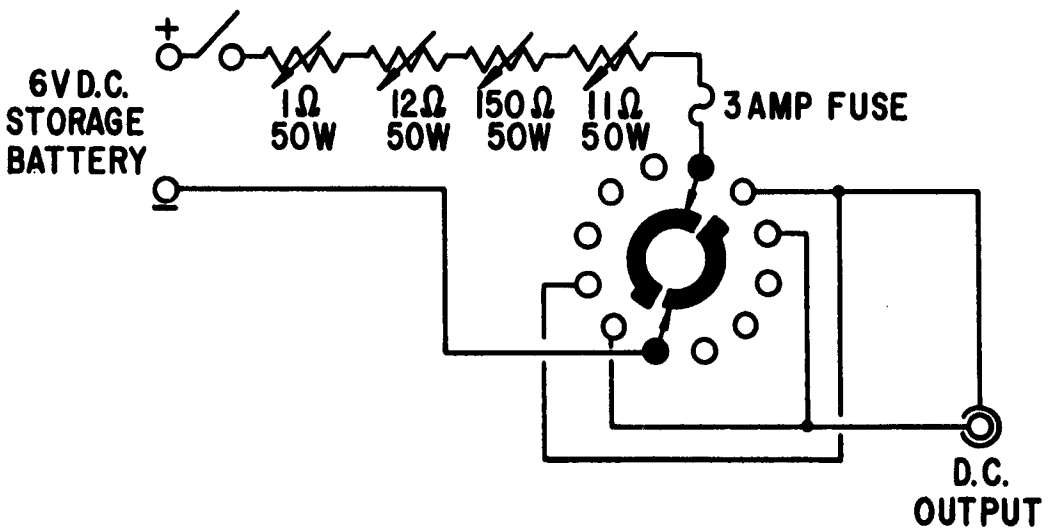

Fig. 4 DC power supply for contact resistance studies

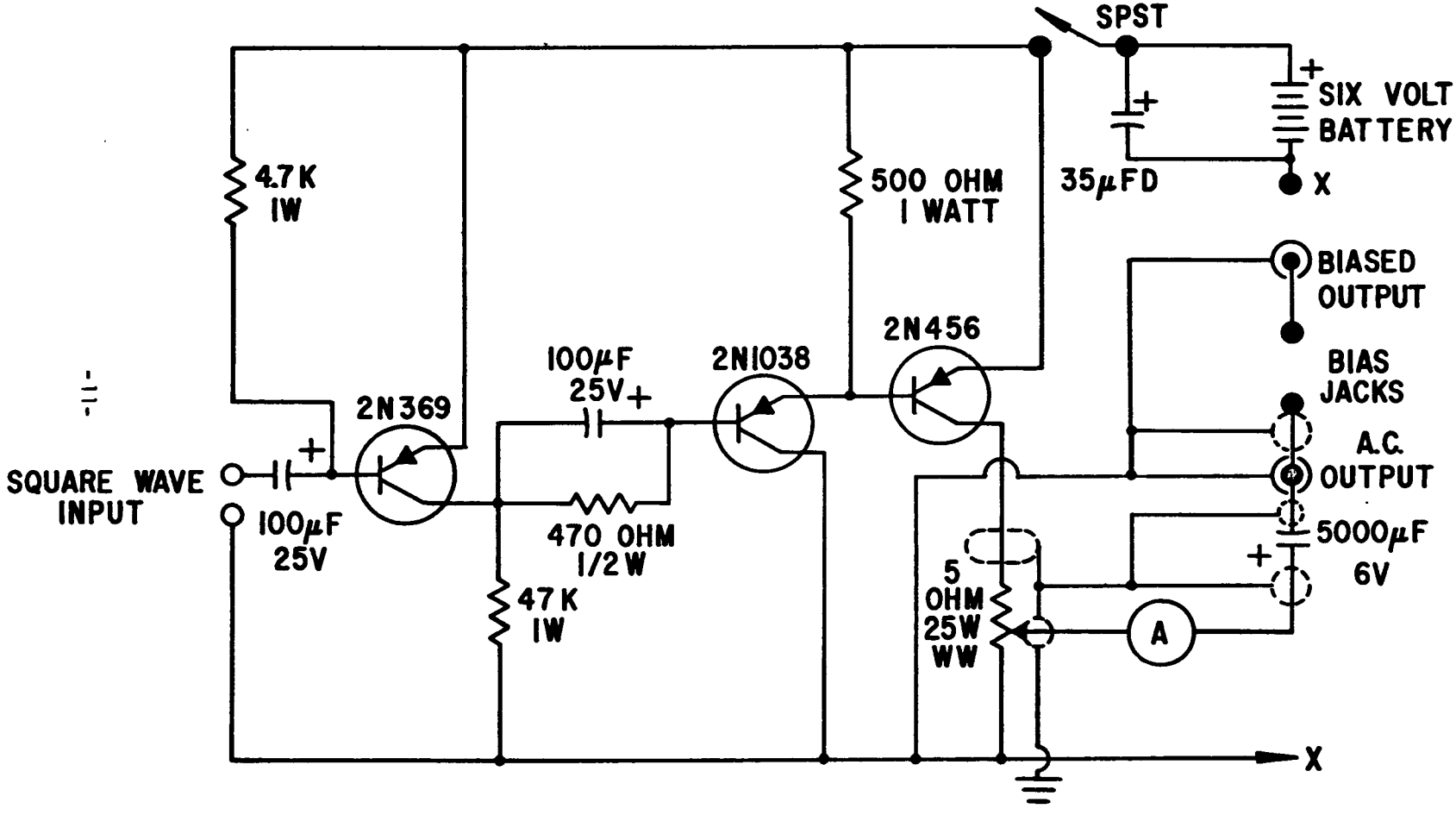

Fig. 5 Power amplifier for contact resistance studies

an output current determined by a 5 ohm potential divider and the load resistance and I_{co}. Low input impedance allows a minimum of collector current, I_{co}. The stage, then, is simply switched on and off by the emitter signal of the second stage. A 5000μf capacitor feeds a 2 ohm load and allows less than 10 percent tilt of the wave, but prevents appreciable dc polarization of the sample. Up to 1 ampere of square-wave ac to a 2 ohm load is supplied by current amplifier. Rise times are about 50μsec and the symmetry is excellent. Distortion causes less than 0.2 percent error in potential measurements.

Probe and Carriage (Fig. 6)-- The sample is placed with the end contacts bridged to nickel blocks by indium held under pressure between the jaws of a lateral vise. Electric current contacts are made to the nickel blocks. The vise is attached to a movable stage which may be translated laterally in 0.01 mm intervals and transversely to align the sample under the probe. The probe is an 0.040-in. diameter tungsten wire, initially sharpened by grinding, and finally etched electrolytically to a fine point; it can be mechanically lowered to the sample and held in place by a small adjustable spring.

Measurement Selector -- Two poles of switch A, Fig. 7, allow either ac or dc to flow through a 1 ohm precision resistor and the sample. Switch B permits potential measurements to be made: (1) across the precision resistor for current determination, (2) across the sample, (3) between the front sample contact and probe, or (4) between the probe and rear sample contact. Switch B is wired to permit these operations without reversing the K-3 input. Switch C in position "2" allows a 60-cycle test signal to pass through a 47 K ohm protective resistance across the probe contact. When probe ohmic contact is established, the oscilloscope vertical input is effectively grounded and a horizontal trace displayed. In position "1," the switch allows the wave form of the potentials to be monitored. The remaining 2 poles of switch A permit output of potentials to either the detector circuit or K-3 potentiometer.

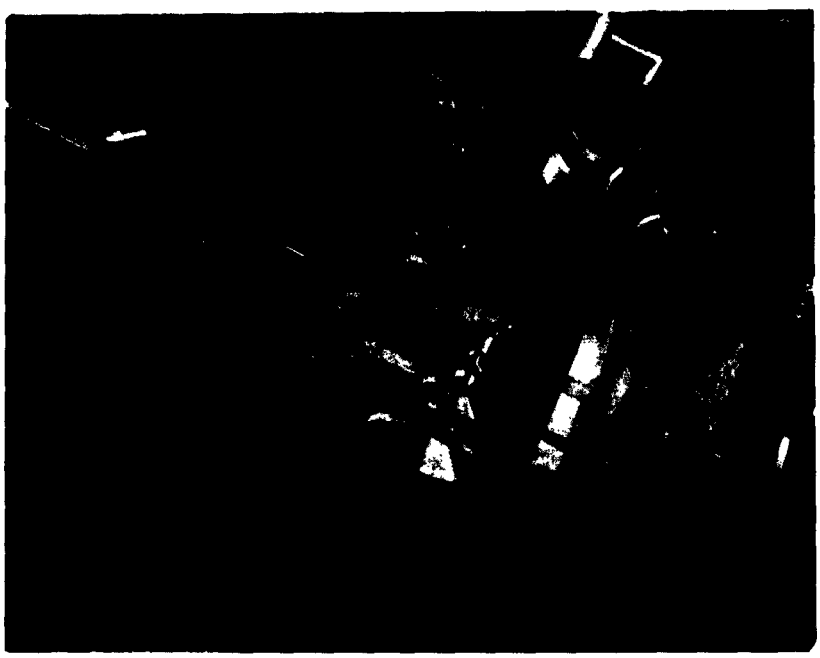

Fig. 6 Photograph of the probe and carriage for contact studies

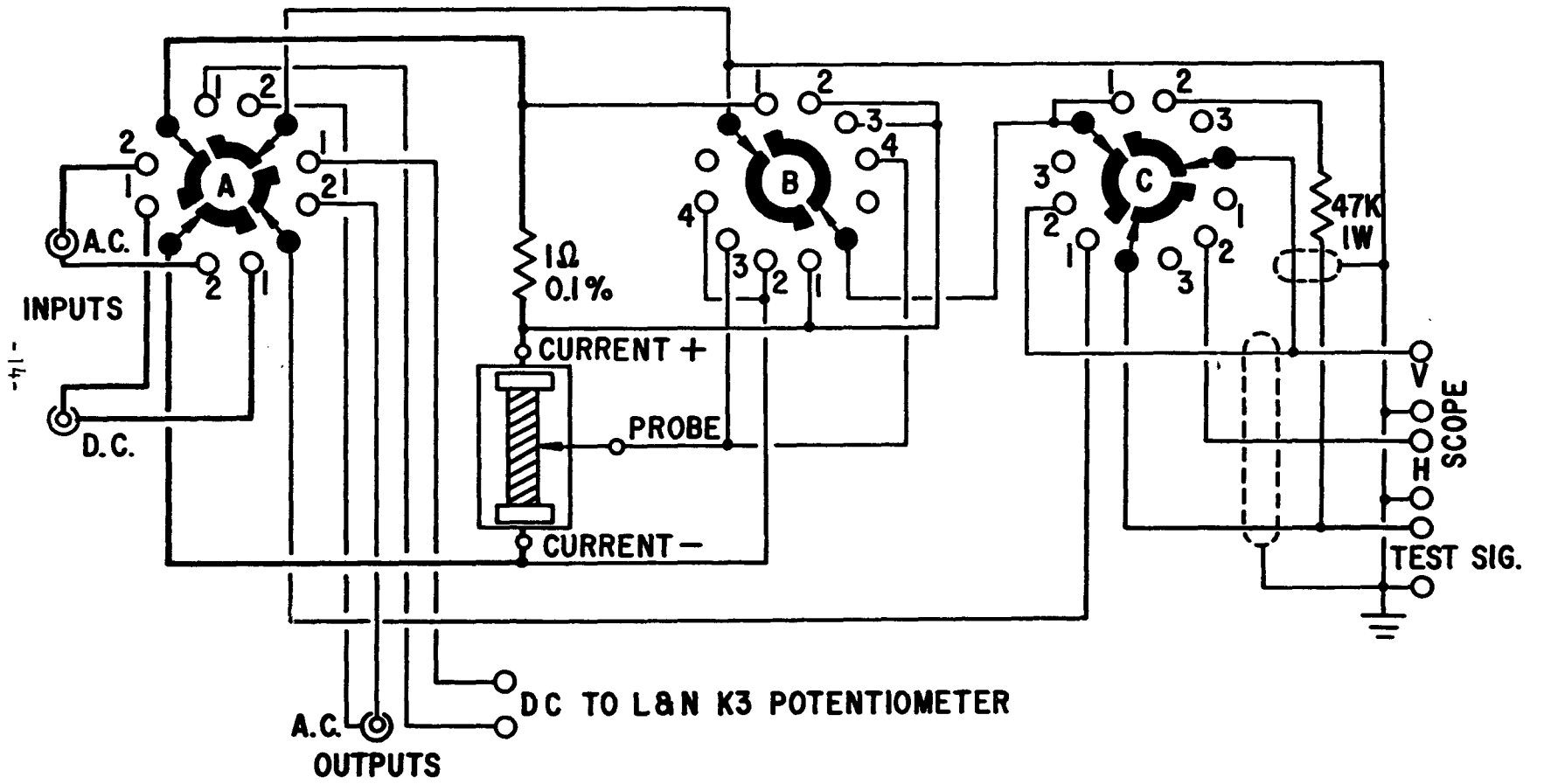

Fig. 7 Measurement selector for contact resistance studies

Detector Circuit (Fig. 8)-- With the toggle switch in peak-to-peak position, the detector is a conventional voltage doubler circuit, loaded by a 1 M-ohm load. A Pi resistance-capacitance network serves as a ripple filter with the toggle switch in peak position; the detector is a shunt rectifier loaded by a 1 M-ohm load. Another 1 M-ohm resistor isolates the Pi filter to prevent the first capacitor from acting as a voltage divided with the Pi filter capacitance. In this condition the detector reads potentials resulting from current flowing unidirectionally through the sample. Potentials corresponding to reverse current flow may be read by throwing the wafer switch, which reverses the diodes. Thus, though square-wave ac flows through the sample, direct current measurements may be made.

The method involves passing a current through a sample of known geometry and dimensions and determining the potential at various points on the sample by precision probing techniques. From the potential drop at the contacts, the sample current, and the cross-sectional area, a value of contact resistance was calculated. Table III shows the results of fourteen different contacting materials investigated initially as ohmic contacts on n- and p-type gallium arsenide, respectively. It should be noted that several of the contacts were non-ohmic, as shown by differences in the values obtained with the current flow in the direction from the contact into the sample from those obtained when the current flow was from the sample to the contact. Figure 9 shows a typical potential profile curve from which the contact resistance values were calculated. Conclusions from these and subsequent experiments showed Au-Zn and Au-Se to be satisfactory ohmic contacts on p- and n-type gallium arsenide, respectively. They are now used in the fabrication of state-of-the-art transistors.

Contact resistances determined from square-wave ac measurements were not significantly different from the values determined from dc measurements. It was concluded that theomoelectric effects were negligible in GaAs. The ac measurement system later proved useful in studying electrical contacts to Bi_2Te_3 and PbTe.

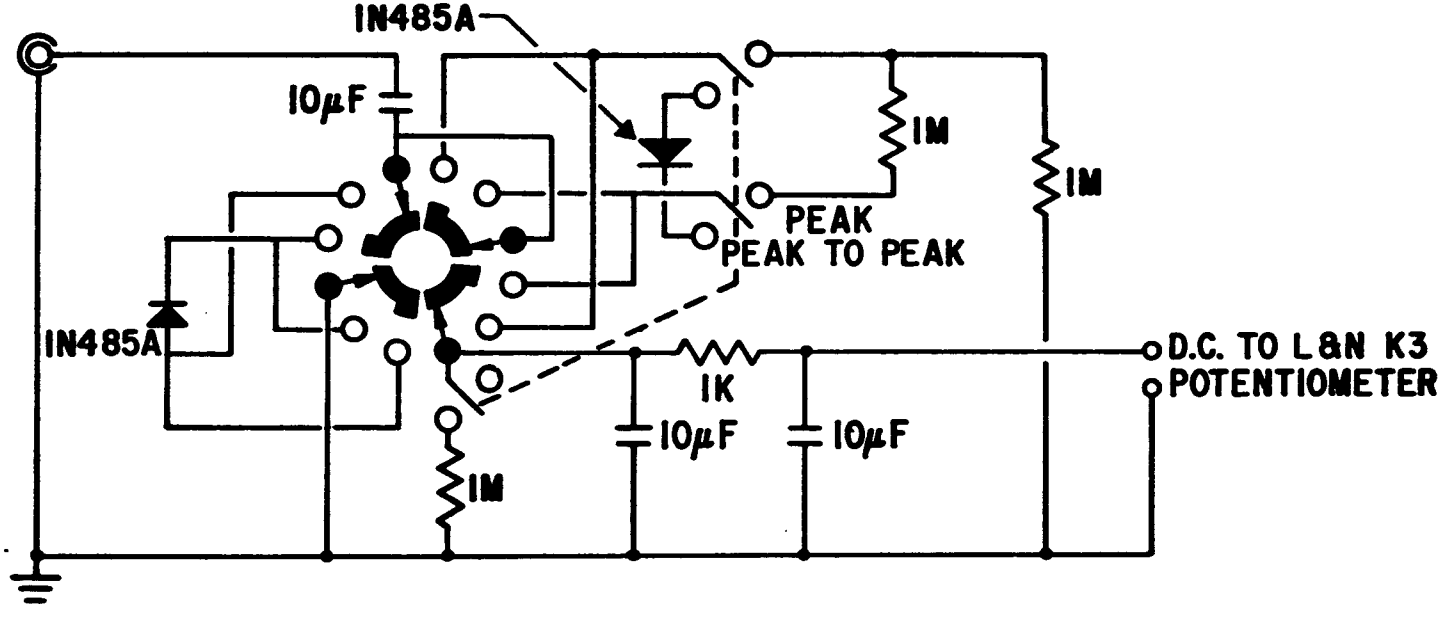

Fig. 8 Detector circuit for contact resistance studies

Table III

Results of Contact Specific Resistance Measurements

GaAs Type	Contact	Specific Resistance ($ohm-cm^2$) Current into Sample	Current out of Sample
n	Ni plate	25.7	0.440
n	Ni plate (preanodized)	78.8	17.1
n	Ni plate (sintered)	0.168	0.184
n	Au (alloyed)	0.516	0.516
n	Au-Sb 95-5 (alloyed and Ni plated)	0.250	0.141
n	Au-Te 95-5 (alloyed and Ni plated)	0.058	0.058
n	Au-Sb 99.4-0.6 (alloyed, Ni plated and sintered)	$2. \times 10^{-3}$	$2. \times 10^{-3}$
n	Ag-Sn 50-50 (alloyed)	3.8×10^{-3}	3.8×10^{-3}
n	Ag-Sn 50-50 (alloyed and Ni plated)	7.6×10^{-4}	7.7×10^{-4}
n	Ni plate (sintered and replated)	6.36×10^{-3}	4.08×10^{-3}
n	Ag-In 99-1 (alloyed)	6.28×10^{-2}	2.91×10^{-3}
n	Au-In 99-1 (alloyed)	4.9×10^{-3}	3.9×10^{-3}
n	Rhodium plate (sintered)	0.50	3.1×10^{-2}
p	Ni plate (sintered)	5.4×10^{-4}	5.0×10^{-4}
p	Ni plate (sintered and replated)	2.1×10^{-4}	1.4×10^{-4}
p	Au-Zn 99-1 (alloyed)	5.0×10^{-4}	1.6×10^{-3}
p	Au-Zn 99-1 (alloyed and Ni plated)	6.8×10^{-5}	1.2×10^{-4}
p	Rhodium plate (sintered)	7.3×10^{-3}	2.1×10^{-2}
p	Ag-Al 72-28 (alloyed)	7.5×10^{-3}	2.8×10^{-3}
p	Ag-Mn 95-5 (alloyed)	2.7×10^{-4}	1.6×10^{-4}
p	Ag-Mn 95-5 (alloyed and Ni plated)	1.9×10^{-4}	9.5×10^{-5}

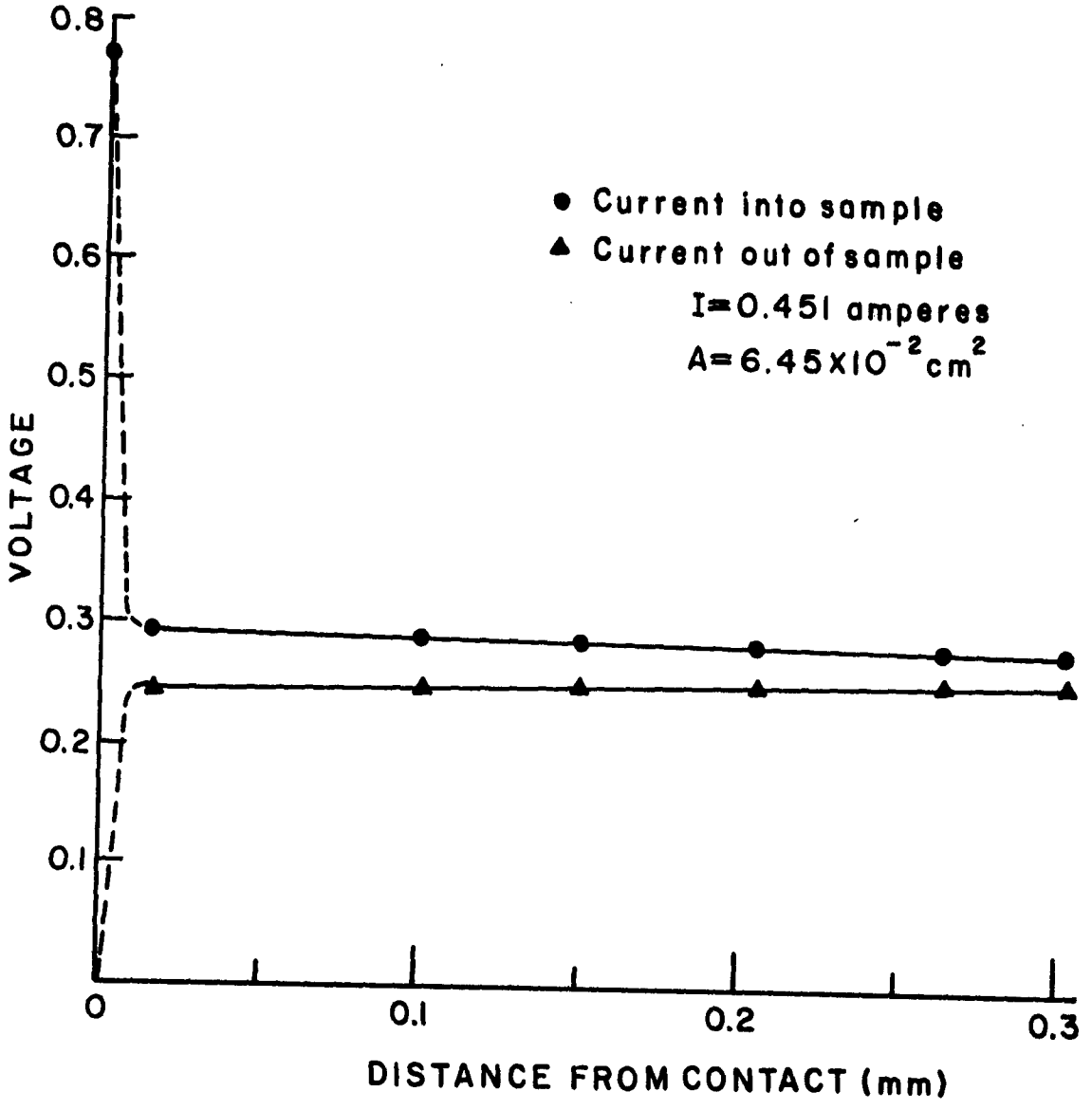

Fig. 9 Potential vs distance from a contact made by alloying an evaporated film of 95% Au - 5% Sb into N-type gallium arsenide and nickel plating surfaces

B. Rectifying Contacts

Studies of rectifying alloyed contacts on gallium arsenide were designed primarily to find a high injection efficiency, high temperature emitter alloy on p-type material. Many alloys such as Au-Te, Au-Sn, Au-Se, Ag-Sn, Sn-Te, Sn-Se, Si-Sn, Au-Ge-Sb, and Sn were investigated. The method for determining the high injection efficiency of the contacts was first to observe the forward I-V trace of the diodes on a curve tracer, then attempt to fabricate a transistor incorporating the alloy as an emitter.

Pure Sn was found to be a donor and a good standard for comparison with other alloys for injection efficiency. Diodes were fabricated on 10^{17} atoms/cc p-type gallium arsenide with pure Sn and were found to exhibit the characteristic 0.8 Volt forward breakover voltage for gallium arsenide. Transistors made with Sn emitters exhibited current gains, β, as high as 3000, certainly indicating good injection efficiency. However, Sn, with its low melting point of 232°C, limited the maximum temperature operation of the transistors far below the expected 350°C.

Of the previously mentioned alloys, the only other one that exhibited desired diode and transistor characteristics was Au-Sn 62% - 38% by weight. Diodes made with this material had the same characteristics as Sn and transistors with β's of about 100 were fabricated. Again, however, the maximum operating temperature of the transistor was limited to about 300°C. The 62%Au - 38%Sn alloy melts at 418°C, but alloying with gallium arsenide lowers this melting point considerably.

Search for an ultimate good alloy emitter is being continued and all state-of-the-art gallium arsenide transistors are now being fabricated using the Sn emitters.

C. Evaporated Contacts

The goal in this study was to evaporate and alloy all the necessary contacts on the transistor. The ohmic base and collector contacts were successfully evaporated and alloyed. The base contact consisted of Au-Zn and the collector contact, of Au-Se. Much effort was expended on evaporating and alloying the 62%Au - 38%Sn alloy as the emitter before we found that it did not exhibit the desired high temperature properties.

Initially, we experienced difficulty in obtaining good melting and alloying of the Au-Sn alloy over the entire area of contact. This resulted in a surface barrier contact with a much lower contact potential than the actual p-n junction, with which it is in parallel, and therefore yielded 0.5 volt forward breakover voltages instead of the characteristic 0.8-1.0 volt for GaAs. However, this problem was finally resolved by proper preparation of the GaAs surface, just prior to the evaporation. Stripes, 1 x 3 mils and 3 microns thick, were evaporated and alloyed. They yielded 0.6 micron thick regrowth regions over the entire area of contact. The alloying cycle was carried out at 600°C in a reducing atmosphere. The diodes obtained exhibited the expected 0.8 to 1 volt breakover voltage on the forward I-V curves.

It was not until this study was completed that we found that the 62%Au - 38%Sn alloy would not withstand temperatures in excess of 300°C after alloying with the GaAs. Work will be continued in this area when a suitable high temperature, high injection efficiency emitter alloy is found.

III. DIFFUSION STUDIES IN GALLIUM ARSENIDE

A. General

Diffusion of zinc, cadium, manganese, sulfur, magnesium, and mercury in gallium arsenide have been studied and are reported here. Diffusion of zinc has been studied in some detail because zinc seems to behave in an anomalous manner. The diffusion coefficient of zinc varies by some 4 to 5 orders of magnitude over a relatively small range in concentration.[1,2]

Cadmium diffusion is also quite interesting, because it seems to diffuse in a direction opposite to its concentration gradient; that is, "uphill-diffusion" seems to occur. We have shown that this results primarily from the independent diffusion of the decay daughter of the radioactive cadmium used. A mechanism that seems to explain these results assumes an outdiffusion of dislocation generated vacancies from the interior of the sample while the cadmium is diffusing inward.

Manganese diffusion results utilizing electrical methods are also reported. The diffusion coefficients of manganese are considerably higher than those of zinc at equivalent concentrations. We believe this is because manganese diffuses interstitially, although the electrically active manganese is probably substitutional; this indicates an interstitial-vacancy reaction.

Sulfur diffusion results using both electrical and radioactive tracer results are also shown. Our values for the diffusion coefficient are much higher than those obtained in the only other published data.[3] We found very serious surface erosion occurred unless suitable precautions were taken. Our data were taken where the surface erosion was reduced considerably, and we believe the reported values are accurate.

Magnesium results are presented as obtained from electrical measurements. No concentration dependence of the diffusion coefficient

of magnesium was observed, but it obeyed a complementary error function distribution in GaAs. No tracer data could be obtained on magnesium to substantiate these observations, because of the extremely short half-life of the isotope.

Mercury diffusion data was secured by the tracer technique and found to obey the complementary error function distribution with extremely low values of diffusion coefficients.

In the theory section that follows, we develop a broad based diffusion theory from first principles. With this theory, based on the diffusion of an atom by several possible modes simultaneously, we can examine the following special cases: (1) an atom that can exist and diffuse in more than one state of ionization, (2) an atom diffusing by both interstitial and substitional modes, (3) an atom diffusing primarily by an interstitial mode, and (4) an atom diffusing primarily by a substitutional mode.

B. Theory of Diffusion by Parallel Modes

If we propose that diffusion may occur by several modes in a crystal, equations can be developed to treat the situation. We choose to treat diffusion at a given region of the crystal as being characterized by an effective diffusion coefficient, $\bar{D}$, and we assume as a first approximation that Fick's first law is obeyed.* Hence the flux J, of a given type of atom in a crystal is given by:

$$J = -\bar{D}\,\frac{dN}{dx}\,, \tag{1}$$

where N is the total concentration of the diffusing atom, and x the distance. If diffusion occurs by several modes, the flux of each mode can be taken into account with the expression

$$J = \sum_i J_i = -\sum_i D_i\,\frac{\partial N_i}{\partial x}\,, \tag{2}$$

* We ignore any effect from interaction of concentration gradients.

where J_i, D_i, and N_i are the flux, diffusion coefficient, and concentration, respectively, of atoms in the i'th mode.

For diffusion by two parallel modes, this becomes:

$$J = - D_1 \frac{\partial N_1}{\partial x} - D_2 \frac{\partial N_2}{\partial x} ,$$

or, remembering that $N = N_1 + N_2$, we have

$$J = -[D_1 \frac{\partial N_1}{\partial N} + D_2 \frac{\partial N_2}{\partial N}] \frac{\partial N}{\partial x} .$$

Now the term in brackets can be identified with the effective diffusion coefficient of Eq. (1), so:

$$\bar{D} = D_1 \frac{\partial N_1}{\partial N} + D_2 \frac{\partial N_2}{\partial N} \tag{3}$$

$$= (D_1 - D_2) \frac{\partial N_1}{\partial N} + D_2 . \tag{3a}$$

If the fraction in each mode is not a function of concentration, this expression becomes:

$$\bar{D} = D_1 \frac{N_1}{N} + D_2 \frac{N_2}{N} , \tag{4}$$

$$= (D_1 - D_2) \frac{N_1}{N_2} + D_2 . \tag{4a}$$

Equations (3) and (4) may now be used to develop several special cases. Equation (4) will generally be used because of its simplicity, although the more exact expression, (3), is also calculated in the first case discussed.

1. Diffusion by Different Charge States

As an example of the use of the above equations, consider an atom in a semiconductor that can be either un-ionized (neutral), or ionized (charged). The fraction of the atom in each state will, in general, be a function of the impurity concentration, or in the language of band theory, the fraction is a function of the position of the Fermi level. Further, it should be clear that in general the diffusion coefficient of the atoms in different states of charge will be different.

Following is a discussion of the diffusion of an acceptor which becomes negatively charged when ionized. The treatment of a donor would proceed similarly. The acceptor is chosen specifically because Allen[4] proposed the above mechanism to explain the large concentration dependence of the diffusion coefficient of zinc in GaAs. Unfortunately, he did not develop his equation so that an effective diffusion coefficient could be calculated. We show in the following that this mechanism predicts a diffusion coefficient variation that is in very poor agreement with the experimental results of Cunnell and Gooch[1] and with our work.

The reaction by which an un-ionized acceptor, A°, becomes ionized by giving up a hole, e^+, (or stated equivalently, "accepting an electron from the valence band") is

$$A^\circ \rightleftharpoons A^- + e^+ \quad .$$

Reiss[5] has shown that if the acceptor concentration is not too high this type reaction can be treated using the laws of chemical equilibria, namely the Law of Mass Action. The Mass Action equation governing the above reaction is

$$\frac{N_A^- P}{N_{A^\circ}} = K_A \quad , \tag{5}$$

where N_{A° and N_A^- are the neutral and ionized acceptor concentrations, P the hole concentration, and K_A an equilibrium constant given by:

$$K_A = \frac{N_V}{2} \exp\left[-(E_A - E_V)/kT\right] \quad . \tag{6}$$

N_V is the density of states in the valence band, E_A the ionization energy of the acceptor, E_V the energy at the top of the valence band, k Boltzmann's constant, T the absolute temperature, and the factor 2 takes account of spin degeneracy. This latter factor can be omitted if desired and included in a modified ionization energy.

Utilizing two other relations, namely the expression for electron-hole recombination and the charge neutrality condition, we can calculate the fraction in each state at any acceptor concentration. With these results we can calculate an effective diffusion coefficient from Eq. (3) or (4). The relations needed to complete the set are from the electron-hole equilibria.

$$np = n_i^2 \quad , \tag{7}$$

where n_i is the intrinsic electron concentration, the charge neutrality condition (ignoring any compensating donors),

$$n + N_A^- = p \quad , \tag{8}$$

and conservation of species

$$N_A = N_A^- + N_{A^\circ} \quad . \tag{9}$$

These equations can be manipulated to give the following expression involving N_{A° and N_A:

$$\left(\frac{N_{A^\circ} K_A}{N_A - N_{A^\circ}}\right)^2 - N_{A^\circ} K_A - n_i^2 = 0 \tag{10}$$

This is a cubic equation in N_{A°, and not easily solved, but at very low acceptor concentrations, i.e., $N_A \ll n_i$ the fraction un-ionized, as well as the partial derivative, is

$$\frac{N_{A^\circ}}{N_A} = \frac{\partial N_{A^\circ}}{\partial N_A} = \frac{n_i}{n_i + K_A} \quad . \tag{11}$$

Further, at moderate and high acceptor concentrations where $N_A \gg n_i$, we have for the un-ionized fraction:

$$\frac{N_A^\circ}{N_A} = \frac{2N_A + K_A}{2N_A} - \left[\left(\frac{2N_A + K_A}{2N_A}\right)^2 - 1\right]^{1/2}, \quad (12)$$

and for the partial derivative

$$\frac{\partial N_A^\circ}{\partial N_A} = 1 - \left(\frac{K_A}{4N_A + K_A}\right)^{1/2} . \quad (13)$$

The effective diffusion coefficient can be obtained by inserting (12) or (13) into (4) or (3), respectively. We have done this for the acceptor zinc in GaAs at 1000°C and compared it with the experimental results of Cunnell and Gooch.[1] The parameters used in the calculation were $n_i = 3.8 \times 10^{17}$ cm^{-3}, $E_A - E_V = .11$ eV., $K_A = 2.43 \times 10^{19}$ cm^{-3}, and $N_V = 1.3 \times 10^{20}$ cm^{-3}. These values, except for the zinc ionization energy, were calculated using the data of Ehrenreich.[6] The choice of zinc ionization energy is somewhat arbitrary, since there is no reliable published value.*

The results of the calculation are shown in Fig. 10, compared with the experimental results. The diffusion coefficient of the un-ionized species is assumed to be dominant. Allen[4] claimed qualitative fit with this theory and the data shown, but it is clear that quantitatively the agreement is very poor.

2. Parallel Interstitial and Substitutional Diffusion

Consider an atom that can diffuse either substitutionally (via vacancies) or interstitially. The flux of each species depends on

---

* Implicit in these arguments is the assumption that the ionization energy stays well defined even at high acceptor concentrations. We present evidence in Section D that this is indeed the case at diffusion temperatures.

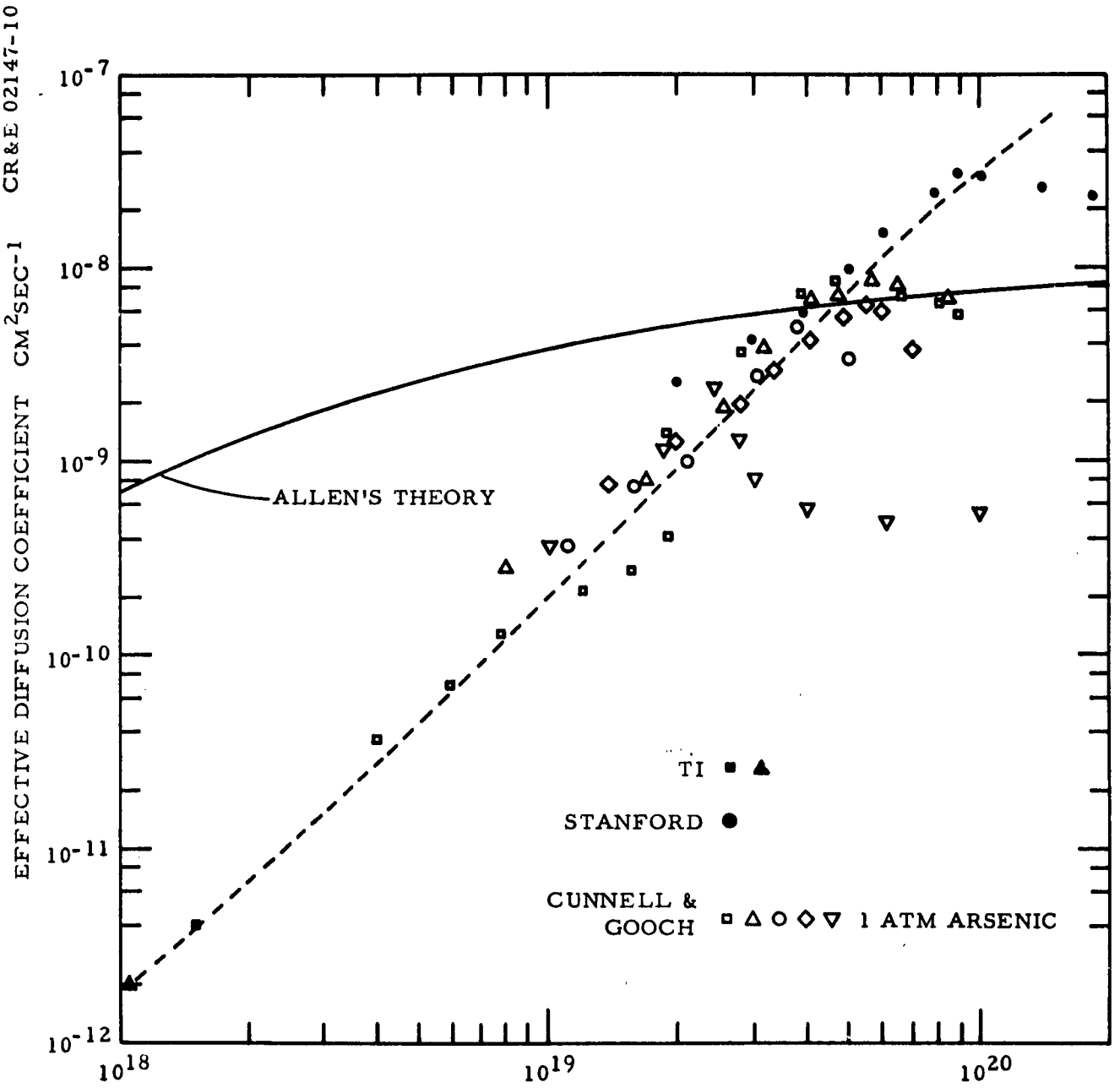

Fig. 10 Zinc diffusion in GaAs at 1000°C where the solid line demonstrates the poor fit with Allen's theory

the concentration gradient of each, and an effective diffusion coefficient can be calculated using Eq. (3) or (4). In the following we will use Eq. (4) as an approximation even where the fraction in a given state is a function of concentration. Doing this will introduce little error and will greatly simplify the considerations. Rewriting Eq. (4) in terms of the interstitial and substitution concentrations, N_I and N_S, and diffusion coefficients, D_I and D_S, we have:

$$\overline{D} = D_I \frac{N_I}{N_I + N_S} + D_S \frac{N_S}{N_I + N_S} \quad , \tag{14}$$

where the first term will dominate if an interstitial mechanism is dominant and the latter will be important if a substitutional mechanism dominates. In most systems of interest, the fraction interstitial, $N_I / N_I + N_S$, is small (i.e., 10^{-2} - 10^{-8}), but D_I is so much greater than D_S, that the interstitial mode may still dominate $\overline{D}$. This is so for the diffusion of copper and gold in silicon and germanium. On the other hand, for groups III and V atoms in silicon and germanium, the evidence suggests that the substitutional mode dominates, which implies negligible interstitial concentration for these impurities. In the following sections we develop defect equilibria that will enable us to calculate the expected concentration dependence of $\overline{D}$ when either of the two modes is dominant.

a. Dominant Interstitial Mode

Consider an impurity that is an acceptor when in a substitutional position, but is a donor (positively charged) when interstitially placed.* There will be an equilibrium reaction in the crystal between these two forms, namely

*A substitutional donor can be treated in a similar manner.

$$2\ e^+ + A^- \rightleftarrows A^+ \quad , \tag{15}$$

and the Law of Mass Action will relate the concentration of these species as:

$$\frac{N_A^+}{N_A^-} = K_I\ p^2 \ ,$$

where N_A^- and N_A^+ are the substitional and interstitial concentrations, and p is the hole concentration. We could have included a vacancy in the reaction above, since it is certainly involved in the transfer of an atom from one mode to another, but this would merely introduce a constant vacancy concentration term into the equilibrium constant K_I. The important point is that the fraction interstitial is proportional to p^2. It can also be shown in the same manner that the fraction interstitial is proportional to p^3 if the interstitial atom becomes a doubly ionized donor. Longini[8] recently made this suggestion to explain our results for zinc diffusion in GaAs.

We have not treated the case of a diffusing <u>un-ionized</u> interstitial because we feel that this interstitial form is likely to diffuse much more slowly through the lattice and hence, is not likely to dominate the diffusion process. However, if such a species <u>were</u> important, the effective diffusion coefficient would be proportional to the first power of the hole concentration.

The companion problem of substitutional donor can be treated in the same way. However, if the interstitial is also a singly ionized donor, then the fraction interstitial will be independent of electron concentration. If the interstitial is a doubly ionized donor, $\bar{D}$ will be depressed at high substitutional donor concentrations. If the interstitial form can diffuse significantly in the un-ionized state or exist in acceptor form, then $\bar{D}$ will be proportional to the electron concentration to some power. The latter possibility is believed to be extremely remote because of the large ionic radius expected of a negatively charged interstitial.

In summary, we feel that the concentration dependence of $\overline{D}$ will help support an interstitial process in the following cases:

(1) The effective diffusion coefficient of a substitutional acceptor square or cube of the acceptor (hole) concentration.

(2) The effective diffusion coefficient of a donor being depressed with high donor (electron) concentrations.

b. Dominant Substitutional Mode

Now consider the case where the second term in Eq. (14) is important. The fraction substitutional will be essentially unity at all concentrations and the diffusion coefficient D_S will be a function of impurity concentration. This occurs because D_S is a function of the vacancy concentration, which in turn is affected by the impurity concentration. We will assume that D_S is directly proportional to the vacancy concentration. If the vacancy exists in several states of ionization, the substitutional diffusion coefficient of the impurity may consist of several modes, each term of which will be proportional to the concentration of each vacancy type. Although we will retain this fact, we will discuss next the simplest situation in which D_S (and hence $\overline{D}$) is a function of one type of vacancy only.

Consider the case of a vacancy that ionizes to become positively charged, namely:

$$e^+ + V^\circ \rightleftharpoons V^+ \quad .$$

Using the Law of Mass Action again, we have:

$$N_V^+ = K_V N_V^\circ \; p \quad , \qquad (16)$$

where N_V^+ and N_V° are the positively charged and neutral vacancy concentrations, p the hole concentration, and K_V an equilibrium constant that is a function of the ionization energy of the vacancy. The neutral vacancy concentration, N_V°, is not a function of impurity concentration, at least to a first approximation.[9] Hence, the positively charged vacancy concentration will be proportional to the first power of the hole concentration. If the vacancy can become doubly or triply ionized, the concentration of these multiply ionized vacanies will be proportional to the second and third powers of the hole concentrations.

Then summarizing the case for a dominant substitution mode diffusion of an acceptor, one should expect the diffusion coefficient to be enhanced to some power of the hole concentration if positive vacancies are important. If negatively charged vacancies are the only ionized vacancy allowed, the $\overline{D}$ should be depressed with increasing acceptor (hole) concentration. The depression of $\overline{D}$ will continue until the neutral vacancies begin to dominate, when $\overline{D}$ will become independent of concentration.*

The above arguments will apply to paired vacancies (divacancies) as well as to simple vacancies. If divacancies are the predominant mode of diffusion in III-V compounds, the divacancies could be supplied by a reaction such as

$$V_{Ga} + V_{As} \rightleftharpoons W^\circ \quad ,$$

where W° is the symbol chosen for neutral divacancy. The Mass Action Law expression for this reaction is

---

* Exactly complementary arguments apply to the effect of high donor concentrations on the concentration of negative and positive vacancies, which will be enhanced and depressed, respectively.

$$N_{VGa} N_{VAs} = K_W N_W^{\circ} \quad . \tag{16a}$$

Since the product of the simple vacancy concentration is usually taken as constant,[15] the equilibrium neutral divacancy concentration will also be constant. This implies that the diffusion coefficient of an impurity that is dominated by divacancy diffusion will not be a function of the pressure of either component over the compound. The concentration of ionized divacancies will still be a function of hole and electron concentration, of course.

C. Zinc Diffusion in GaAs

The pages immediately following contain a discussion which shows the results of diffusing zinc into gallium arsenide with particular emphasis on the concentration dependence of $\bar{D}$. A critical analysis of these data is also included.

1. Experimental Procedure

The GaAs used was n-type with about 10^{17} donors cm^{-3}. Sample sizes ranged from rectangular samples, 6 mm x 8 mm, to square ones, 10 mm x 10 mm. Sample thicknesses before diffusion ranged from 0.5 mm to 1 mm. Most slices were prepared for diffusion with 1400 carborundum, and then fine lapped on a flat glass plate with American Optical polishing compound 309W. This treatment produced a surface that was monitored for flatness using simple interference effects by utilizing a precision optical flat and oblique viewing. The surfaces were flat to better than 1 micron. The samples were cleaned by boiling in an HCl-methanol solution, then rinsed in deionized water.

All the diffusion runs were made in sealed quartz ampoules with sufficient zinc or zinc-gallium alloy, not in contact with

the GaAs, to maintain equilibrium conditions during the run. The zinc-gallium alloy was used to control the surface concentration. After the sample was diffused with radioactive Zn^{65}, the edges were lapped off. Zinc distribution was measured by lapping off successive layers 0.5 - 5μ thick. The amount removed was monitored by weighing the sample with a Mettler microbalance. All lapping was done by hand with AO 309W polishing compound on 2-inch diam optically flat glass or pressed alumina discs. Occasional checks with a precision optical flat were made to ascertain that reasonable flatness (better than 1 micron) was maintained on both optical flats and the sample. The samples were rotated often during lapping to favor plane parallel material removal. Continuous monitoring of the conductivity type of the sample using a thermoelectric probe served as a check on the wedging. For most samples, the type change occurred simultaneously across the whole slice. After lapping, the sample was wiped with a small piece of tissue paper placed on the optical flat. The optical flat with lapping compound and tissue paper was then wrapped with a single layer of Saran Wrap and approximately centered on a well counter. The exact position of the radioactive material on the 2-inch plate was not critical. After a count was made, the optical flat was washed in hot aqua regia.

The specific activity of the zinc was about 100 mC/gm. This relatively low activity limited the concentration determinations to greater than about 5×10^{17} cm^{-3}. However, after this limit was reached, lapping was continued in small increments until the p-n junction was reached. This junction depth provided an accurate zinc concentration determination at about 10^{17} cm^{-3}. The remainder of the sample was n-type in almost all cases, with the bulk resistivity only slightly higher after diffusion. Little or no zinc penetration to the interior of the sample was indicated.

2. Results

The results of most of the radioactive tracer runs we have made are shown in Table IV and in Figs. 11-14. The individual data-points on the diffusion profiles at the higher concentrations should be within 5% of the true concentration. In the range of 10^{19} cm^{-3} and 10^{18} cm^{-3} the uncertainties are estimated to be about 10% and 50%, respectively.

All the profiles measured deviated sharply from those expected for a constant diffusion coefficient. The profiles were analyzed for the effective diffusion coefficient of zinc as a function of zinc concentration using the Boltzmann-Matano method discussed by Crank.[7] $\overline{D}_1$ at a given concentration, C_1, on a diffusion profile is given by:

$$\overline{D}_1 = 1 \frac{1}{2t\ dC/dx} \int_0^{C_1} x\ dC = - \frac{\text{Area under } C_1}{2t\ dC/dx} 1 \quad , \qquad (17)$$

where t is time. The concentration gradient at C_1 and the area under the curve are easily obtained from a plot of C vs x on a linear scale. The area may be measured with sufficient accuracy by counting squares or by using a planimeter.

In principle, the complete concentration dependence of $\overline{D}$ can be obtained from a single profile. However, as Crank points out, the values at the extremes of concentration may be in considerable error, especially if the $\overline{D}$ variation is large. The region near the surface may be in error because of out-diffusion during the cooling cycle or other effects associated with the surface. Errors may be introduced in the regions of low concentration from the difficulty in recording the exact slope in this vicinity. Diffusion profiles for the zinc in GaAs system have quite high concentration gradients in the region near the p-n junction and the $\overline{D}$ values measured are invariably higher than expected. This may be from mild wedging of the samples during analysis, but could also be from a non-equilibrium effect in this vicinity.

Table IV

Zinc Diffusion in GaAs

Run	Percent Zn in Source	Temperature (°C)	Time (Hrs)	Surface Concentration (cm^{-3})	p-n Junction Depth (μ)
1	100.0	900°	2.0	3×10^{20}	208
2+	100.0	900°	1.5	8×10^{19}	71
3	1.0	900°	87.5	9×10^{18}	60
4	0.25	900°	166.0	4.7×10^{18}	23
5*	3.0	900°	16.0	2×10^{19}	
6	100.0	750°	5.5	1.1×10^{20}	75
7	5.0	750°	25.0	$8\text{-}10 \times 10^{18}$	13-15
8	2.2	750°	25.0	$6\text{-}7 \times 10^{18}$	9-10
9	1.0	750°	303.0	$4\text{-}5 \times 10^{18}$	15-16
10++	100.0	692°	8.0	$3\text{-}4 \times 10^{19}$	14

+ Amount of zinc limited to provide 130 torr vapor pressure; incremental resistivity also measured to determine electrically active concentration.

* Iso-concentration run diffusing radio-zinc into already zinc-doped sample.

++ Both sides of sample analyzed to check for orientation effects.

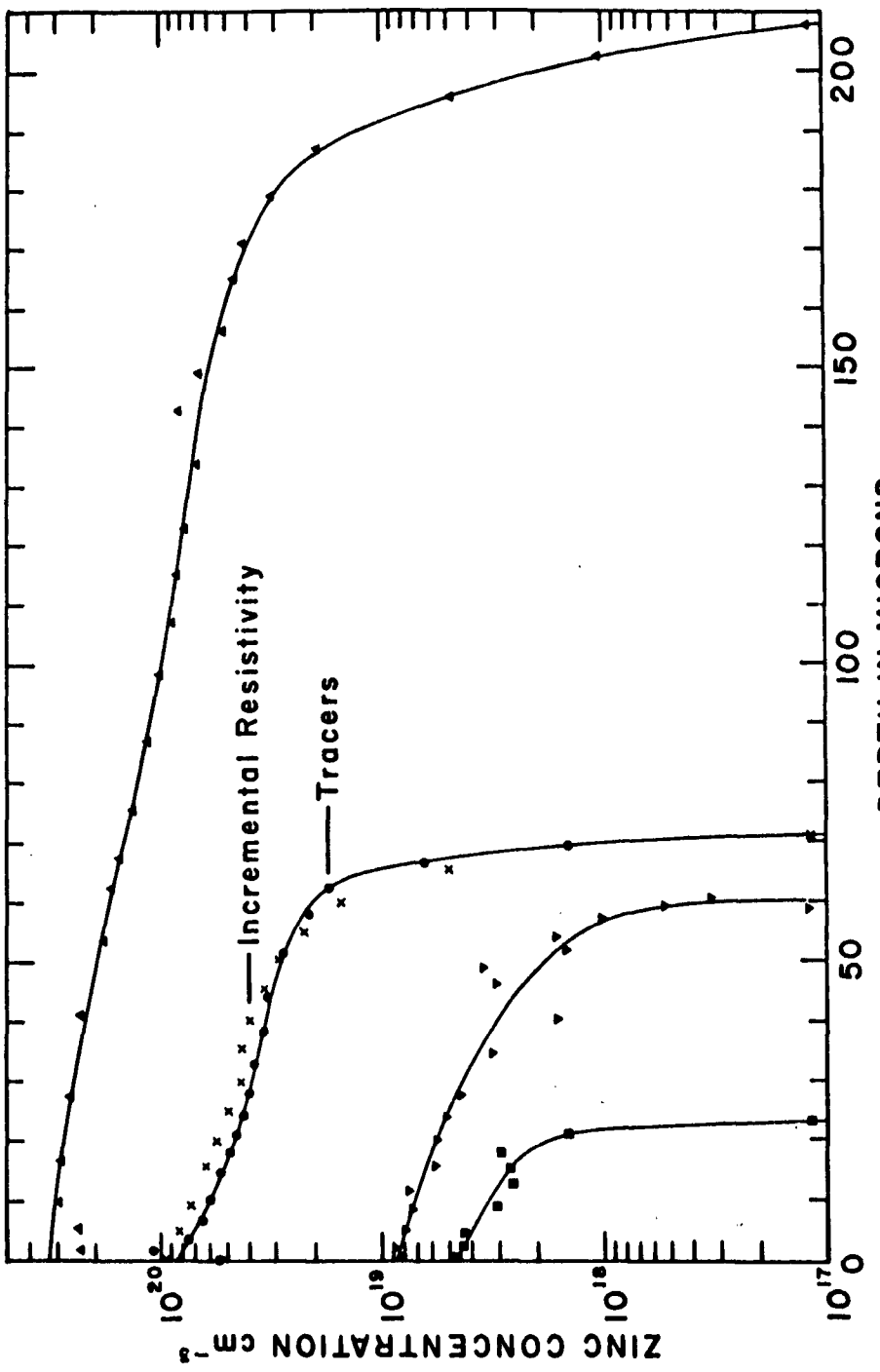

Fig. 11 Zinc diffusion profiles in GaAs at 900°C

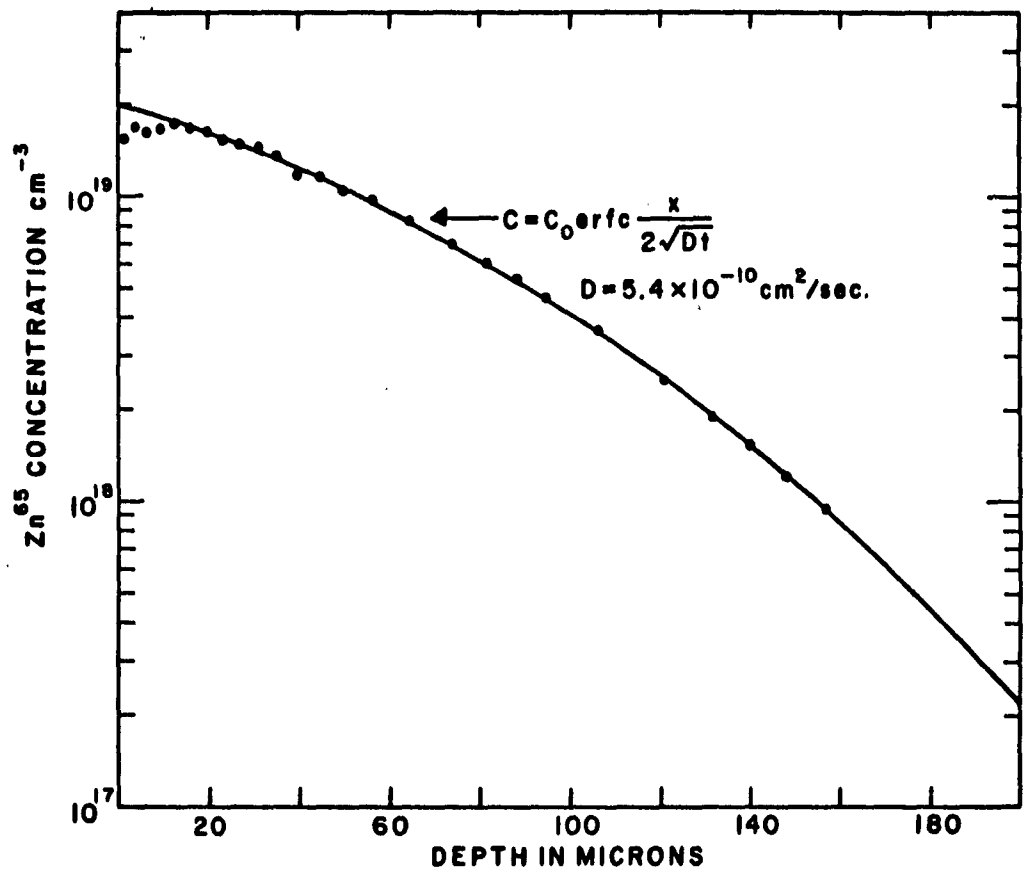

Fig. 12 Iso-concentration run. Surface concentration with tracer zinc maintained at same concentration as non-tracer bulk

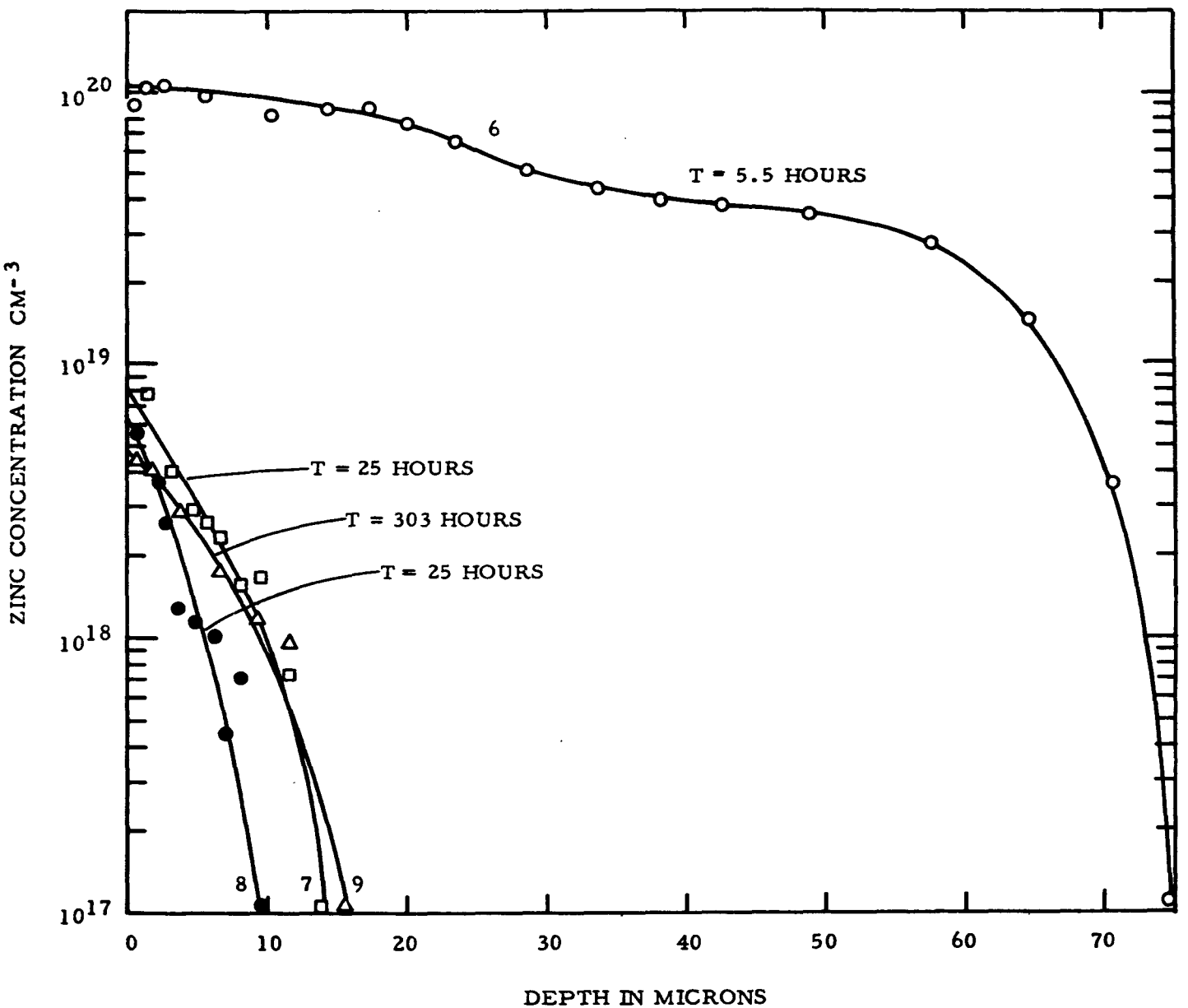

Fig. 13 Zinc diffusion profiles in GaAs at 750°C

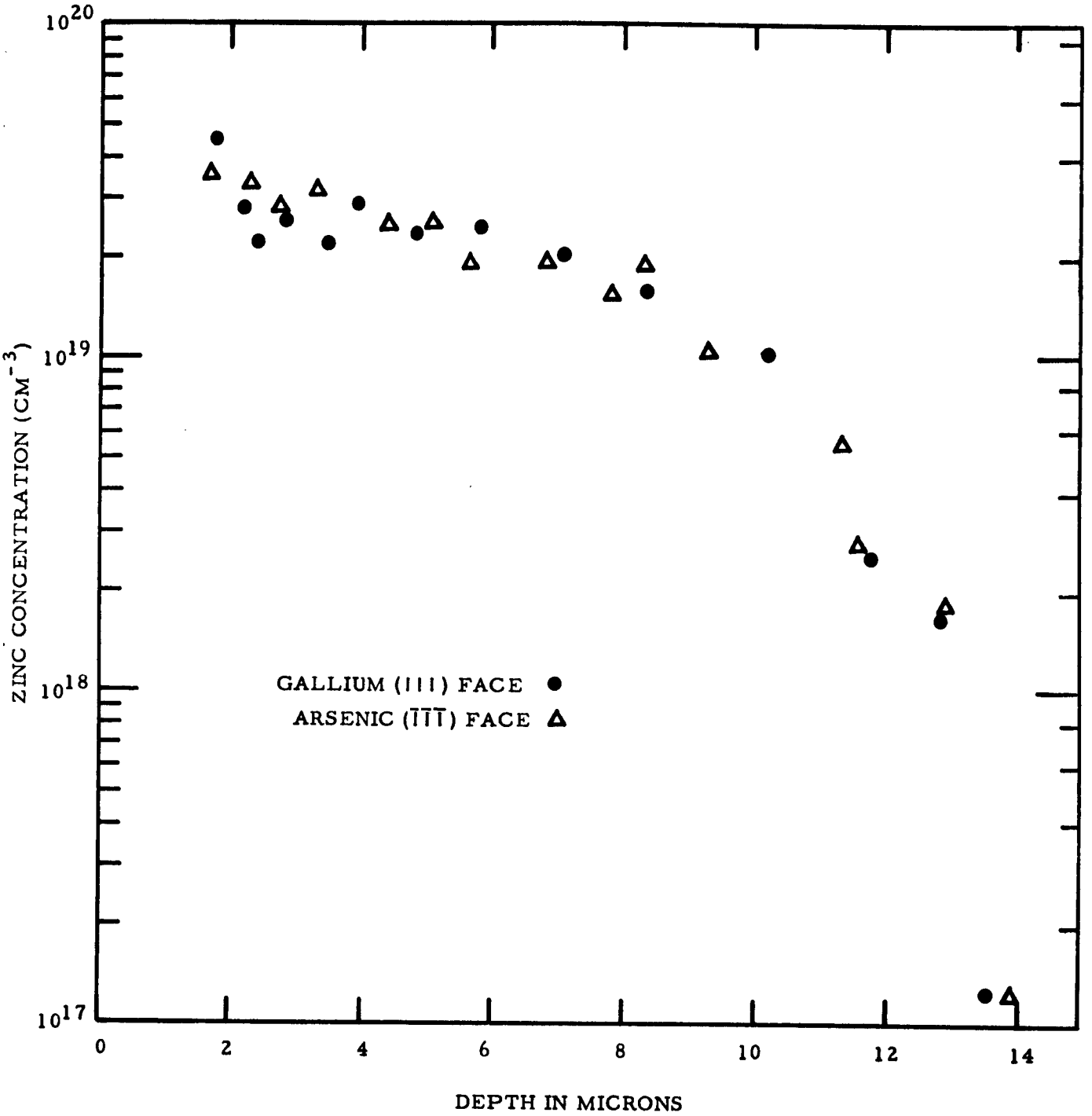

Fig. 14 Zinc diffusion profile in gallium arsenide at 692°C showing absence of orientation effects

For the reasons discussed above, we have ignored values of $\bar{D}$ taken from regions very near the surface and near the junction. Results of the analysis of the profiles at 900°C are shown in Fig. 15. Also shown is our analysis of the Cunnell and Gooch[1] profiles at this temperature and the results obtained at Stanford by Pearson and co-workers.[10] Agreement among these three laboratories is striking for runs made under similar conditions. For example, note the run made at the highest concentration by each group, in which an apparent maximum in $\bar{D}$ is recorded by each group at about 7×10^{19} cm^{-3}. The effective diffusion coefficients at a given concentration agree to within about 10%, which is extremely good for such a complex system. This agreement in data is especially surprising in view of the quite different experimental technique employed. They used a two-temperature method to control their surface concentration instead of the zinc-gallium source. For runs made at lower concentrations, the same sort of effect was observed, but the apparent maxima occurred at a lower concentration.

These efforts indicate that the measured effective diffusion coefficient is <u>not only a function of concentration</u>, but also a function of some other variables, such as time and distance. The method used in the analysis of $\bar{D}$ is good only if $\bar{D}$ is a function of concentration <u>only</u>. Since this is obviously not the case for Zn in GaAs, we have developed a technique which subordinates these difficulties. It involves diffusing with radioactive zinc into material <u>already doped</u> with non-radioactive zinc. Diffusion conditions are set up so the expected surface concentration is identical to the zinc concentration already present in the bulk. We call this an <u>iso-concentration diffusion</u>, since the indiffusing radioactive zinc always finds itself in a constant <u>total</u> zinc concentration ambient. Because there are no complicating zinc concentration gradients, the expected profile is of a system with constant diffusion coefficient and constant surface concentration, namely a complementary error function.

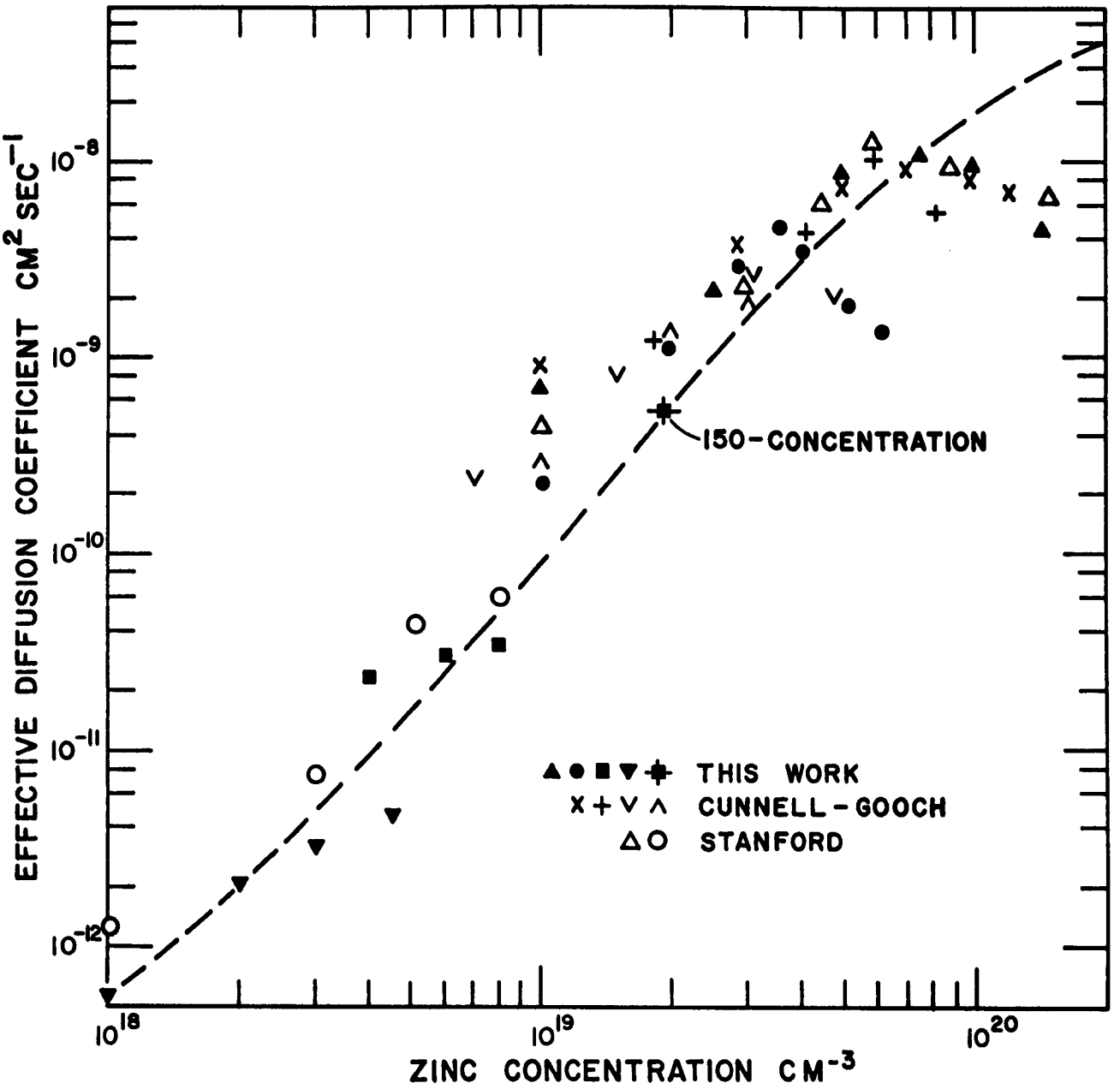

Fig. 15 Zinc diffusion in GaAs at 900°C

Figure 12 shows the results obtained by diffusing radioactive zinc from an alloy of Zn^{65} and gallium (3% Zn), known from previous data to control the surface concentration at about 2×10^{19} cm^{-3}, into GaAs already doped during crystal growth at this same level with non-radioactive zinc. The expected erfc distribution is followed quite closely, and the diffusion coefficient is about a factor of 2 lower than that determined by the previous method.

An alternative method for obtaining a non-radioactive sample at the desired concentration is by a lengthy pre-diffusion process under exactly the same diffusion conditions as the proposed tracer run. This method has been successfully applied by the Stanford group and a $\bar{D}$ value obtained at a zinc concentration of 3×10^{20} cm^{-3}, of about 6×10^{-8} cm^2/sec[10]. This result is much higher than the values obtained by analyzing the normal diffusion profiles, so the apparent depression of $\bar{D}$ at extremely high concentrations probably results from some kinetic effect such as non-equilibrium vacancy and/or interstitial conditions. Utilizing these facts, we have drawn a curve to indicate where we think the "true" effective diffusion coefficient should fall. This curve should be regarded as quite tentative, of course, since it heavily favors only two points, namely the iso-concentration runs.

Also shown in Fig. 11, on run 2, are the results of an incremental resistivity method[11] which was undertaken in conjunction with radioactive sectioning. This was done to determine the extent to which the zinc was electrically active. To convert from resistivity to a carrier concentration, we used the combined data of Haisty and Kellett[12] shown in Fig. 16. The agreement is within about 15% at most concentrations, which is within the probable error of the resistivity measurements. Zinc is apparently completely electrically active at room temperature in these concentrations. At still higher concentrations evidence shows this is not so. For example, with zinc concentration of about 3×10^{20} cm^{-3}, the hole concentration in one sample was only about 1×10^{20} cm^{-3}. We take this as evidence that

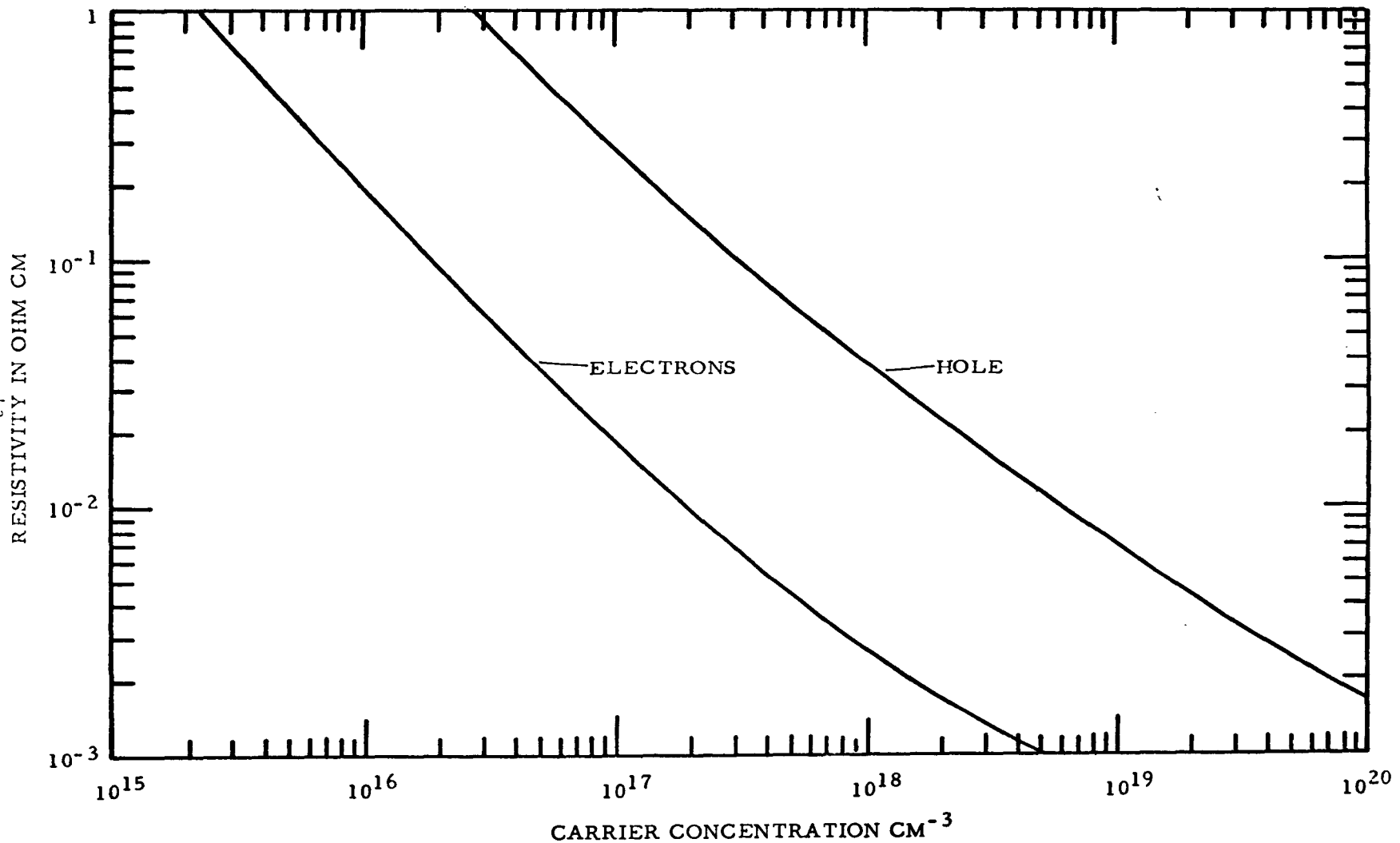

Fig. 16 Resistivity-carrier concentration data for GaAs at 27°C used for diffusion calculations

at these very high concentrations the zinc precipates significantly during the cooling cycle.

To prove that precipitation could actually occur, even at the relatively low temperature of 220°C, we continuously monitored the resistivity of one sample for several months at this temperature. Contacts were applied using a high temperature solder. These results are shown in Fig. 17, with the average hole concentration being estimated from the resistivity at 220°C.

A diffusion coefficient of 10^{-13} to 10^{-14} cm^2/sec can be estimated at 220°C for the initial part of the precipitation by making certain simplifying assumptions concerning the shape of the precipitate and the concentration of precipitation centers. The process slowed somewhat as the average active zinc concentration decreased, but not as much as expected. Several zinc-doped crystals in the range 10^{16} cm^{-3} to 10^{18} cm^{-3} were monitored in the same manner at 220°C and only negligible increases in the resistivity were observed (less than 3% in 64 days).

The implications of the above measurements are clear. As an emitter in a transistor or in tunnel diodes, some precipitation of zinc should be expected at concentrations above 10^{19} cm^{-3}. At concentrations of 10^{18} cm^{-3} and lower, the zinc should remain in solid solution for extended periods, even at reasonably high operating temperatures.

Results at 750°C shown in Figs. 13 and 18 are similar to those at 900°C. The apparent maximum in $\overline{D}$ occurs at about 4×10^{19} cm^{-3}. An additional diffusion coefficient has been provided by D'Asaro[14] at an average zinc concentration of about 7×10^{17} cm^{-3}. At this concentration he obtained a value of about 3×10^{-14} cm^2/sec for $\overline{D}$, off scale on Fig. 18, but consistent with the dotted line representing our estimate of the effective diffusion coefficient.

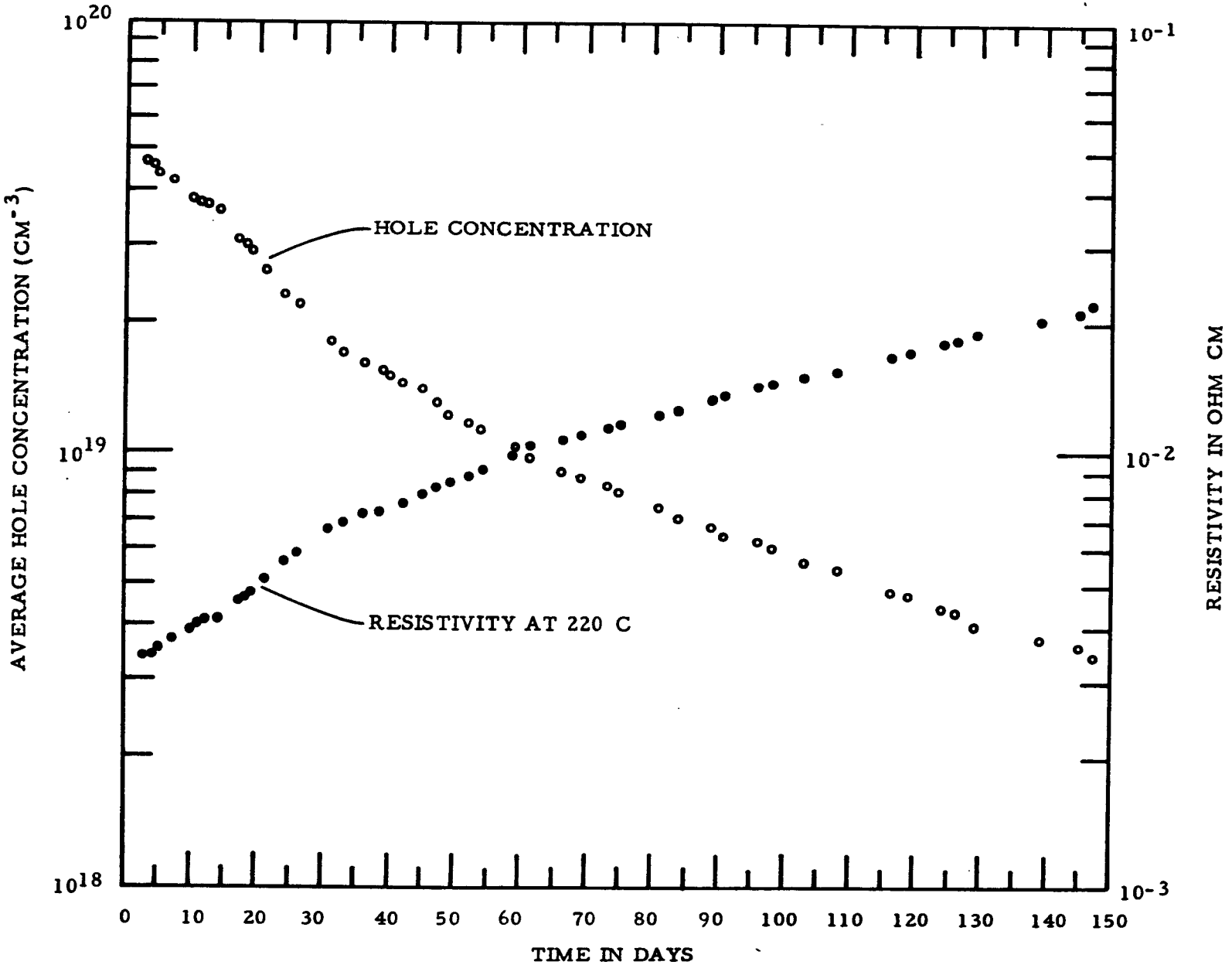

Fig. 17 Effect of heat treatment at 220°C on heavily zinc doped GaAs demonstrating precipitation.

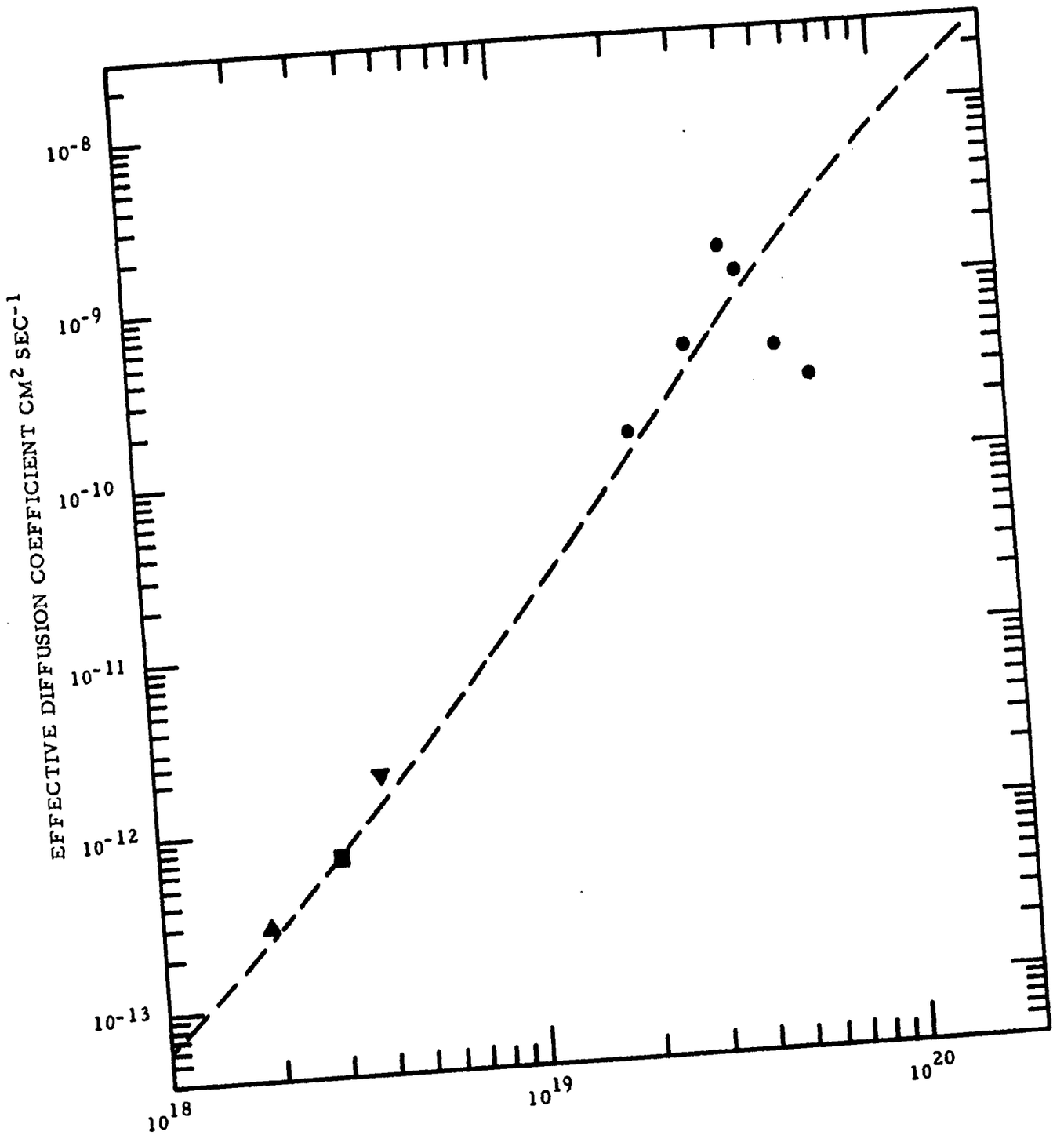

Fig. 18 Zinc diffusion in GaAs at 750°C

The results at 1000°C were considered in the theory section, where it was shown that Allen's suggestion that the variation in $\overline{D}$ was due to the different diffusion rates of ionized and un-ionized zinc was not valid. Most the data shown is from reference 1, although one set of data at high concentration is from the Stanford group.[10] At low concentrations, the recent data[13] are shown. The dotted line again is a tentative estimate of the effective diffusion coefficient.

Our analysis of the Cunnell and Gooch data taken with excess arsenic in the ampoule at 1000°C is also shown in Fig. 10. The effective diffusion coefficient is apparently markedly reduced under these conditions near the surface, but not affected significantly deeper in the sample. We are not sure if this is an equilibrium or a kinetic effect.

An apparent activation energy for diffusion,[11] Q_a for zinc in GaAs can be obtained from the three sets of data <u>at a given concentration</u>. The apparent activation energy is significantly reduced at high concentrations. The expression relating $\overline{D}$ to temperature is

$$\overline{D} = D_{oa} \exp\left[-Q_a/kT \right] , \qquad (18)$$

where both D_{oa} and Q_a are a function of concentration. The values obtained for Q_a and D_{oa} at several concentrations follow:

Zinc Concentration	Q_a (eV)	D_{oA} (cm^2/sec)
3×10^{19}	0.6 ± 0.2	6×10^{-7}
1×10^{19}	1.0 ± 0.2	2×10^{-6}
1×10^{18}	1.6 ± 0.2	4×10^{-6}
Intrinsic	2.3 ± 0.2	5×10^{-4}

Values quoted for intrinsic GaAs were obtained by extrapolation of the experimental data to zinc concentrations below the intrinsic electron concentration at a given temperature where $\overline{D}$ is expected to become independent of zinc concentration. It should be emphasized that the estimated $\overline{D}$ at 220°C obtained from the precipitation experiment leads to an activation energy of about 0.7 ± 0.2 at high zinc concentrations. This is consistent with the Q_a estimated above in this range of concentrations.

A few of the tracer runs made were analyzed on both sides of the sample. A run at 692°C, shown in Fig. 14, demonstrating that there is no significant effect of crystal orientation on $\overline{D}$. Although none was expected, there was a possibility that the surface equilibrium conditions would be different on opposite sides of a <111> slice, since a different type atom predominates on each side. No such effect was observed in this run, however.

As an engineering aid, we have compiled most of the existing zinc data as to p-n junction depth and have shown them in Fig. 19 plotted against zinc surface concentration. Surface concentration can be predicted accurately from the diffusion conditions from data to be presented in Section D. The junction depth is that expected for an n-type bulk concentration of 10^{17} cm^{-3} and for a time of 10^4 seconds. The values were calculated by assuming the junction depth advanced as the square root of time. This is a valid assumption even for a sharp concentration diffusion coefficient, but assumes that $\overline{D}$ is a function of concentration only. The anomalous effects discussed earlier indicate that $\overline{D}$ is evidently a function of time and distance in this system, but the data of Fig. 19 can be used as a first approximation. The inflection points in both the 900°C and 1000°C are believed due to the kinetic effects discussed earlier. In most runs reported, it is likely that the surface concentration had reached a constant value.

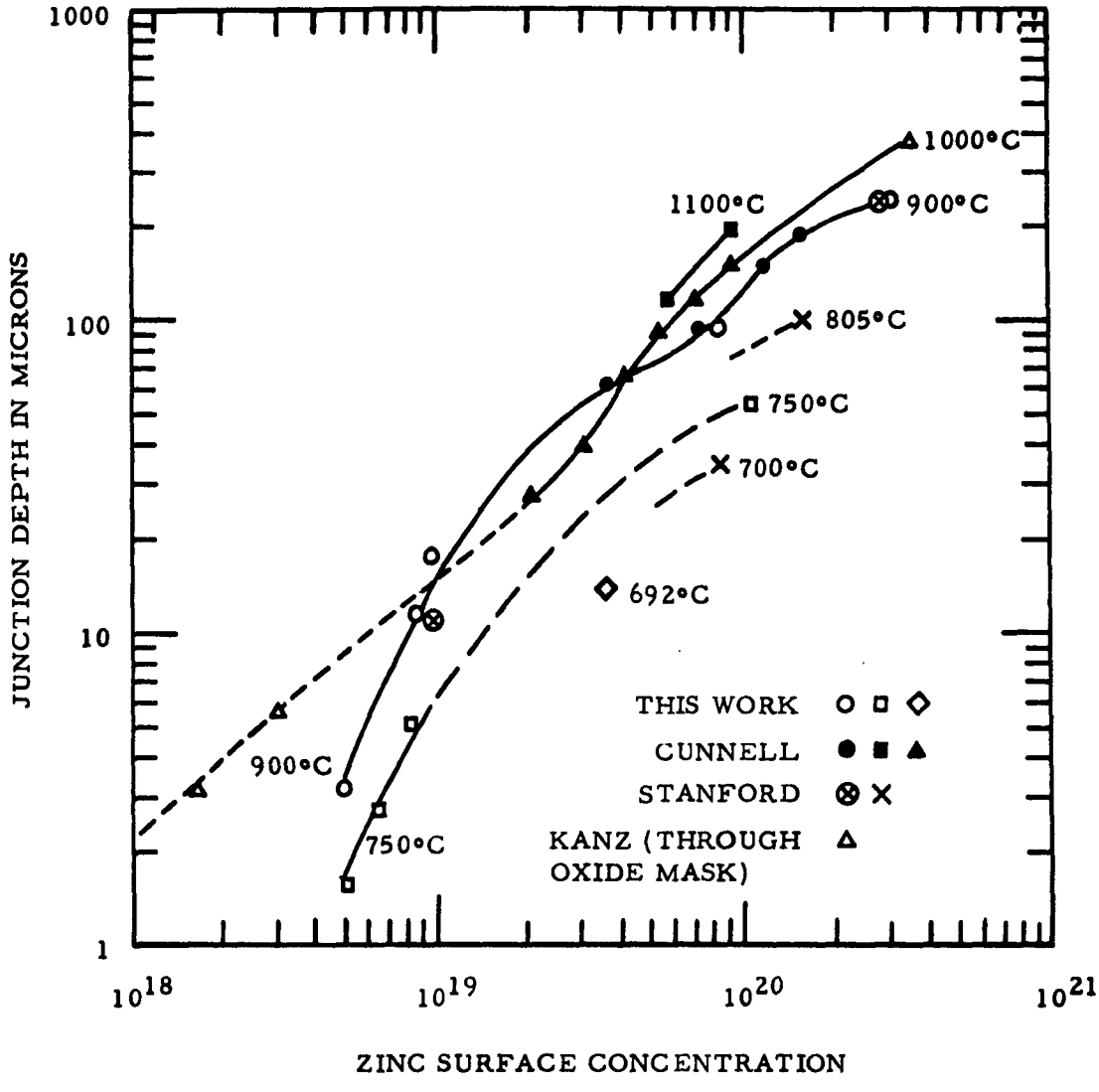

Fig. 19 P-N junction depth for zinc diffusion in GaAs for a normalized time of 10^4 seconds and 10^{17} cm^{-3} bulk donors

We have evidence, however, that the attainment of an equilibrium surface concentration is rather sluggish, so short diffusion times will generally lead to shallower junctions than those predicted here.

3. Discussion of Results

The important experimental facts to be explained for the zinc in GaAs system at any given temperature are:

(1) $\overline{D}$ is proportional to N_{Zn}^{n} where n ranges from 2 to 2.5.

(2) An apparent maximum in $\overline{D}$ occurs when the diffusion profiles are analyzed.

(3) High arsenic pressures tend to depress $\overline{D}$ near the surface.

These experimental facts can be explained assuming either a dominant interstitial diffusion mode or a dominant substitutional mode.

For an interstitial process: Fact (1) can be explained assuming that the zinc interstitial is a singly (sometimes doubly) ionized donor. Fact (2) can be justified on the assumption that the high diffusion coefficients in the interior are caused by the higher than equilibrium "fraction interstitial" (which dominates $\overline{D}$, as shown in the theory section), since the vacancies in this region must be generated at dislocation, a sluggish process. The region near the surface is nearer the equilibrium fraction interstitial, since the surface is a good source of incoming vacancies, so $\overline{D}$ is lower near the surface than in the interior. Fact (3) can be explained by assuming the gallium vacancies are enhanced in the presence of high arsenic pressure. If the interstitial zinc tends to react predominantly with gallium vacancies, then the enhanced gallium vacancy concentration would cause the fraction interstitial (and hence $\overline{D}$) near the surface to be depressed. In the interior of the sample, $\overline{D}$ will remain high because of the dislocation generated arsenic and gallium vacancies.

For a substitutional process the arguments are the following. Fact (1) requires that the vacancies be doubly (or sometimes perhaps triply) ionized donors. These must be divacancies, since simple gallium vacancies are inconsistent with Fact (3), as will be shown.* Fact (2) can be explained by postulating a flux of dislocation generated vacancies from the interior into the heavily p-type region.+ This will cause higher $\overline{D}$ values than typical of equilibrium at depths near the junction since a flux of vacancies outward causes a net flux of atoms inward. The vacancy concentration near the surface may be depressed by the incoming zinc, because the zinc can enter the crystal only at a vacant site. This would explain the low $\overline{D}$ values near the surface. At long times the net flux of zinc atoms into the crystal would finally decrease and incoming vacancies could maintain their equilibrium. The sluggish approach to the equilibrium surface concentration mentioned earlier may also result from this effect.

Fact (3) cannot be explained under the assumption that simple gallium vacancies are the main mode of diffusion for zinc. This is evident because excess arsenic should enhance the gallium vacancy concentration, which would in turn enhance $\overline{D}$. On the other hand, the way in which the divacancy concentration could be reduced is a non-equilibrium effect due to a sluggish gallium vacancy equilibrium. The arsenic vacancy concentration will be sharply reduced in an excess arsenic atmosphere. The gallium concentration should increase proportionally to keep the gallium-arsenic vacancy product constant. If the latter process is sluggish, the divacancy reaction will not be supplied

---

*An alternative explanation for Fact (1) involves a singly charged divacancy whose ionization energy decreases with increasing acceptor concentration. This could be expected in view of the large orbital of the electron in a material like GaAs. The electronic orbit of a donor would contain several acceptors at these high zinc concentrations.

+ Some very unusual data are presented in a later section about cadmium diffusion that seem to substantiate the outward vacancy flux concept.

properly so the concentration of the latter will decrease, as will $\overline{D}$. Near the junction, $\overline{D}$ will still be high because of bulk generated vacancies.

In looking at the two choices available, one is tempted to accept the interstitial argument and reject the substitional because of the greater simplicity of the arguments in the interstitial case. However, in addition to the cadmium data which substantiates the vacancy flux proposal, there are three other semiconductor systems that can be explained very nicely with substitutional models, whereas the interstitial model is inconsistent in almost every case. In silicon the evidence is that divacancies do indeed dominate diffusion at high temperatures, and furthermore, that they can be singly ionized donors, neutral, or singly or doubly ionized acceptors.

4. Summary

We believe that the results for zinc diffusion in GaAs are ambiguous for determining a diffusion mechanism from the observed concentration dependence of the diffusion coefficient. The preponderance of data in other semiconductor systems seems to favor a substitutional mechanism for them, but this does not shed any direct light on the GaAs problem. We feel that self-diffusion data for gallium and arsenic in heavily doped GaAs will perhaps resolve the question.

D. Zinc Surface Concentration Control

1. Vapor-Solid Equilibria

The surface concentration of an impurity in a semiconductor during diffusion can be specified by controlling the vapor pressure of the impurity over the semiconductor. We will develop

equations relating the equilibrium surface concentration to the vapor pressure.

Consider an acceptor that exists monatomically in the vapor that is in equilibrium with a semiconductor. The reaction involving transfer of the atom from the gas to the solid is

$$A_G \overset{K_G}{\rightleftharpoons} A^\circ \quad ,$$

where the atom in the semiconductor is assumed to be un-ionized until a subsequent reaction occurs, namely:

$$A^\circ \overset{K_A}{\rightleftharpoons} A^- + e^+ \quad .$$

The Mass Action Law applied to the first reaction gives

$$N_A^\circ = K_G P_A \quad , \tag{19}$$

where N_A° is the un-ionized acceptor concentration in the solid, P_A the partial pressure of the acceptor and K_G an equilibrium constant.[16] The second reaction above has already been discussed and the resulting mass-action expression given in Eq. (5) as

$$\frac{N_A^- \; p}{N_A^\circ} = K_A \tag{5}$$

where p is the hole concentration and K_A can be calculated using (6).

By utilizing these expressions and the charge neutrality and conservation of species as before, the following expression can be developed (assuming no compensating donors are present):

$$N_A = K_G P_A + \frac{K_G K_A P_A}{(K_G K_A P_A + n_i^2)^{1/2}} \quad , \tag{20}$$

where N_A is the equilibrium acceptor concentration in the solid, and n_i the intrinsic electron concentration. The left and right terms are the un-ionized and ionized acceptors, respectively.

At low partial pressures where the acceptor concentration in the solid is much less than n_i, the above expression shows a linear dependence of N_A on pressure, namely

$$N_A = K_G P_A \left(1 + \frac{K_A}{n_i}\right) \quad . \tag{21}$$

At higher pressures where N_A is much greater than n_i, Eq. (20) becomes:

$$N_A = K_G P_A + \left(K_G K_A P_A\right)^{1/2} \quad , \tag{22}$$

where the square root dependence dominates at intermediate concentrations and the linear term becomes important at very high acceptor concentrations.

We have plotted the zinc surface concentrations of almost all the runs made in GaAs, as a function of the pressure of zinc, under the assumption that Raoult's law* is valid for the zinc-gallium alloy diffusion source. These data are shown in Figs. 20 and 21, with data from the Stanford group and from reference 1. Pressure in the latter was calculated from the expected vapor pressure of elemental zinc which was placed at the cold end of the tube. The consistency of these points with our data at 900°C is especially gratifying, considering the different experimental conditions.

---

* Raoult's law states that the partial pressure of the solute (zinc) in a solution is $P_A = X_A P_{A^\circ}$, where X_A is the mole fraction of the acceptor and P_{A° is the vapor pressure of the pure acceptor at the temperature in question.

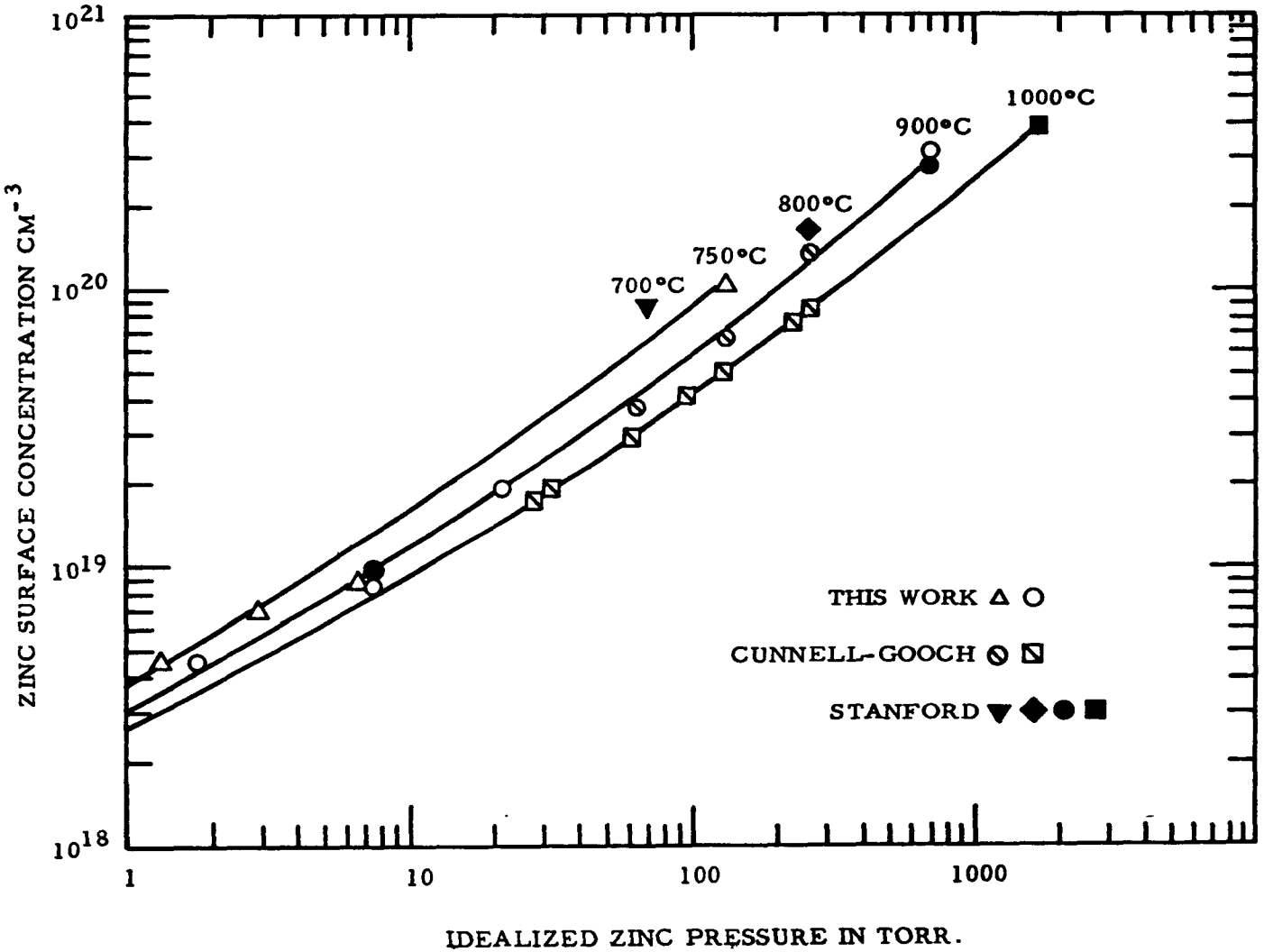

Fig. 20 Effect of zinc partial pressure on surface concentration with theoretical curves assuming zinc ionization energy of .08ev

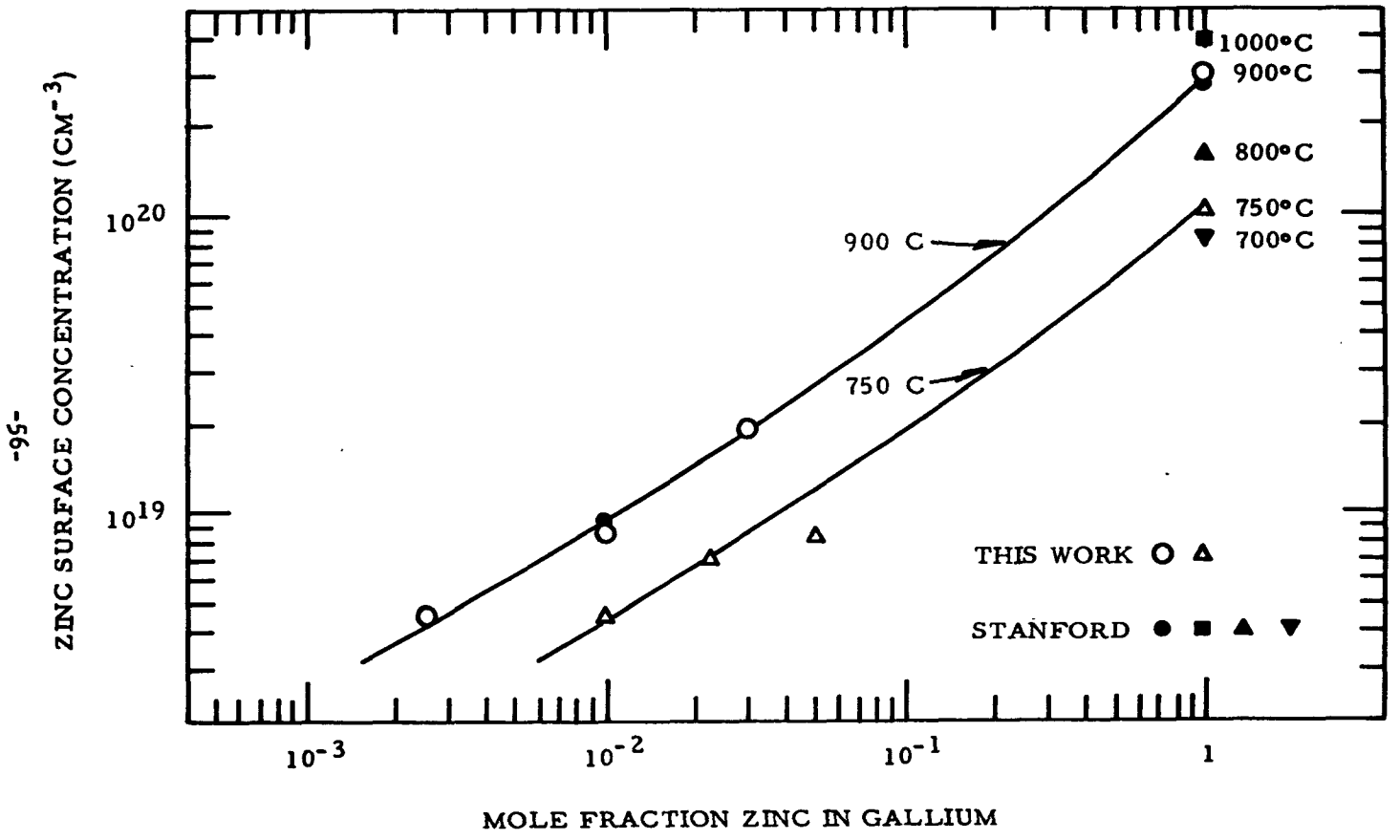

Fig. 21 Zinc surface concentration using a zinc-gallium alloy diffusion source

The theoretical curves shown are calculated from Eq. (22) assuming an acceptor ionization energy of .08 eV, which is a theoretical value assuming a simple hydrogenic model. This choice is somewhat arbitrary, because there are no reliable published values. The data can be fitted reasonably well with any ionization energy in this range. K_a at each temperature was calculated using the band structure parameters of Ehrenreich[6] as discussed in the Theory section.

The equilibrium constant K_G was calculated to give the best fit with the data at each temperature. These values of K_G are shown in Fig. 22, with two points calculated from single runs utilizing elemental zinc. The temperature dependence of K_G is given by:

$$K_G = 1.5 \times 10^{15} \exp\left[.53/kT\right] , \qquad (23)$$

where the units of K_G are cm^{-3} $torr^{-1}$** and the heat of reaction is in electron volts (with an estimated uncertainty of only 0.04 eV). By utilizing this relation for K_G and Eq. (23) (general) or (22) (extrinsic), the equilibrium surface concentration expected of almost any experimental condition should be predictable to within about 10% accuracy. This is based on data from Fig. 20. Only one point of the 23 shown is outside this error.

Note that the heat of transfer for an atom in the vapor going to an un-ionized atom in the solid is <u>negative</u>. This is evident in Fig. 20 because at a given pressure the surface concentration decreases with increasing temperature.

** One torr is a mm of Hg of pressure.

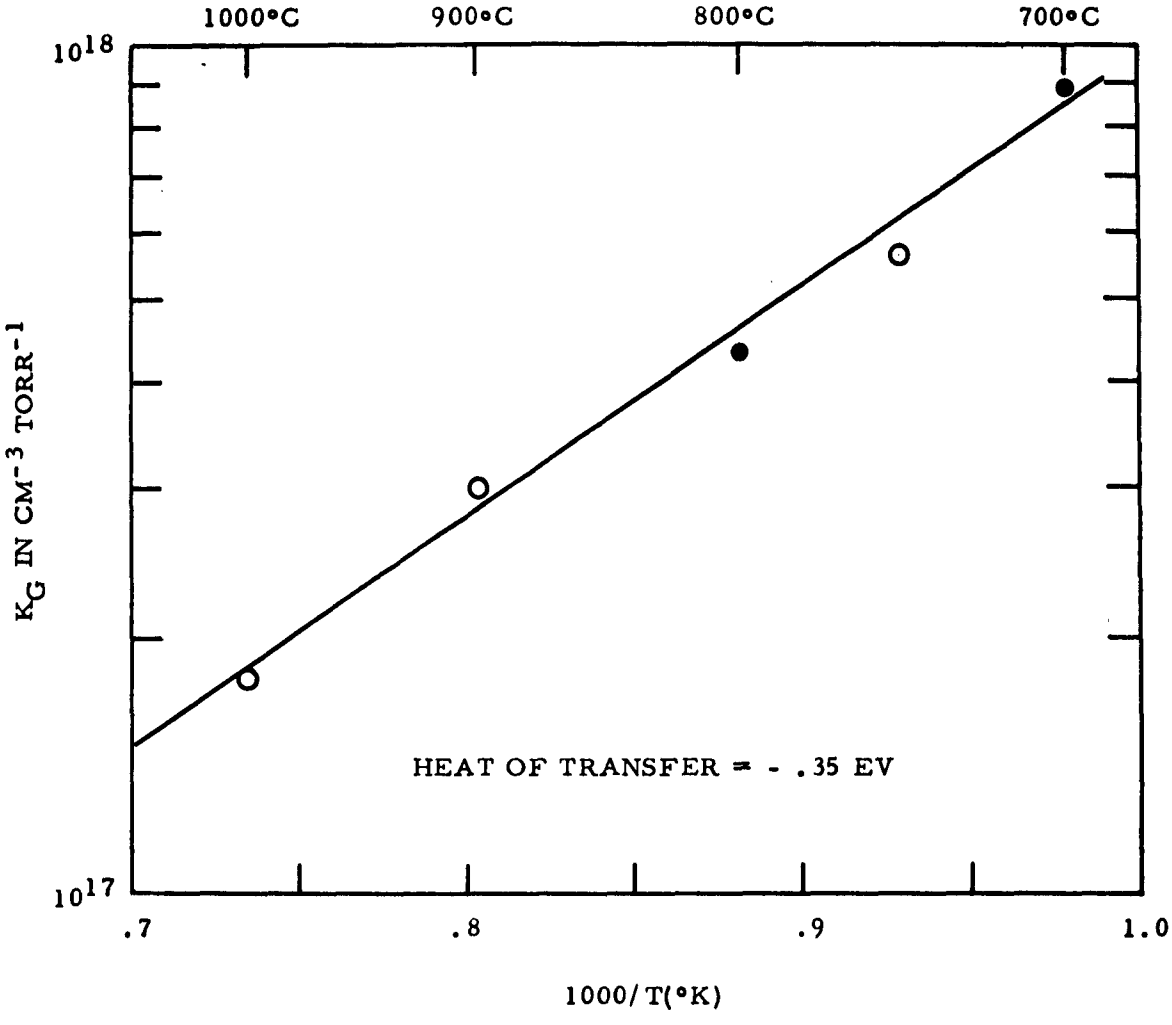

Fig. 22 Temperature variation of the equilibrium constant for the zinc in GaAs vapor-solid equilibria

These data are believed to be the first experimental verification of the concept proposed by Reiss,[16] that vapor-solid equilibria are governed by the un-ionized impurity concentration in the solid rather than by the total impurity concentration. In most other diffusion systems, either the partial pressure of the impurity is unknown or the ionization energy is a function of concentration. This latter effect causes the energy level to merge with the nearest band at high concentrations and the impurity is completely ionized at essentially all concentrations. When this occurs, the theory is not followed.

Some data of the same nature reported here for the zinc in InSb system is in poor agreement with this theory. This is not unexpected in view of the larger expected orbitals in this system. An order of magnitude criterion for the concentration at which merging should occur is given by calculating the concentration at which the donor or acceptor orbitals begin to overlap. On a simple hydrogenic model the radius of the orbital is given by $a_o \epsilon^2 \, m_o/m^*$ where a_o is the radius of the electron orbit of the hydrogen atom (0.53A°), ϵ the dielectric constant and m_o and m^* are the electronic and effective masses, respectively. For acceptors in InSb, merging of the energy level with the valence band on this model should occur at about 3×10^{18} cm^{-3}, so it is not surprising that the theory does not apply to this system, since all our data are for concentrations above this value.

The same calculation for acceptors in GaAs yields a value of 4×10^{20} cm^{-3}, so the theory should fit at concentrations below this value. The good fit with theory is good evidence that the energy level of zinc remains well-defined <u>at these high temperatures</u>. We stress this latter point because there is good evidence that at room temperature the level <u>does merge</u> with the valence

band. This is evident from the Hall data of Haisty and Kellett[12] shown in Fig. 16, which with other data, shows zinc to be completely ionized to at least 10^{20} cm^{-3}. This seems to indicate that the phenomenon of impurity level merging is more likely to occur (that is, at a lower concentration) at low temperatures. We feel this merging is due to the increased degeneracy effects at lower temperatures due to the lower density of states. An interesting consequence of this effect is that the hole or electron concentration of a heavily doped sample may actually <u>decrease</u> as the temperature is raised while the energy levels "unmerge" at high temperatures.

2. Zinc Solid Solubility and Segregation Coefficient

The segregation coefficient, k, is defined (for an acceptor, for example) as

$$k = \frac{N_A}{N_A^L} \quad , \tag{24}$$

where N_A is the acceptor concentration in the solid and N_A^L the acceptor concentration in the liquid. We can introduce a liquid into our vapor-solid equilibria if we imagine that the surface of the semiconductor contains a liquid layer that is in equilibrium with both the acceptors in the vapor and the solid. The pressure of the acceptor is related to the acceptor concentration in the liquid by

$$P_A = \gamma_L X_A^L P_A^\circ \quad , \tag{25}$$

where P_A° is the pressure over pure acceptor, γ_L the activity coefficient for the acceptor in the liquid, and X_A^L the mole fraction of the acceptor in the liquid, ($N_A^L = N_\circ X_A^L$ where $N_\circ$ is the total atom concentration per cm^3, which is 4.4×10^{22} for GaAs).

The segregation coefficient in terms of the liquid concentration can be obtained from (20), (24), and (25) and the result is

$$k = \frac{K_G P_A^\circ}{N_o} \left[1 + \frac{K_A}{(K_G K_A X_A^L P_A^\circ + n_i^2)^{1/2}} \right] , \quad (26)$$

where the activity coefficient (usually of order unity) can be inserted with each P_A°, if necessary.

In terms of the acceptor concentration in the solid, the complete expression is rather complex and will not be given here. At acceptor concentration below n_i, namely <u>intrinsic</u> conditions, the expression reduces to

$$k = \frac{K_G P_A^\circ}{N_o} \left(1 + \frac{K_A}{n_i} \right) , \quad (27)$$

and under <u>extrinsic</u> conditions ($N_A \gg n_i$) the expression for k is:

$$k = \frac{K_G P_A^\circ}{N_o} \left\{ 1 + \frac{K_A}{2N_A} + \left[\left(1 + \frac{K_A}{2N_A} \right)^2 - 1 \right]^{1/2} \right\} . \quad (28)$$

The acceptor concentration must vanish at the melting point, so we are in the intrinsic range near the melting point, and Eq. (27) applies. To calculate the segregation coefficient near the melting point, all we need is a value of K_G and P_A°, since K_A and n_i are both calculable. A value of K_G can be obtained at the melting point of GaAs (1240°C) from Eq. (23), and the pressure of pure zinc at this temperature is available from standard vapor pressure data. The value of n_i is 1.5×10^{18} cm^{-3}, P_A° is 9×10^3 torr, K_G is 8.7×10^{16} cm^{-3} torr^{-1}, and K_A is 4.6×10^{19} cm^{-3} for an ionization energy of .08 eV. Putting these values in (27), we obtain a segregation coefficient of 0.55 at the melting point. The only assumption we have made is that the liquid behaves ideally ($\gamma_L = 1$). The only published

value of k for zinc in GaAs is by Whelan,[17] who says it is somewhere in the range of 0.3 to 0.9. Our calculated value falls in the middle of this range. A more accurate statement of our results is that $k = 0.55\gamma_L$, so knowledge of γ_L would permit a more accurate value of k to be determined.

The solid solubility of zinc in GaAs can be calculated by relating the concentration in the solid to that in the liquid using Eqs. (20) and (25) so we have*

$$N_A = K_G X_A^L P_A^\circ \left[1 + \frac{K_A}{(K_G K_A X_A^L P_A^\circ + n_i^2)^{1/2}} \right]. \quad (29)$$

The temperature dependence of all these terms except X_A^L is known. This, too, can be calculated if the heat of fusion of the semiconductor in known and by making certain simplifying assumptions concerning the ideality of the liquid.[18] This is somewhat complex unless $k \ll 1$, so we will show the data which we think best represent the solid solubility and will indicate the expected temperature dependence as a dotted line. This is done in Fig. 23, where we have also included data from Pearson, et al.[10] The solid solubility was obtained by extrapolating the diffusion profiles to the surface.

E. Cadmium Diffusion in GaAs

Diffusion of radioactive Cd^{115} in gallium arsenide, as a p-type impurity, was investigated. A complication was observed from the simultaneous diffusion of In^{115}, which is a decay daughter of Cd^{115}. It was

---

* The activity coefficient γ_L can be inserted in this and subsequent relations by multiplying into all P_A° terms.

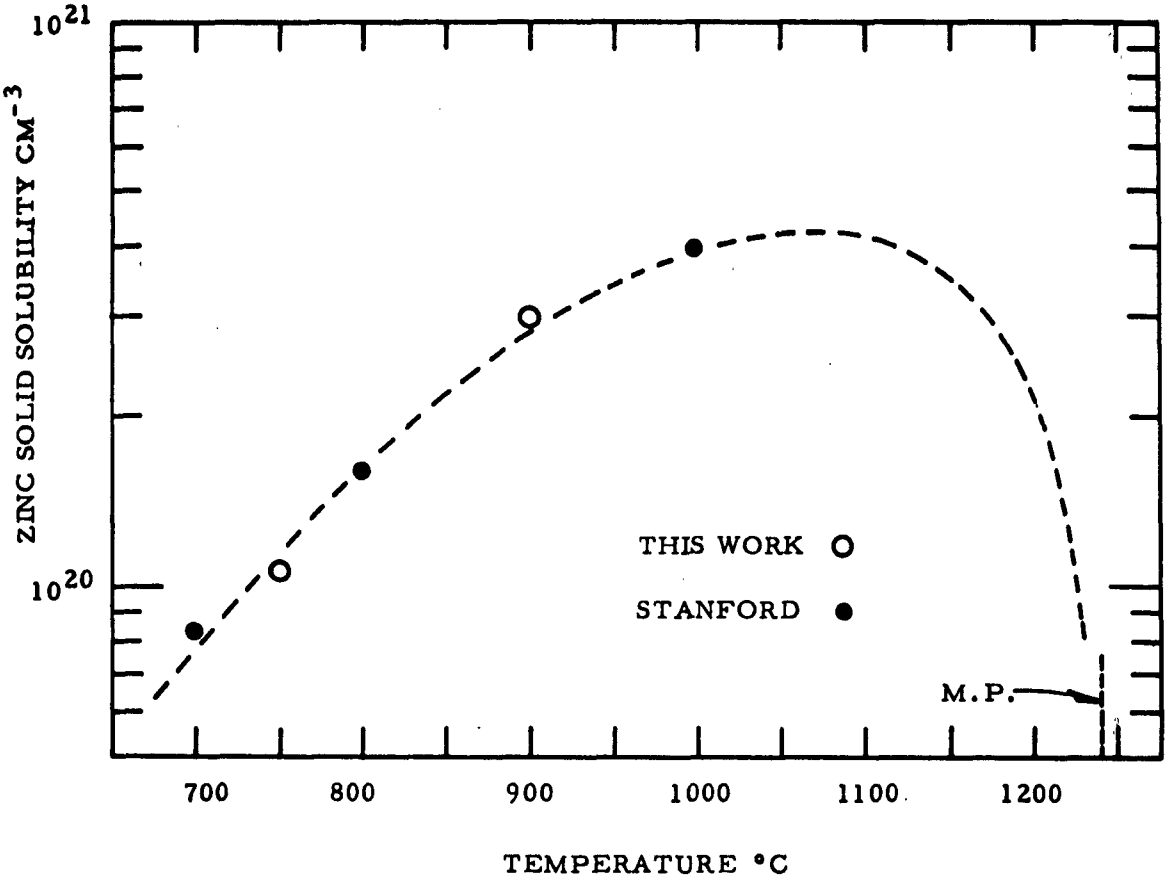

Fig. 23 Solid solubility of zinc in GaAs

found that the indium had a diffusion coefficient slightly higher than the cadmium at 1100°C. Figure 24 demonstrates these results, where the curve showing a value for the diffusion coefficient of 3-5 x 10^{-11} cm^2 sec^{-1} is attributed to the diffusion of the Cd^{115}. These two curves were obtained by evaluating opposite sides of a single wafer, diffused with Cd^{115} for 10 hours at 1100°C, at two different times. The curve showing the higher "apparent" surface concentration and faster diffusion was obtained immediately after the diffusion run. The second curve was obtained on the opposite surface two days later. The difference was attributed to the fact that after two days, the concentration of the 4.5-hour half-life In^{115} was down by 3 orders of magnitude, so only the 53-hour Cd^{115} was seen. It is assumed, therefore, that the second curve with a D = 2 x 10^{-11} cm^2 sec^{-1} is due to Cd^{115} only. This value of diffusion coefficient is lower by a factor of two than that reported by Goldstein[19]; however, his diffusion conditions were somewhat different.

That the aforementioned conclusions are probably correct was later substantiated in a diffusion run by gamma ray spectroscopy. This analysis showed that the sample contained in the regions near the surface an inordinate amount of In^{115} that could not be attributed to the normal equilibrium decay scheme of Cd^{115}. The analysis showed one other point of interest: there was no detectable concentration of either In^{115} or Cd^{115} in the bulk of the sample beyond 30 microns penetration. This is in disagreement with the results of Cunnell and Gooch,[20] which were possibly obtained under somewhat different experimental procedures. Figure 25 shows a concentration profile for Cd^{115} after diffusion at 1000°C for 53 hours. The diffusion coefficient is 8 x 10^{-13} cm^2 sec^{-1}, which is again lower by a factor of four than that reported by Cunnell and Gooch[20] and a factor of ten lower than Goldstein[19] Since our diffusion was done under conditions which gave lower surface concentrations, it could be noted that cadmium, like zinc, is sharply concentration dependent.

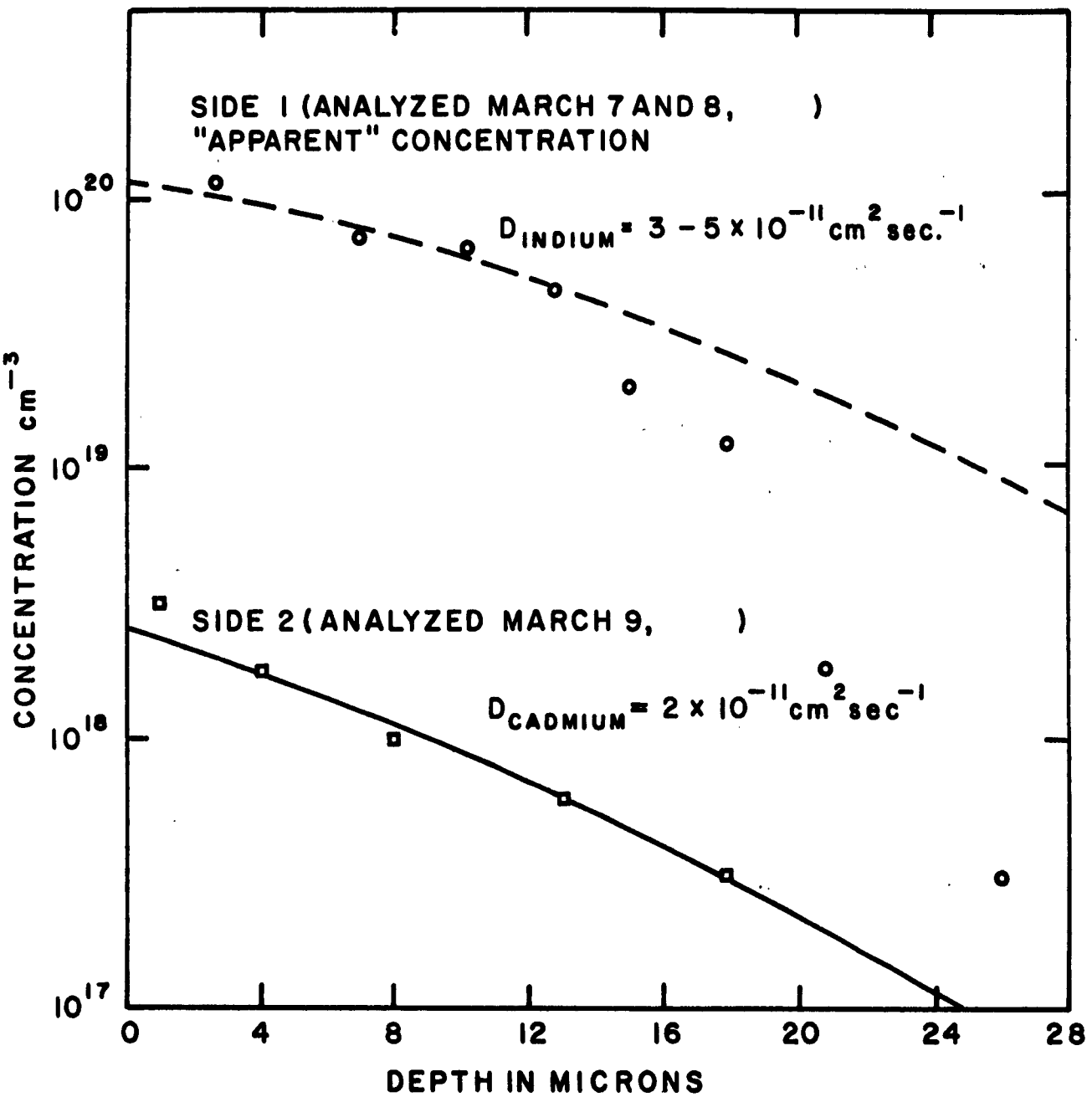

Fig. 24 10 hours at 1100°C with 0.2 atm. cadmium^{115} showing transient effects due to indium^{115}

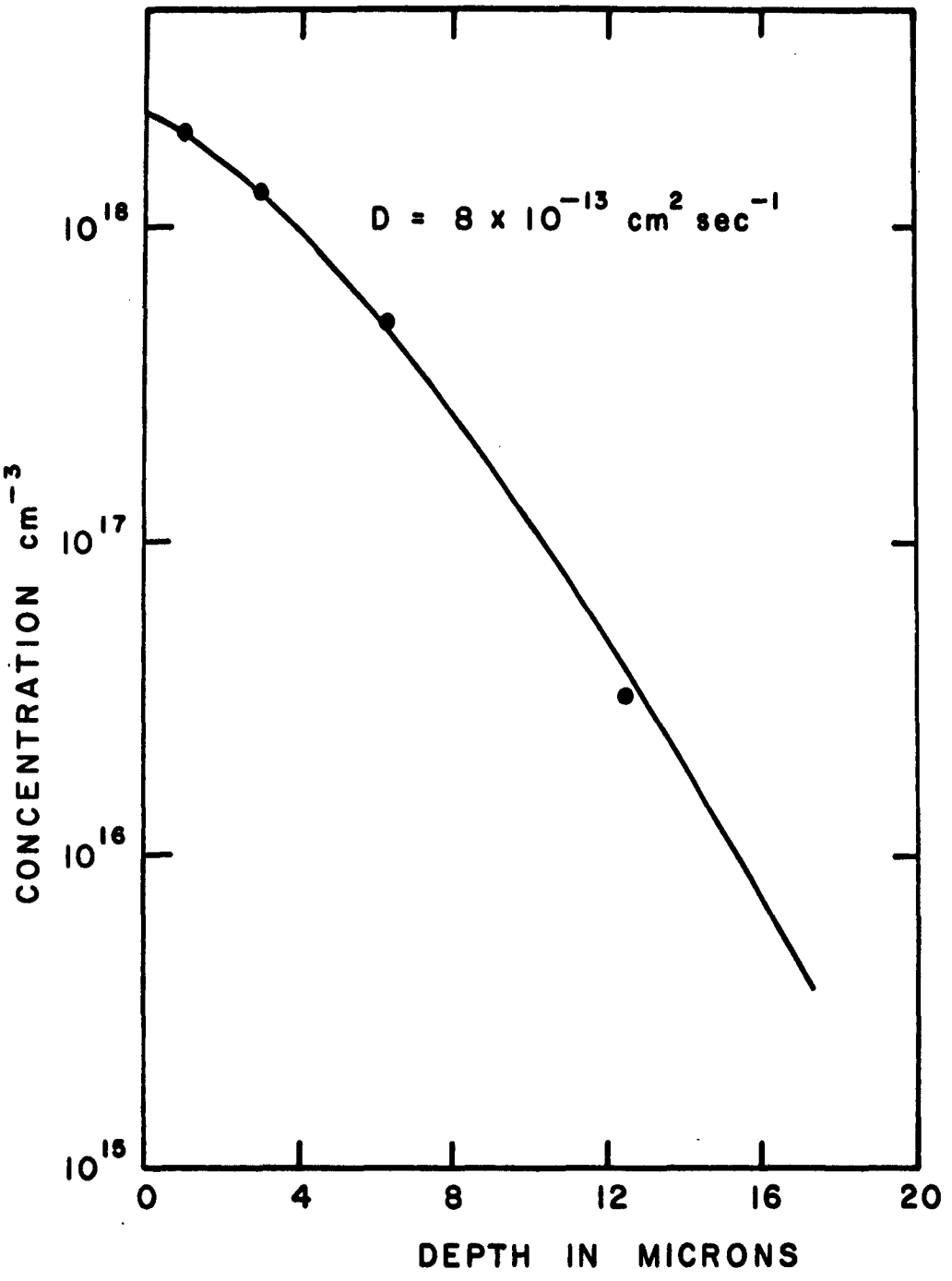

Fig. 25 53 hours at 1000°C with 0.15 atm. of cadmium^{115}

F. Manganese Diffusion in GaAs

Diffusion of manganese as an acceptor in gallium arsenide was investigated. Several diffusion runs were made under different conditions and the resulting manganese distributions determined using incremental sheet resistance techniques. The results were in agreement with those expected from the typical complementary error function distribution,

$$C(x) = C_o \left(1-\text{erf} \frac{x}{2\sqrt{Dt}}\right) . \qquad (30)$$

From Eq. (30), values of D were calculated for the various diffusion conditions and are plotted vs 1000/T(°K) in Fig. 26. The data may be represented by

$$D = 8.5 \times 10^{-3} \, C^{-1.7/kT} . \qquad (31)$$

Figure 27 shows the dependence of the surface concentration of manganese on temperature.

G. Sulfur Diffusion in GaAs

The study of diffusion of sulfur into gallium arsenide was greatly hindered by reaction of the diffusant vapor with the sample at the necessary high temperatures. The surface of sulfur-diffused samples generally showed considerable pitting from the reaction and exhibited appreciable losses in weight. Again data were obtained by the incremental sheet resistance technique. The results showed that the diffusion of sulfur follows a complementary error function distribution in gallium arsenide. With reservations because of the aforementioned difficulties, the data shown plotted in Fig. 28 were obtained. One value on this curve was obtained by the radioactive tracer analysis technique of S^{35}. This diffusion coefficient value at 890° C agrees very well with the values obtained from the sheet resistance technique.

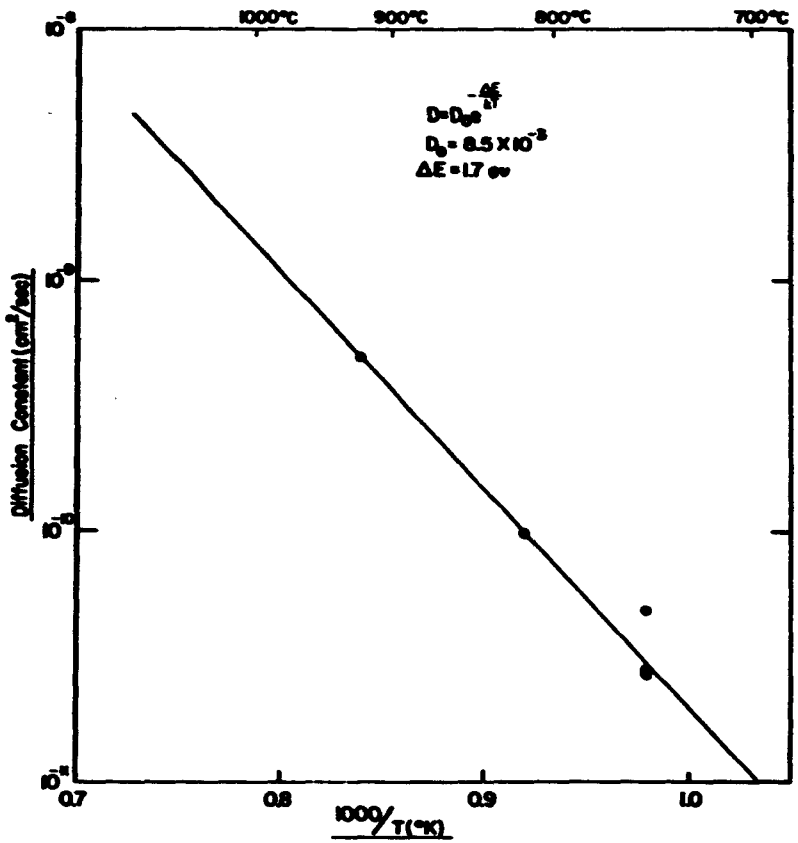

Fig. 26 Dependence of the diffusion constant of manganese on gallium arsenide on temperature

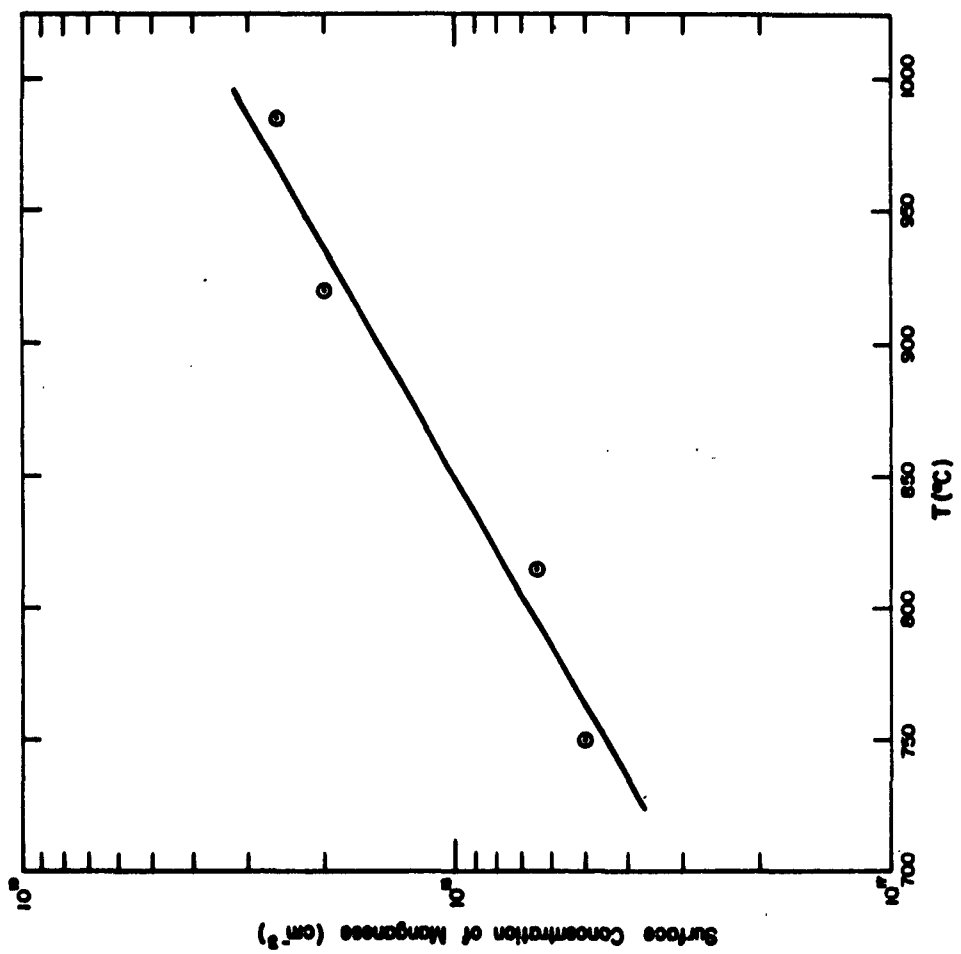

Fig. 27 Surface concentration, C_o, of manganese in gallium arsenide as a function of diffusion temperature

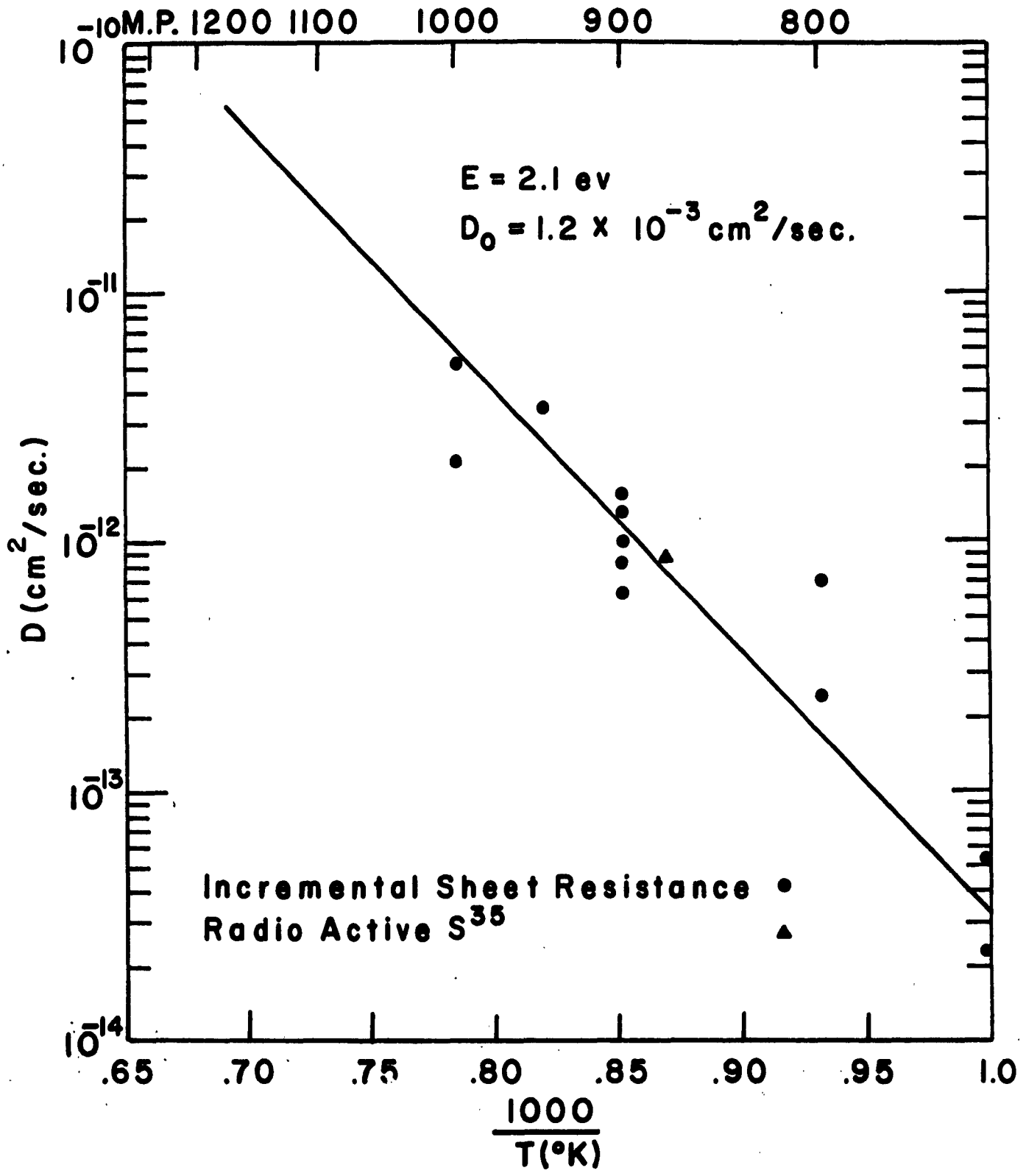

Fig. 28 Diffusion of sulfur in GaAs

H. Magnesium Diffusion in GaAs

Diffusion of magnesium, a p-type impurity, in gallium arsenide was studied in considerable detail. Diffusion runs were made at 800, 900, 1000, 1100, and 1150° C in sealed ampoules. The amounts of gallium (placed in ampoule to prevent copper diffusion) and magnesium (40-60 atomic percent, respectively), volume of ampoule, and size of sample were kept constant throughout the runs. Initially, results were evaluated by measuring the sheet resistance, ρ_s, of the p-layer and the junction depth, x. Values of the surface concentration, C_o, were obtained from a set of curves of C_o vs $\rho_s x$ for various starting n-impurity concentrations, Cx. These curves are valid if the impurity distribution in the p-layer is assumed to be a complementary error function for magnesium diffusion in gallium arsenide. An independent set of experiments validated this assumption. Figure 29 shows a plot of C_o vs temperature where C_o ranged from 4.5×10^{17} atoms/cc at 800° C to 5×10^{18} atoms/cc at 1150° C. Calculation of the diffusion coefficients, D, for these C_o values yielded $D = 1 \times 10^{-13}$ cm^2/sec at 800° C to 2.3×10^{-11} cm^2/sec at 1150° C. A plot of these values of D vs T (temperature) is shown in Fig. 30. Values at 800° C are believed to be somewhat in error because of inaccurate measurement of the small values of x ($\lesssim$ 1 micron after 20 hours of diffusion). There may also be some error at the higher temperatures, where considerable surface loss of arsenic is possible.

Figures 31, 32 and 33 show plots of concentration, C. vs depth of penetration, x, at 1100, 1000, and 900° C for magnesium diffusion if gallium arsenide. These curves tend to support the validity of the assumption that magnesium obeys a complementary error function distribution. One can calculate D at various points on the curves and find them to correlate with those shown in Fig. 30. The results in Figs. 31, 32 and 33 were obtained by incremental sheet resistance measurements, ρ_s, vs depth of penetration, x, for the p-layers.

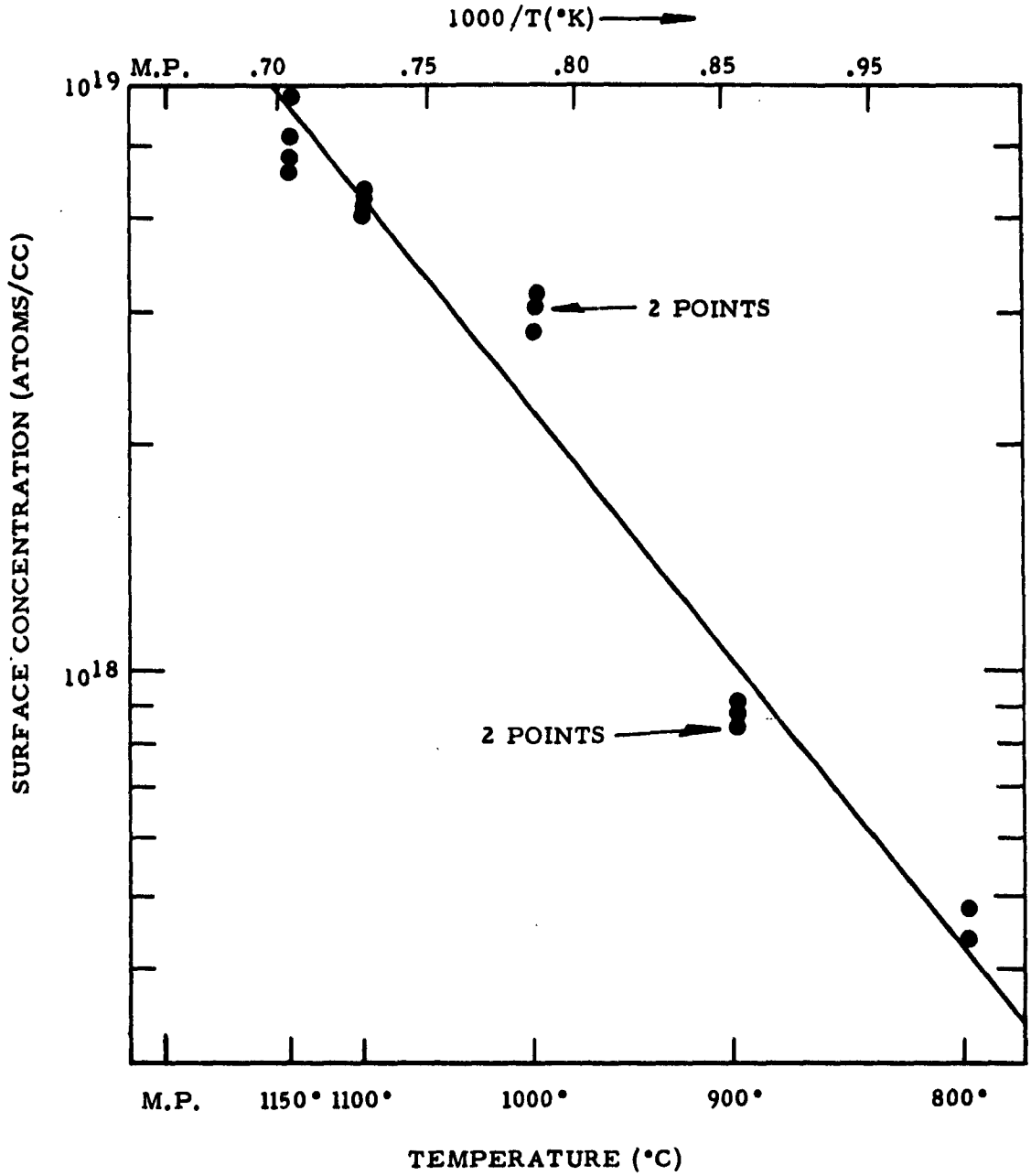

Fig. 29 **Diffusion of magnesium in GaAs (n-type). Source, 60 atomic % Mg.**

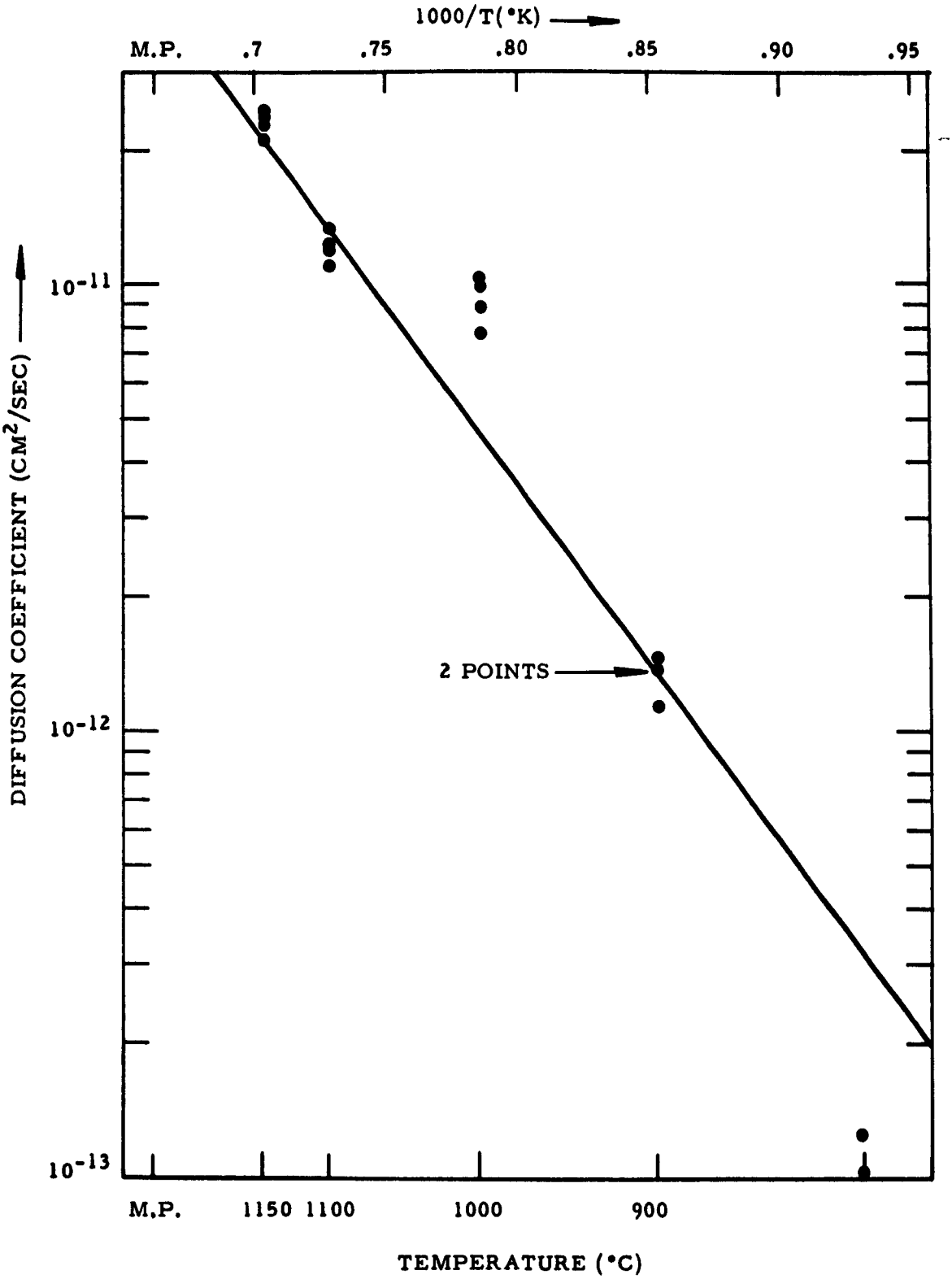

Fig. 30 Diffusion of magnesium in GaAs (n-type). Source 60 atomic % Mg.

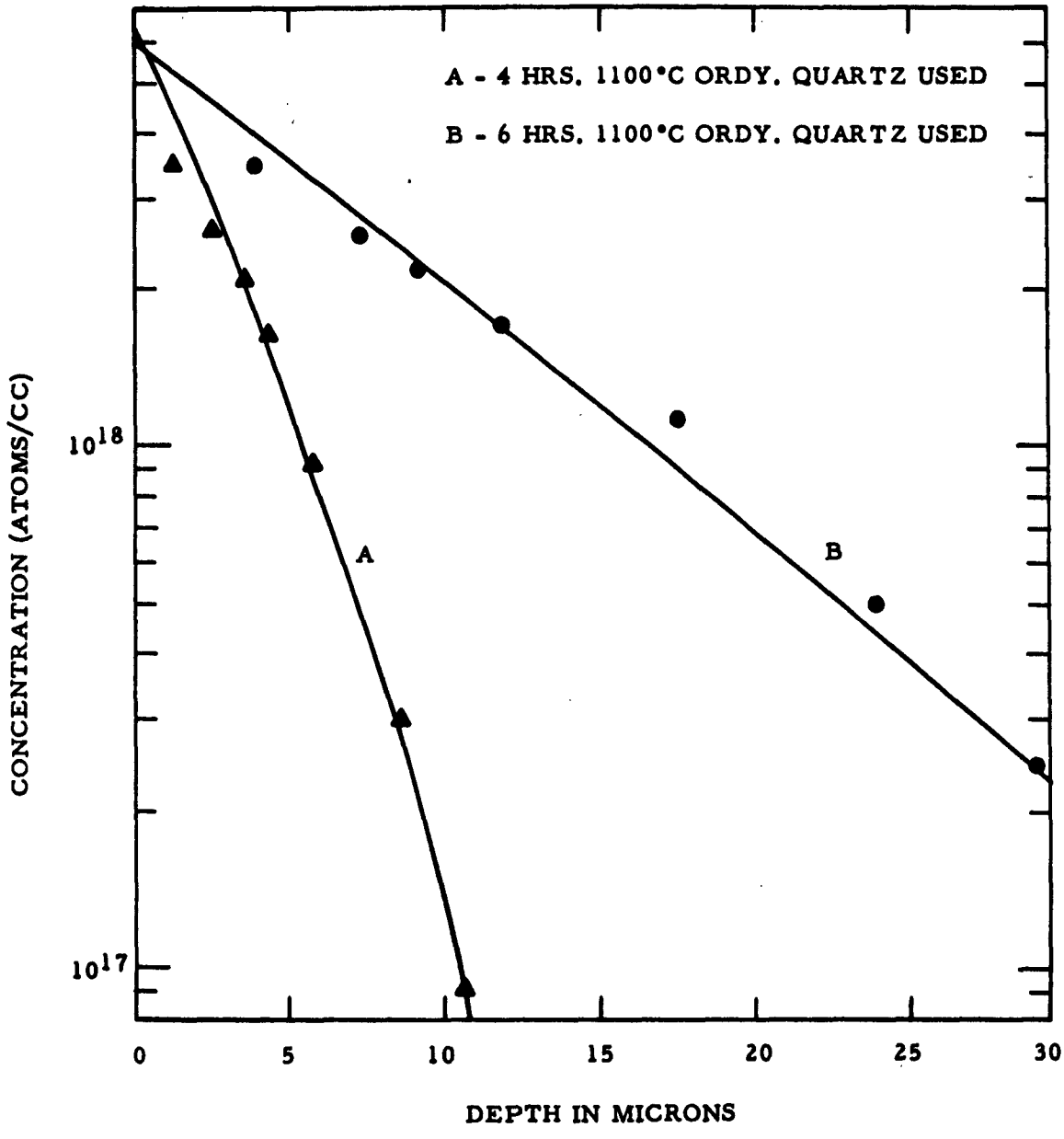

Fig. 31 Concentration as a function of diffusion depth. Source 60 atomic % Mg.

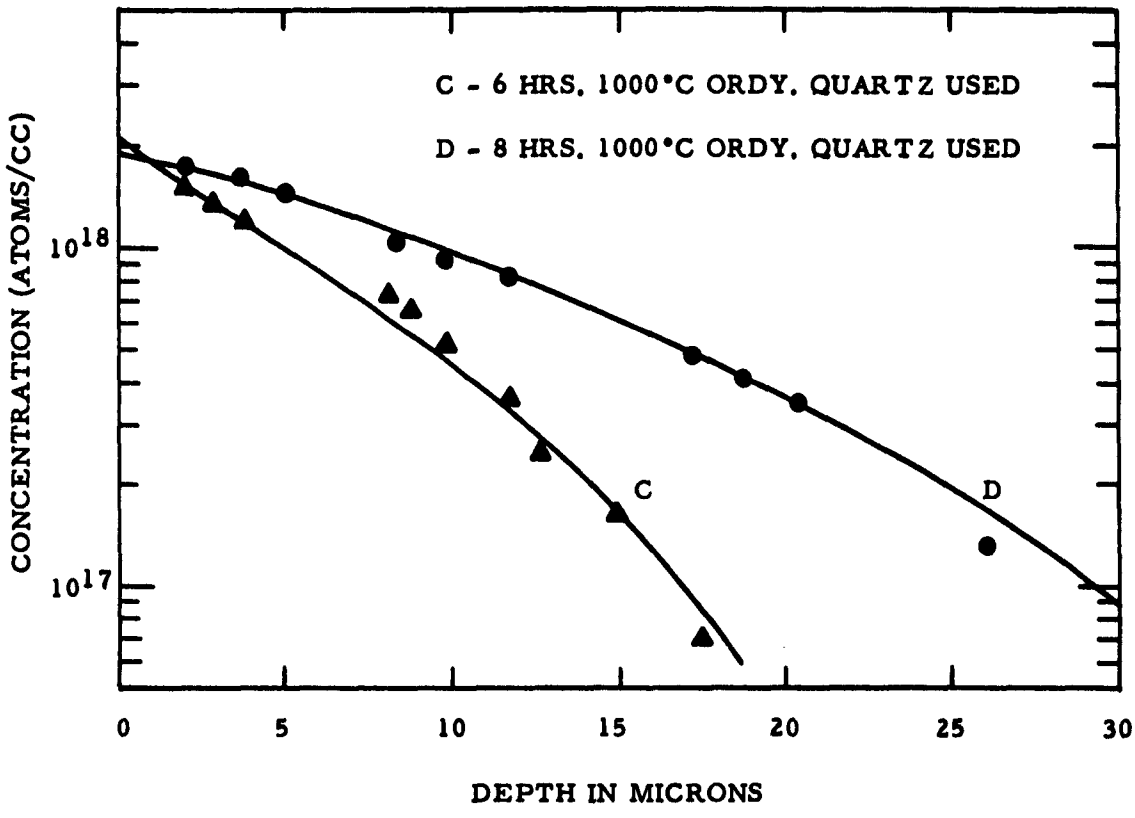

Fig. 32 Concentration as a function of diffusion depth. Source 60 atomic % Mg.

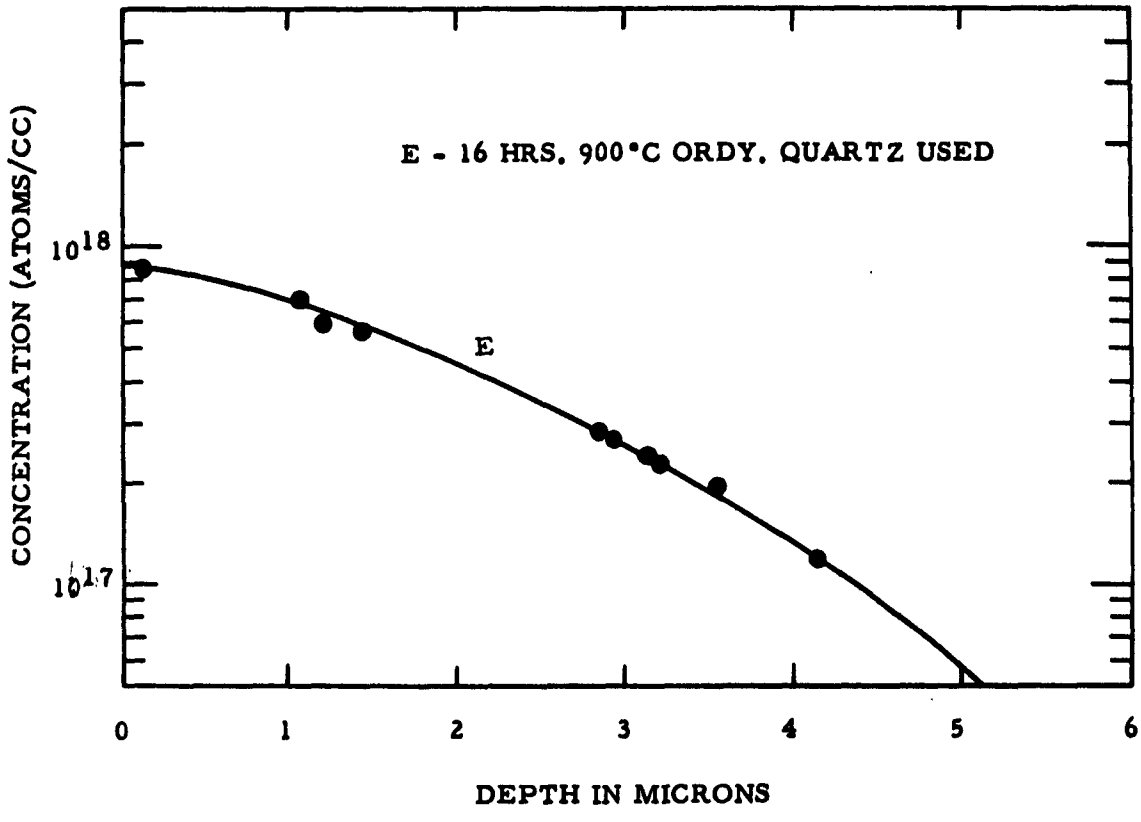

Fig. 33 Concentration as a function of diffusion depth. Source 60 atomic % Mg.

I. Mercury Diffusion in GaAs

The diffusion of mercury, as an acceptor, in gallium arsenide was investigated. Two samples of gallium arsenide were diffused 44 hours at 1000° C with the radioactive isotope Hg^{203}, at a mercury pressure of 1.0 atmosphere. Data from both samples are shown in Fig. 34. The limits are shown for a 90% confidence level (see Appendix A); within these limits the diffusion coefficient may be no greater than 7.3×10^{-14} cm^2/sec. For a more accurate determination, Hg^{203} with a higher specific activity than was available would be required. The value 7.3×10^{-14} cm^2/sec was determined by assuming a complementary error function distribution and finding the highest D that would fall within the predetermined statistical limits of the data taken. This is not intended as an actual value, but merely the maximum. Because of this low diffusion coefficient for mercury at 1000° C, no further investigation of mercury diffusion in gallium arsenide was deemed necessary.

J. Thermal Conversion

A study of contamination as a cause for the "thermal conversion" of gallium arsenide from n- to p-type during diffusion, was accomplished. Copper was established as the offending agent. The exact sources of contamination were not defined, although the possibilities are numerous.

In the experimental procedure a slice of n-type gallium arsenide of known concentration was sealed in a thoroughly cleansed quartz ampoule, with either a known amount of gallium or arsenic, at a vacuum of about one micron. In each run the preparation of slices and tubes was identical; samples were heated at 1100° C for one hour with the same cooling cycle on each run. After each experiment conductivity type and carrier concentration of each sample were ascertained and a spectrographic analysis made for existing impurities. In the case of a control slice, which was not heated, a spectrographic analysis was made to

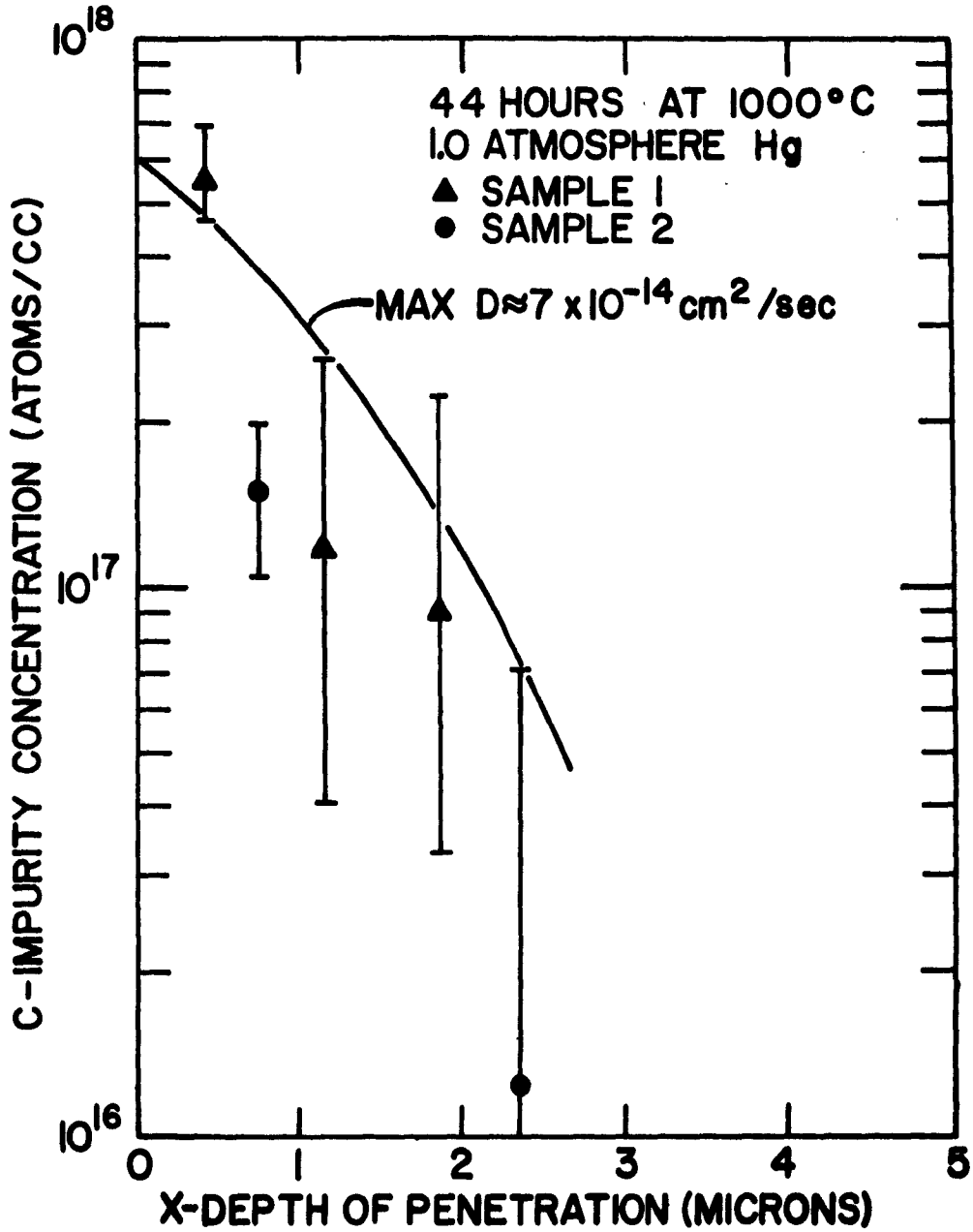

Fig. 34 Hg^{203} diffusion in GaAs

determine the original impurities in the crystal. Table V shows the results of these experiments, from which the following conclusions can be made.

(1) Copper (a) is not found in the grown crystals used in the experiments, but (b) is introduced during the heat treatment process.

(2) The number of acceptors added during the treatment is proportional to the amount of copper added.

(3) Various chemical treatments of the gallium arsenide surfaces reduce the amount of copper introduced, but do not eliminate it.

(4) Contamination from the quartz ampoule appears to be a larger factor in sample preparation.

(5) Excess gallium in the ampoule significantly reduces the amount of copper introduced into the gallium arsenide and permits the use of n-type material with starting concentration as low as 5×10^{16} atoms/cc to make transistors. Placing the gallium in contact with the slices does not aid further reduction.

(6) Excess arsenic in the system has much less effect than gallium on copper contamination.

Attempts to eliminate the copper contamination completely have not yet been successful.

Table V

Experimental Results on Thermal Conversion of Gallium Arsenide

Run Number	Ampoule Content	Original Excess Electron Concentration x 10^{16} cm^{-3}	Excess Carrier Concentration After Heat Treatment cm^{-3}	Spectrographic Analysis Results Concentrations x 10^{16} cm^{-3}				
				Iron	Tin	Silicon	Copper	Aluminum
1	Control[+]			4.1	4.0	3.1	ND	10.0
2	Nothing	8.2	1.4×10^{16} p-type	ND[++]	5.7	5.8	55.0	<.1
3	.43 mg Gallium	8.2	3×10^{14} p-type	ND	5.4	4.1	14.5	<.1
4	5.6 mg Gallium	9.0	3.9×10^{16} n-type	ND	3.8	3.0	7.0	9.3
5	12.8 mg Gallium	7.8	4.8×10^{16} n-type	ND	3.0	2.5	4.2	4.5
6	26 mg Arsenic	3.5	3.5×10^{14} p-type	ND		2.7	15.0	<.1
7	5.5 mg Arsenic	6.0	$<3 \times 10^{13}$ p-type	ND	4.3	2.5	9.5	7.0
8	.68 mg Arsenic	6.5	1.6×10^{16} p-type	10.3	6.5	5.2	70.0	<.1
9	9.7 mg[+++] Gallium	8.0	7×10^{15} n-type	ND		2.5	2.6	4.8

+ Control slice not heated
++ ND stands for "not detectable"
+++ Gallium was placed in actual contact with the sample

IV. SILICON DIOXIDE MASKING ON GALLIUM ARSENIDE

A. General

A study of the effect of reactively sputtered silicon dioxide films on the surface of gallium arsenide as a mask against impurity diffusion was initiated. Preliminary investigations were made on zinc and magnesium diffusion through 12,000 Å layers of silicon dioxide on partially coated n-type gallium arsenide slices. Figure 35 shows the result of zinc diffusion in the presence of the film. Zinc was diffused from a 1% zinc-gallium alloy in a sealed ampoule at 800° C for five hours and showed no penetration on the protected regions, but a two-micron penetration on the uncoated regions. Figure 36 shows the result for magnesium diffusion. The magnesium diffused from a 60% magnesium-gallium alloy in a sealed ampoule at 1000° C for one hour showed no penetration in the area of the silicon dioxide coating but penetrated 1.3 microns in the unprotected region. Diffusion was carried out for these impurities with thinner films ($\approx$ 2000 Å), through which visible diffusion was observed. Hence, it can be concluded that the masking effect is dependent on the silicon dioxide thickness for a given diffusion temperature and time. To fully evaluate this silicon dioxide mask, both n- and p-impurities for gallium arsenide should be thoroughly investigated by the radioactive tracer technique. Results should indicate the eventual feasibility of a gallium arsenide planar transistor structure.

From this initial masking study it was observed that impurities may be effectively diffused through this mask with no dissociation of the gallium arsenide during the course of the diffusion. With gallium arsenide and other compound semiconductors similar in volatility at diffusion temperatures, the surface of the crystal is lost in varying degrees whether the diffusion is accomplished by sealed ampoule, semiclosed, or open-tube technique. To depress this loss, a closed

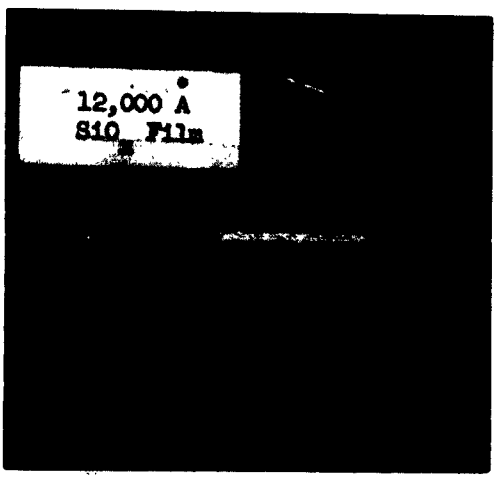

Fig. 35 Zinc diffusion with 1% Zn-Ga alloy in sealed ampoule at 800°C for 5 hours. Magnification 70X

Fig. 36 Mg diffusion with 60% Mg-Ga alloy in sealed ampoule at 1000°C for one hour. Magnification 140X

system and/or lower diffusion temperature is usually used. However, even by this method the surface loss was still undesirable for electronic devices. The advent of this oxide mask will permit two-zone open-tube diffusion and a more accurate evaluation of the semiclosed system. Preliminary investigations in both cases, in the presence of the silicon dioxide, showed surface loss of gallium arsenide to be nonexistent.

In a simultaneous diffusion, two slices of gallium arsenide were diffused 5 1/2 hours at 800° C with 1% Zn-Ga alloy in the semi-closed system. Both slices had been chemically polished, but only one was protected with a 2000 Å layer of silicon dioxide. After diffusion, the film was removed with hydrofluoric acid. The surface under the oxide layer of the protected slice showed no evidence of arsenic loss. The unprotected surface was covered with small droplets of gallium, definitely showing loss of arsenic. Junction depths measured on both slices were approximately 1.6 microns. However, diffusion depths of the two samples cannot be directly compared, since it is impossible to determine accurately the amount of surface loss from the unprotected slice.

We also made a two-zone, open-tube diffusion run which further verified effectiveness of the silicon dioxide as protection against surface loss. Figure 37 shows the results very dramatically. The slice was coated in stripes with a 12,000 Å layer. Diffusion was carried out with the slice at 800° C, zinc source at 360° C, and a helium carrier gas at the rate of 1 cu ft/hr. No visible diffusion was observed in either the protected or unprotected areas. However, the surface loss in the uncoated areas was 12.5 microns, with none observable in the coated area. These results open a whole new avenue of diffusion techniques for the more volatile compound semiconductors.

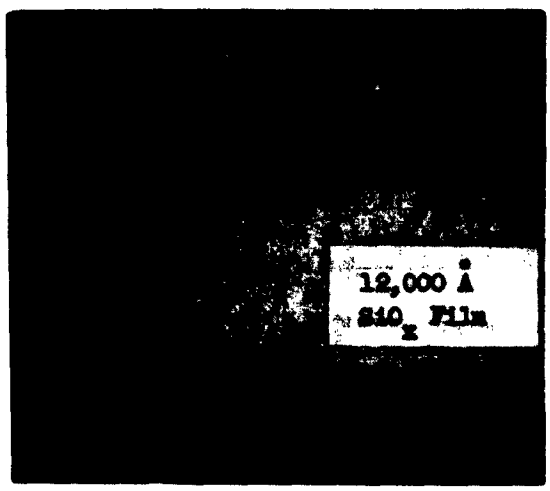

Fig. 37 Two-zone open tube diffusion at 800° C, Zn source at 360°C in He flow (1CHF) for 1 hour 12,000°A film blocked diffusion

B. Magnesium Diffusion Through SiO_2 Film into GaAs

Magnesium diffusion into gallium arsenide through a silicon dioxide film was analyzed. Initially, an experiment was performed to evaluate the distribution of magnesium in both the film and the gallium arsenide. The slices were coated with a 1000 Å layer of silicon dioxide on chemically polished surfaces, and then diffused at 1000° C for six hours from a 60% Mg - 40% Ga source. To find the behavior of this diffusion, the concentration in the film was determined by spectrographic analysis on the samples prepared by dissolving the film incrementally in 10% HF. In the gallium arsenide the concentration was obtained by the standard incremental lapping and sheet resistance technique. The results are shown in Fig. 38, where a $D = 6.76 \times 10^{-12}$ cm^2/sec was found in the gallium arsenide. As expected, this value of D is in fair agreement with those previously reported without SiO_2 films. This film should have no effect on the value of D in the gallium arsenide.

Consequently, a series of diffusion runs were made at temperatures from 800° C to 1150° C, and diffusion was analyzed on both protected and unprotected surfaces. The gallium arsenide slices were cut 500 x 400 mils from approximately 0.01 ohm-cm tin-doped <111> grown crystals. Mirror finish and good planarity were obtained on the slices by chemical polishing, and the possibility of impurity contamination during the lapping process was eliminated. Thus, final sample thickness was about 20 mils. These slices were then coated with 2000 Å thick silicon dioxide films on the $(\bar{1}\bar{1}\bar{1})$ face and diffused from a 60% Mg - 40% Ga source in an ampoule evacuated to approximately one micron. The oxide film was then removed with HF, and effects were studied by measuring the diffusion parameters on both surfaces. Sheet resistance was measured with the four-point probe, and the diffusion depth by the standard lap-stain technique. The surface concentration and diffusion coefficients were calculated assuming the complementary error function distribution previously shown valid for magnesium in gallium arsenide. Figure 39

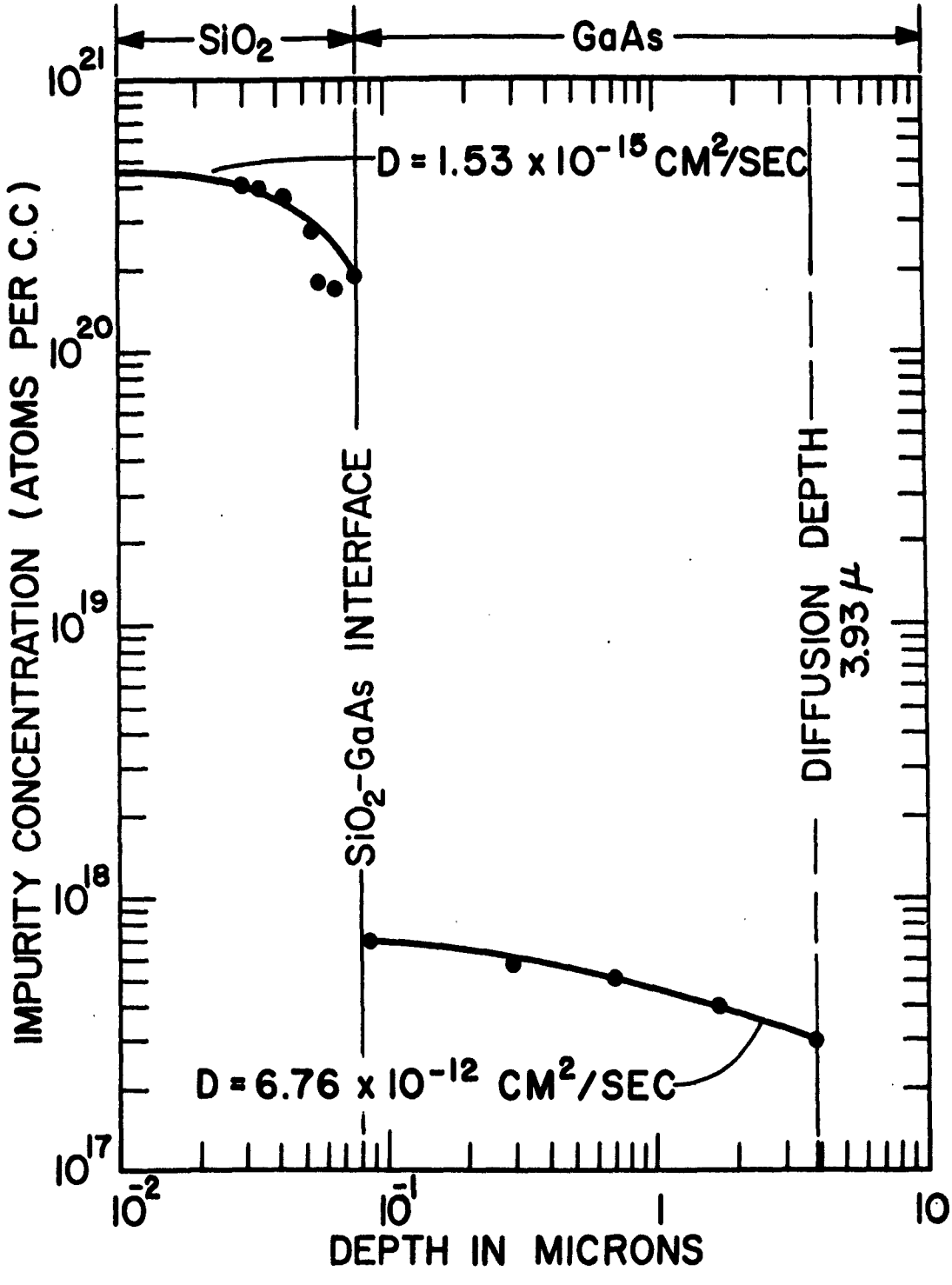

Fig. 38 Diffusion of magnesium in GaAs - N-type for 6 hours at 1000°C (source diluted with 40% gallium)

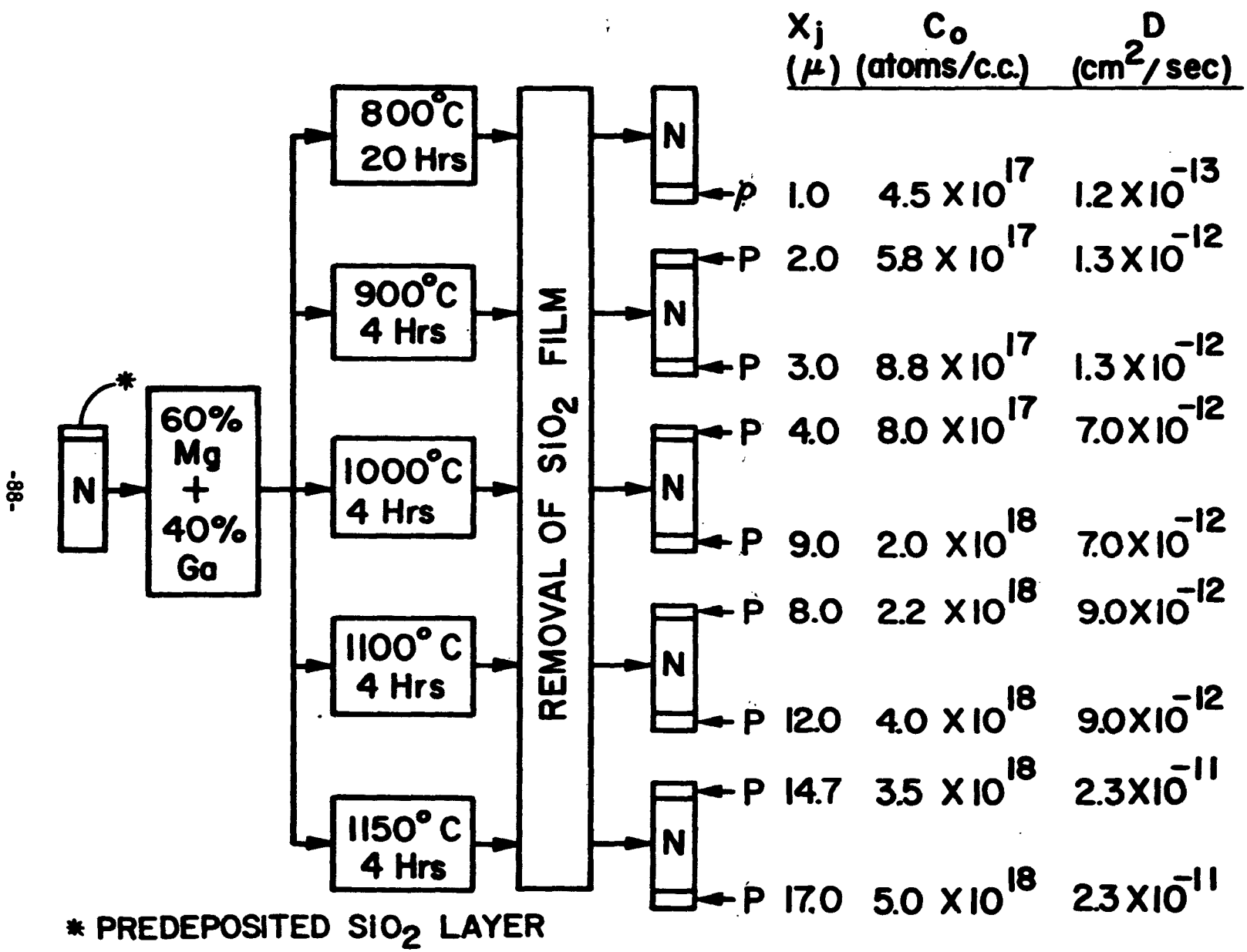

X_j (μ)	C_o (atoms/c.c.)	D (cm^2/sec)
1.0	4.5×10^{17}	1.2×10^{-13}
2.0	5.8×10^{17}	1.3×10^{-12}
3.0	8.8×10^{17}	1.3×10^{-12}
4.0	8.0×10^{17}	7.0×10^{-12}
9.0	2.0×10^{18}	7.0×10^{-12}
8.0	2.2×10^{18}	9.0×10^{-12}
12.0	4.0×10^{18}	9.0×10^{-12}
14.7	3.5×10^{18}	2.3×10^{-11}
17.0	5.0×10^{18}	2.3×10^{-11}

Fig. 39 Effect of SiO_2 film against Mg diffusion in gallium arsenide

shows the results of this investigation. As expected, the film had no effect on the values of D. However, the silicon dioxide definitely did have a masking effect; junction depths and surface concentration were reduced on the coated surfaces.

Appendix B of this report presents the analytical solution for magnesium diffusion in the SiO_2-GaAs system.

C. Zinc Diffusion Through SiO_2 Film into GaAs

Zinc diffusion through a SiO_2 film into gallium arsenide was studied. The slices of gallium arsenide were tin-doped crystals to a concentration of 1×10^{17} atoms/cc with chemically polished surfaces. Half the slices were then coated with a 6500 Å thick silicon dioxide layer and one coated slice and an uncoated slice placed in a sealed ampoule with a Zn-Ga source. In all cases the diffusion temperature of 1000° C and diffusion time of 18 hours were held constant. Only the percentage of Zn in the source was varied in the three runs made. The radioactive isotope of Zn^{65} was used, allowing tracer technique use for the diffusion profile analysis.

Figures 40-42 show the concentration profiles for a 1.0% Zn, 0.1% Zn, and 0.01% Zn source, respectively. In all cases the surface concentrations under the film are significantly lower than on the unprotected surfaces. The depth of penetration is also considerably less on the protected surfaces, indicating very definitely that the SiO_2 film serves as a mask against zinc diffusion. Note also that when the zinc surface concentration is less than 10^{18} atoms/cc, the distribution approximates a complementary error function. Figures 41 and 42 show diffusion coefficients calculated for these cases, and they agree very well.

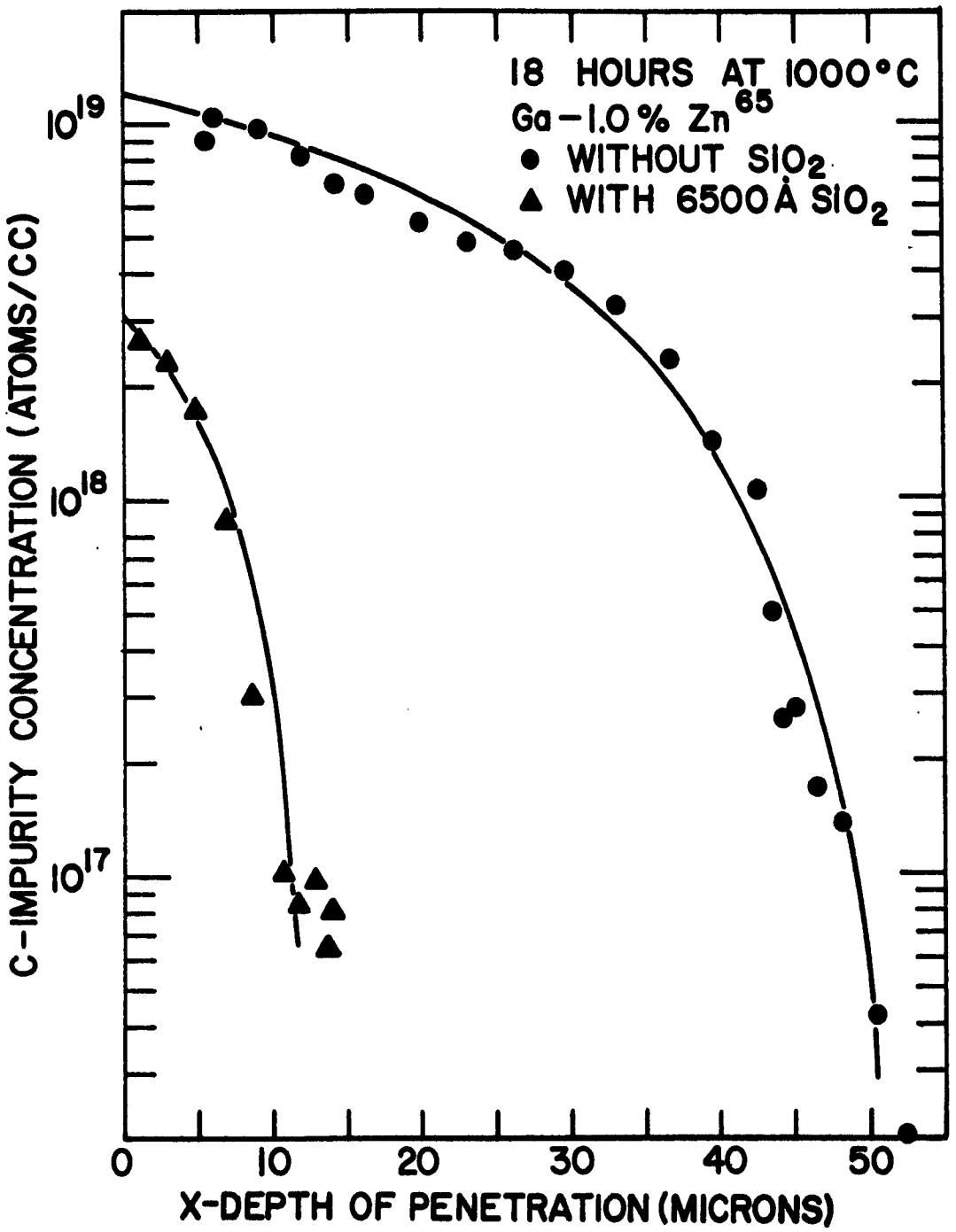

Fig. 40 Zinc diffusion in GaAs

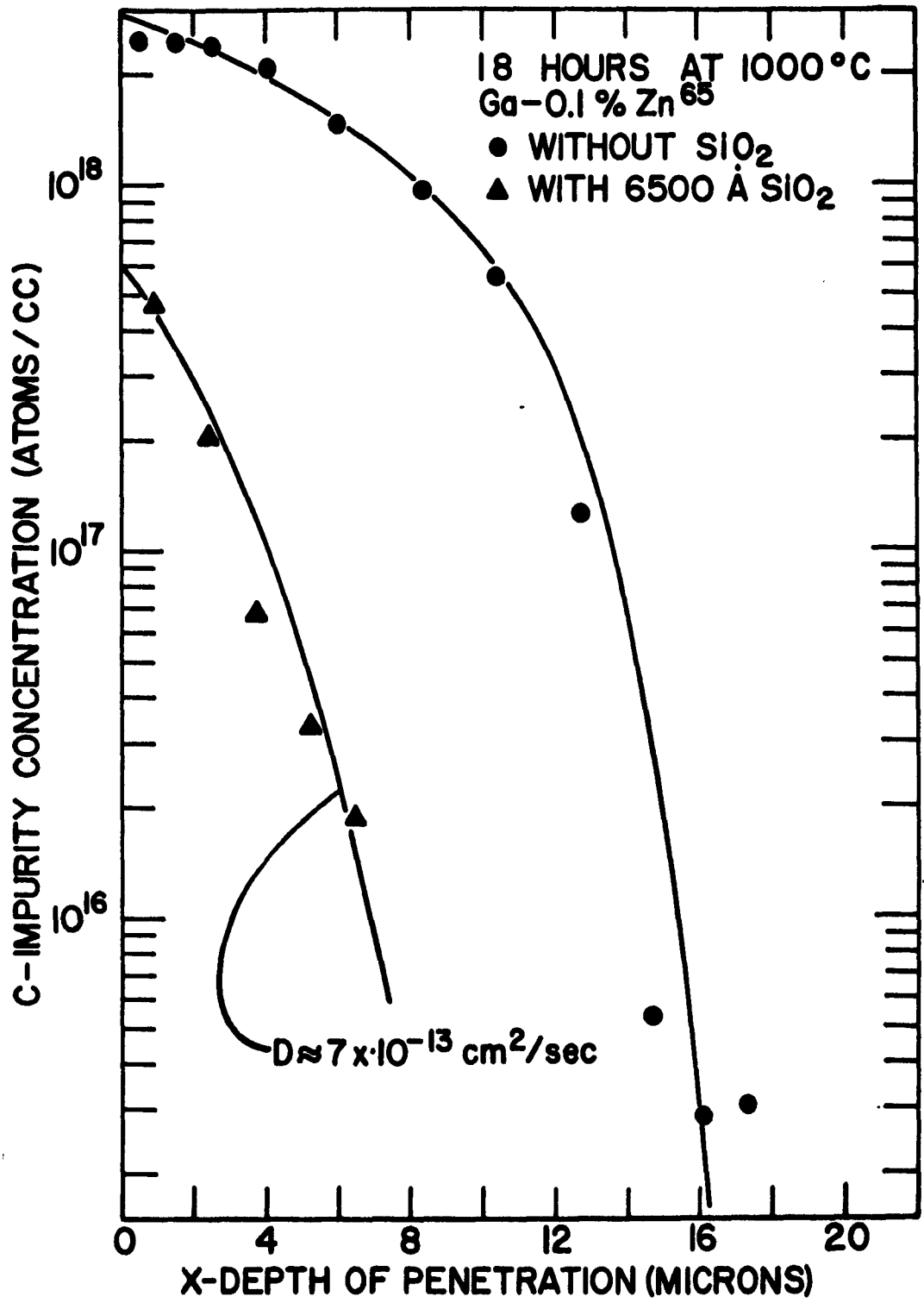

Fig. 41 Zinc diffusion in GaAs

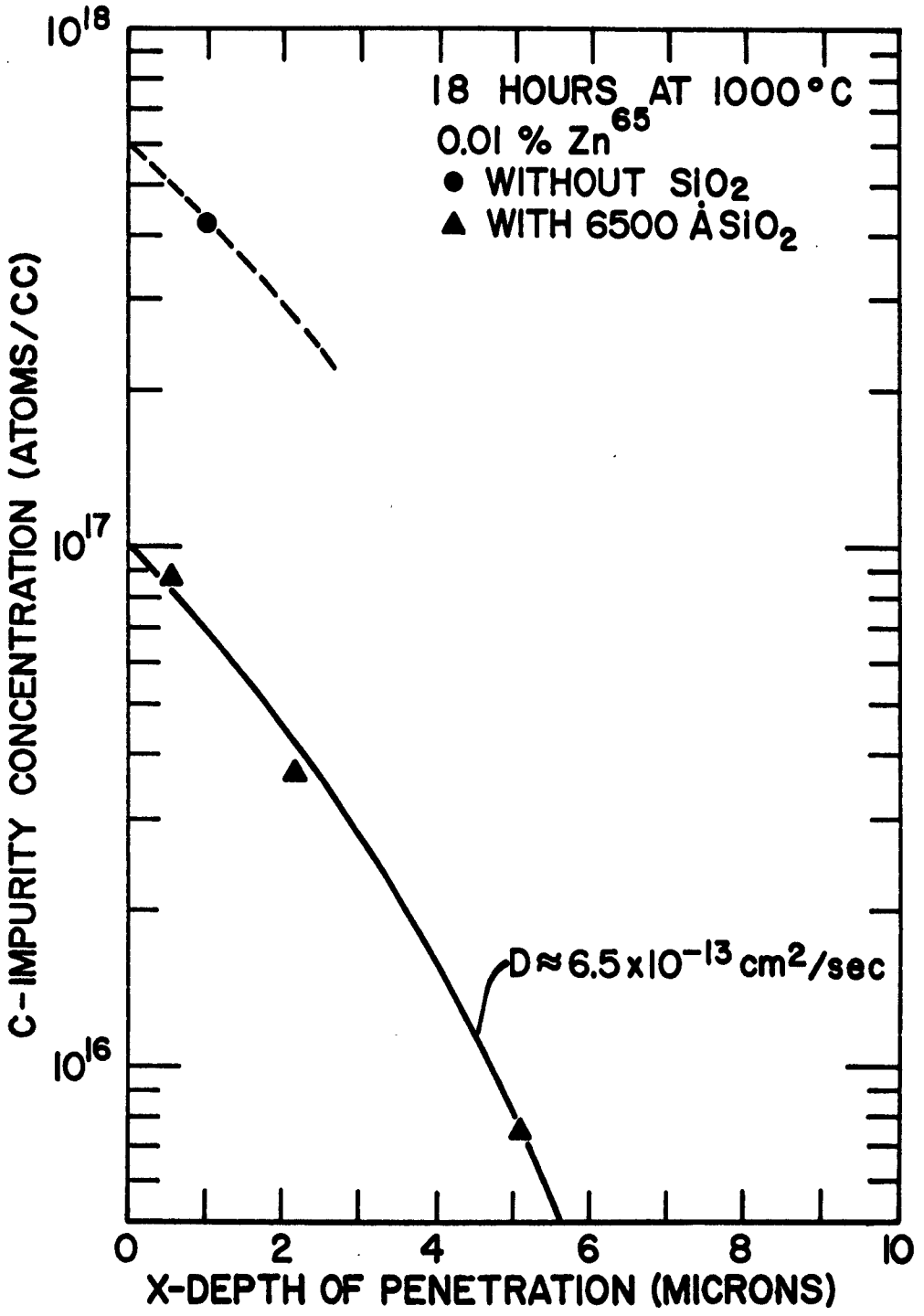

Fig. 42 Zinc diffusion in GaAs

The validity of the meager data exhibited on Fig. 42 is supported by electrical measurements. The uncoated slice was p-type on the surface after diffusion but the masked sample was still n-type. Thus, in regard to electrical conductivity this sample was effectively masked against zinc; but because the tracer technique was used, zinc diffusion at a level below the bulk donor level was detected.

Diffusion coefficients of 7×10^{-13} cm^2/sec and 6.5×10^{-13} cm^2/sec shown were calculated assuming the surface concentration under the film to be constant during the time of diffusion. Since little is known about the actual diffusion of zinc through the SiO_2 film itself, this may or may not be a valid assumption. Work will be carried out to determine whether the surface concentration of the zinc under the film is time dependent.

V. MISCELLANEOUS TECHNOLOGY STUDIES ON GaAs

Several miscellaneous technology studies made on gallium arsenide included: chemotaxially polishing of surfaces, delineation of junctions by etch or stain techniques, post-alloy diffusion studies, and surface "passivation" of gallium arsenide transistors.

A. Chemotaxial Polished Surfaces

Because of the adverse effects of surface damage to device characteristics, as introduced by mechanical polishing, another method for preparing gallium arsenide surfaces was sought. In particular, attention was focused on a chemical polishing process reported by the Bell Telephone Laboratories.

The process which finally evolved, consisted of placing the gallium arsenide slices between two teflon discs which are submerged in a solution of 80 parts H_2SO_4, 10 parts H_2O_2 and 10 parts H_2O in a rotating inclined teflon beaker. Figure 43 is a picture of the system as presently used.

This system has yielded excellent optically polished surfaces, free of surface damage and negligible lensing on the outside periphery of the slices. An important observation was that the above solution would only polish the (111) or arsenic face of the slice. If attempts were made to polish the gallium face, a very rough, pitted surface would result. This chemotaxial polishing technique is now being used exclusively to prepare slices for diffusion and device studies.

B. Delineation of Junctions

Many etches and stains were investigated for delineating the diffused and alloyed junctions. This is of considerable importance in evaluating diffusion depths, alloyed regrowth regions and the base widths in transistors.

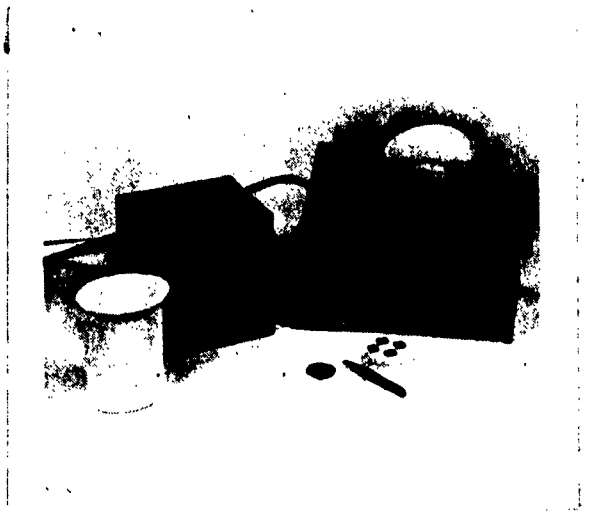

Fig. 43 Chemotaxial polishing system

A very satisfactory stain for decorating diffused p-n junctions in gallium arsenide was found. It consists of 2 parts HF, 2 parts acetic acid, 4 parts HNO_3, 1 part methanol, and 1 part H_2O. This mixture is more effective if allowed to age prior to use. Wafers containing diffused layers are lapped and polished with a 5° bevel and stained to reveal the junction. The nature of the stain is such that the n-region will stain black. This stain is now used in evaluating all diffusion depths.

An etch that has been used successfully in delineating junctions (both diffused and alloyed) consists of 5 parts HCl, 1 part HNO_3, and 2 parts of H_2O. This solution will etch the p-region preferentially. Both alloyed p-n junctions and alloyed emitters-diffused base n-p-n transistors have been cross-sectioned and delineated with this etch. Figure 44 shows a cross-section through the active region of a transistor that has been etched with the above solution. The light region at the bottom on the photograph is the n-type collector, while the darker band is the diffused p-type base region. The light stripe penetrating into the base is the n-type regrowth region which acts as the emitter. This particular transistor had an emitter diameter of 0.002 in. with a base width of approximately 3μ. This process is being used routinely in delineating junctions in diodes and transistors.

C. Post-Alloy Diffusion

Only a token effort was applied in the post-alloy diffusion technique in gallium arsenide. Investigation of this area was limited to one alloy, Au-Sn-Zn. A major problem was encountered with this alloy. The concentration of Zn in the alloy had to be maintained at a level of less than 0.01% to avoid compensation of the Sn in the n-regrowth region. This is because of the 2 orders of magnitude difference in the segregation coefficients of Zn and Sn. The net result is that the Zn level in the alloy has to be maintained at a low level comparable to other unknown and probably undesirable impurities present. Conse-

Cross section of the active region of a diffused base-alloyed emitter Gallium Arsenide transistor. Magnification 1000 X.

Fig. 44

quently, very erratic results are obtained with this alloy. However, several transistors which exhibit β's $\approx$ 1 were realized by this technique. This area of endeavor was replaced by more promising techniques.

D. Surface "Passivation" of GaAs Transistors

A small effort was made to improve and possibly "passivate" the state-of-the-art gallium arsenide transistors by chemical treatment. As is known, the current gain, β, of the transistors falls off rapidly at low current levels and is very surface sensitive. A chemical etch of 5 parts NaOH to 1 part H_2O_2 improves on the low current level β and increases the value by as much as an order of magnitude. Figure 45 demonstrates the effect of a 20 second etch on a gallium arsenide transistor. The low current level β is seen to improve dramatically after this etch, with β increasing from 100 to 480 at 5 volts and 5 ma. This improvement may be attributed to a lowering of the surface recombination velocity in the vicinity of the emitter. Device stability of the units was also improved by this treatment. It was observed that if more than a 20 second etch was applied no further improvement in β was realized, but that the saturation voltage, V_{CE}, was considerably degraded.

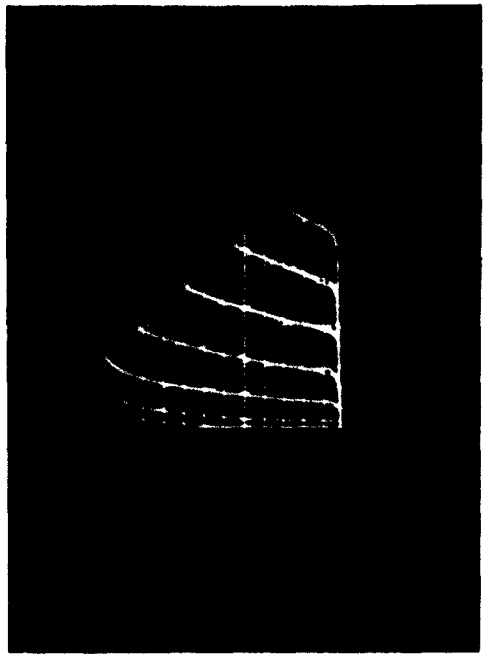

Before Etch

I_c = 1 ma/div

V_c = 1 Volt/div

I_b = .02 ma/step

β = 100 at 5V, 5 ma

I_c = 1 ma/div

V_c = 1 Volt/div

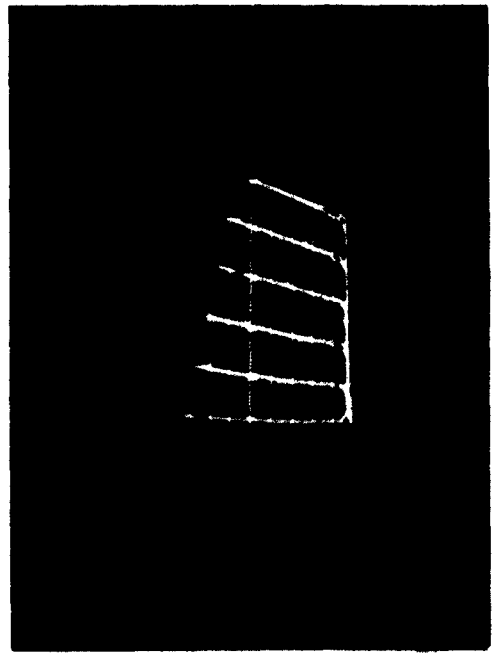

After 20 Sec. Etch

I_c = 1 ma/div

V_c = 1 Volt/div

I_b = .005 ma/step

β = 480 at 5V, 5 ma

I_c = 1 ma/div

V_c = 1 Volt/div

Fig. 45 Common Emitter Output Characteristics Before and After NaOH, H_2O_2 Etch

VI. TUNNEL DIODES

A. General

A considerable portion of the device effort on this program was devoted to the evaluation of the feasibility of GaAs as a tunnel diode material and development thereof. The theory of operation of tunnel diodes indicated that gallium arsenide should be superior to both germanium and silicon in all respects. Because of the high energy gap, 1.35 eV, the voltage swing over the negative resistance region should be greater than that obtained for either of the other materials. Since the band structure of gallium arsenide does not require the introduction of phonon interactions to conserve momentum during tunneling transitions, as do the structures of both silicon and germanium, the probability of such transistions may be expected to be higher for GaAs. In addition, the probability will also be enhanced by the lower value of the electron effective mass in GaAs. Therefore, the same junction dimensions and geometry in gallium arsenide should result in higher peak currents and, since the valley current does not depend on these factors, should yield higher peak-current to valley-current ratios. As is known, these assumptions were verified on n- on p-type gallium arsenide. However, as is also now known, a serious degradation problem of the peak current, I_p, is noted on these units at elevated temperatures and operation at current levels of greater than 2 I_p. To date this problem still has not been resolved as to the exact mechanism of failure or means of resolving it.

B. Fabrication Technology and Characteristics

However, since gallium arsenide did appear to be a favorable material, attempts were made to construct tunnel diodes from it. The experiments involved the formation of sharp, heavily doped, p-n junctions by alloying acceptor-containing impurity pellets to degenerate n-type base material and by alloying donor-containing impurity pellets to degenerate p-type base material.

Diodes were constructed from selenium or tellurium-doped n-type GaAs by alloying impurity elements such as zinc and cadmium diluted in metals such as gold, silver and tin. The best results were obtained using the selenium-doped ingot and alloying a 90% tin - 10% zinc pellet. Peak-to-valley ratios up to 4:1 were obtained. The fact that the tin-zinc alloy used for forming the heavily doped p-region yielded the best results is somewhat surprising since tin itself is an excellent donor impurity. It is probably that higher peak-to-valley ratios were not obtained with p- on n-junctions because the doping levels in either or both sides were not sufficiently degenerate.

The results obtained using zinc-doped p-type base material and alloying pellets of tin, or tin containing small amounts of other donors such as selenium or tellurium, were considerably more promising. The best characteristics realized were on p-type gallium arsenide which was doped to a level of about 5×10^{19} zinc atoms/cc. A degenerate n-type regrowth region, forming a sharp junction, was formed by alloying tin. Generally pellets of 0.002 in. nominal diameter were alloyed at a temperature of 550-600° C. Rapid cooling was used to limit diffusion and prevent broadening of the transition region. Diodes made by this process yielded peak-to-valley current ratios as high as 70:1. Figure 46 shows a photograph of the V-I characteristics of one such diode. As is seen, the voltage swings in the negative resistance region were generally about 0.4 volts.

One problem with this process was the wide variations obtained in peak current value. This was and still is a inherent problem in the fabrication of tunnel diodes. To bring these peak current values to a given level, an electrolytic etching technique utilizing a 5% sodium hydroxide solution and 10 ma etching current was employed. During etching the peak current value was monitored and when the desired value was obtained, etching was stopped. Table VI shows typical values for the peak current after fabrication of diodes and after etching to a nominal value of 10 ma. Generally, peak current

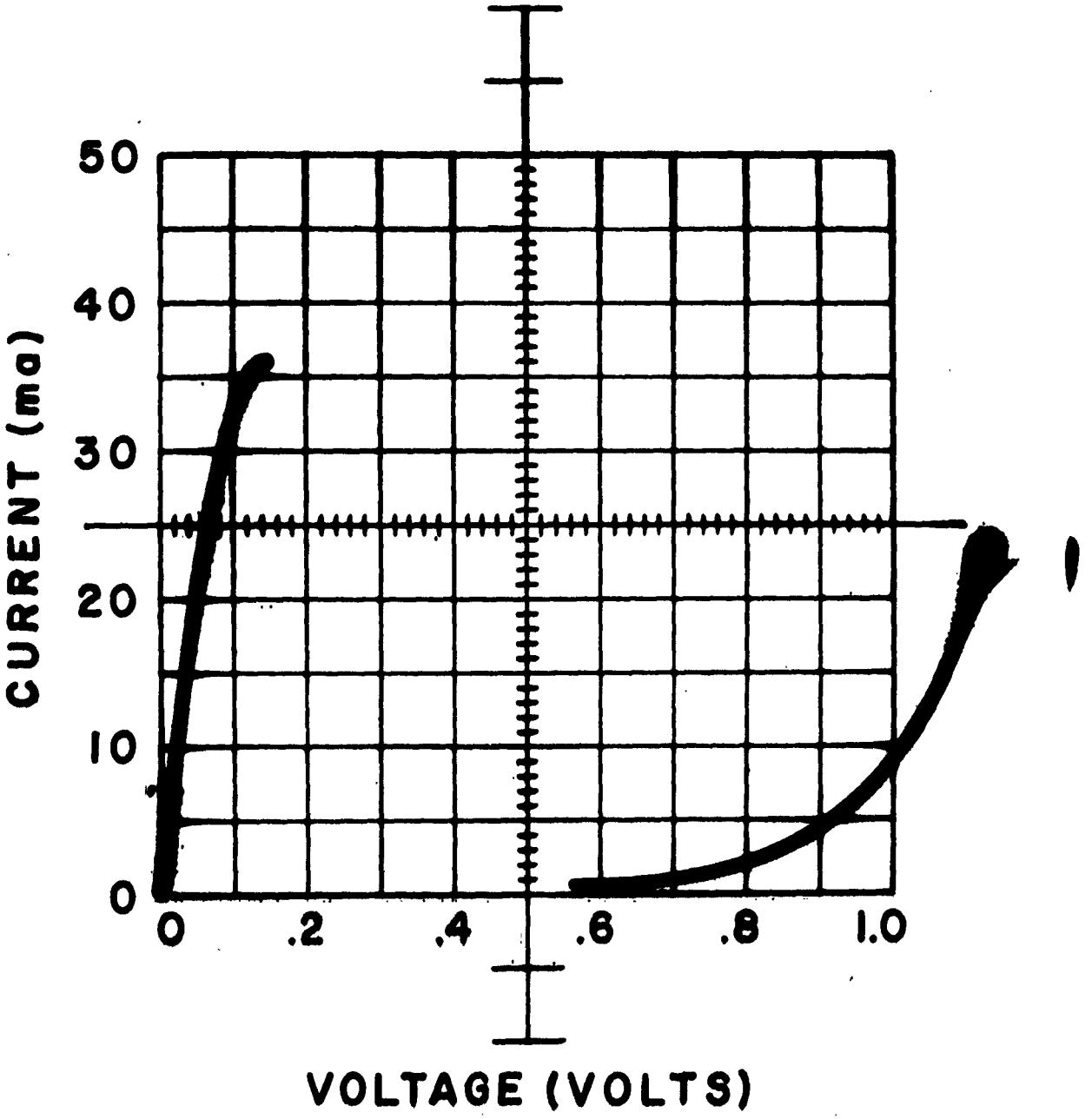

Fig. 46 V-I characteristics of a gallium arsenide tunnel diode

Table VI

Results of Controlled Electrolytic Etching
of Gallium Arsenide Tunnel Diodes

Unit No.	I_p (before etching)	After Etching in 5% NaOH
1	66	9.7
2	290	10.0
3	39	12.0
4	50	9.5
5	50	11.2
6	54	9.6
7	46	9.3
8	20	8.0
9	81	12.0
10	25	10.6
11	50	9.0
12	50	9.2
13	25	10.2
14	29	10.0
15	24	10.0

densities of about 500 amperes/cm^2 were obtained, although values of an order of magnitude and more higher had been realized. Capacitance, measured at the valley point, as low as 2-4 picofarads for a peak current of 10 ma were obtained. Switching times of less than 1 nanosecond were also realized.

C. Anomalous Characteristics

At the time of these studies several anomalies were observed. On some diodes a hump or inflection was observed on the V-I curves in the diffusion current region. Figure 47 shows a photograph of this effect. Experiments were performed in an attempt to find the source of this effect. An ingot of degenerate zinc-doped gallium arsenide was purposely saturated with oxygen when prepared. This element was known to cause a deep lying level in gallium arsenide. Tunnel diodes were constructed by the normal process. On a few of the units a hump was again observed on the V-I curve. However, here it occurred near the center of the valley. Figure 48 shows a photograph of such a curve. It was believed that these humps correspond to a second tunneling process into a deep impurity or defect level in the material. Different impurities which give levels in different positions in the forbidden gap would cause the hump to occur at different values of bias voltage, as was observed. A degenerate zinc-doped sample was doped with copper during the compounding operation to determine whether it would also lead to a hump in the characteristic curve. Although no such effect was observed, diodes constructed from the material had peak current densities from two to three orders of magnitude lower than normally obtained. This result was unexpected and its causes were not understood.

Another interesting observation concurrent with the above phenomena was the decrease in peak/valley current ratio with increasing zinc concentration. In general, the degenerate p-type gallium arsenide used for the diodes had a zinc concentration of about 5×10^{19}/cc. If this concentration was increased, the peak current on fabricated

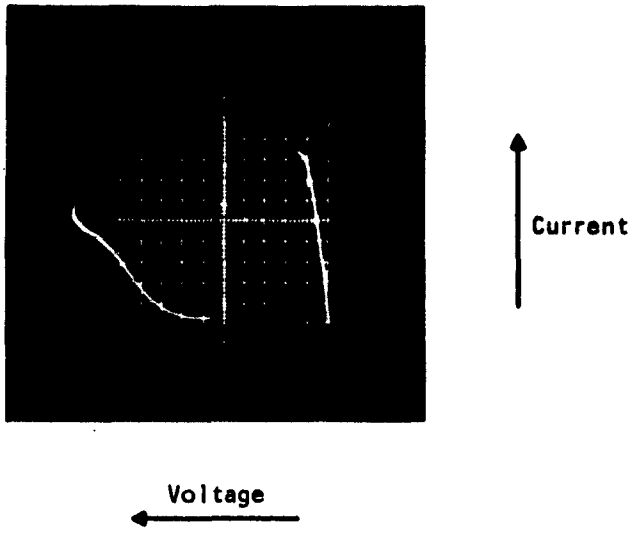

Fig. 47 V-I Characteristics of a Gallium Arsenide Tunnel Diode Showing Anomalous Hump in the Curve

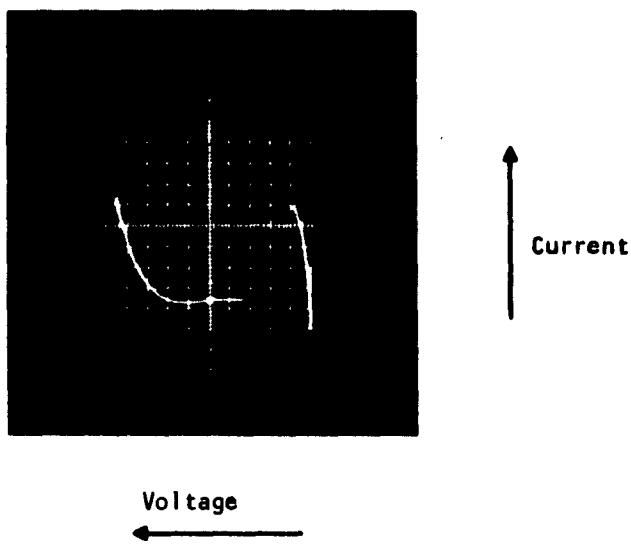

Fig. 48 V-I Characteristics of a Gallium Arsenide Tunnel Diode made from Oxygen Containing Material Showing Anomalous Hump in the Valley Region

diodes increased because of the increased tunneling probability. However, the valley current also increased at a rate sufficient to cause a decrease in the peak/valley current ratio. This increase in valley current was believed to result from an effect similar to that caused by neutron irradiation, where the same behavior was reported. Zinc, in these very heavy concentrations, could strain the crystal lattice sufficiently to cause the introduction of defect bands in the forbidden energy gap. Additional current would then result from tunneling into these defect bands, the carriers subsequently undergoing a transition to the valence band. In addition, some interstitial zinc levels could be introduced. This explanation for the aforementioned phenomena was never verified or discredited.

D. Temperature Behavior of Characteristics

An interesting study that we made was to evaluate the gallium arsenide tunnel diode over a wide temperature range. Although the physical properties of gallium arsenide should allow device operation to temperatures in excess of 350° C, the presence of the previously mentioned tin placed an upper limit of about 200° C. Hence, considerable effort was spent in search of a more satisfactory donor alloy. Successful results were obtained from the 62% Au - 38% Sn (by weight) alloy, mentioned under alloy studies of this report. However, great care had to be taken when raising these devices to temperatures in excess of 300° C. Figure 49 shows the V-I characteristics for a GaAs tunnel diode for temperatures from -196° C to 345° C. At room temperature the unit has a peak/valley current ratio of 17:1 and increases to 32:1 at -196° C. At 345° C the ratio decreased to about 4:1. A better understanding of this can be obtained by looking at Fig. 50 where the peak and valley currents are plotted against temperature. The valley current is seen to increase monoatomically with an increase in temperature, and in the range of 77° K to 300° K increases by 55%, whereas in the same temperature range the peak current changes by only 10%. Consequently, the peak-to-valley ratio increases considerably in lowering

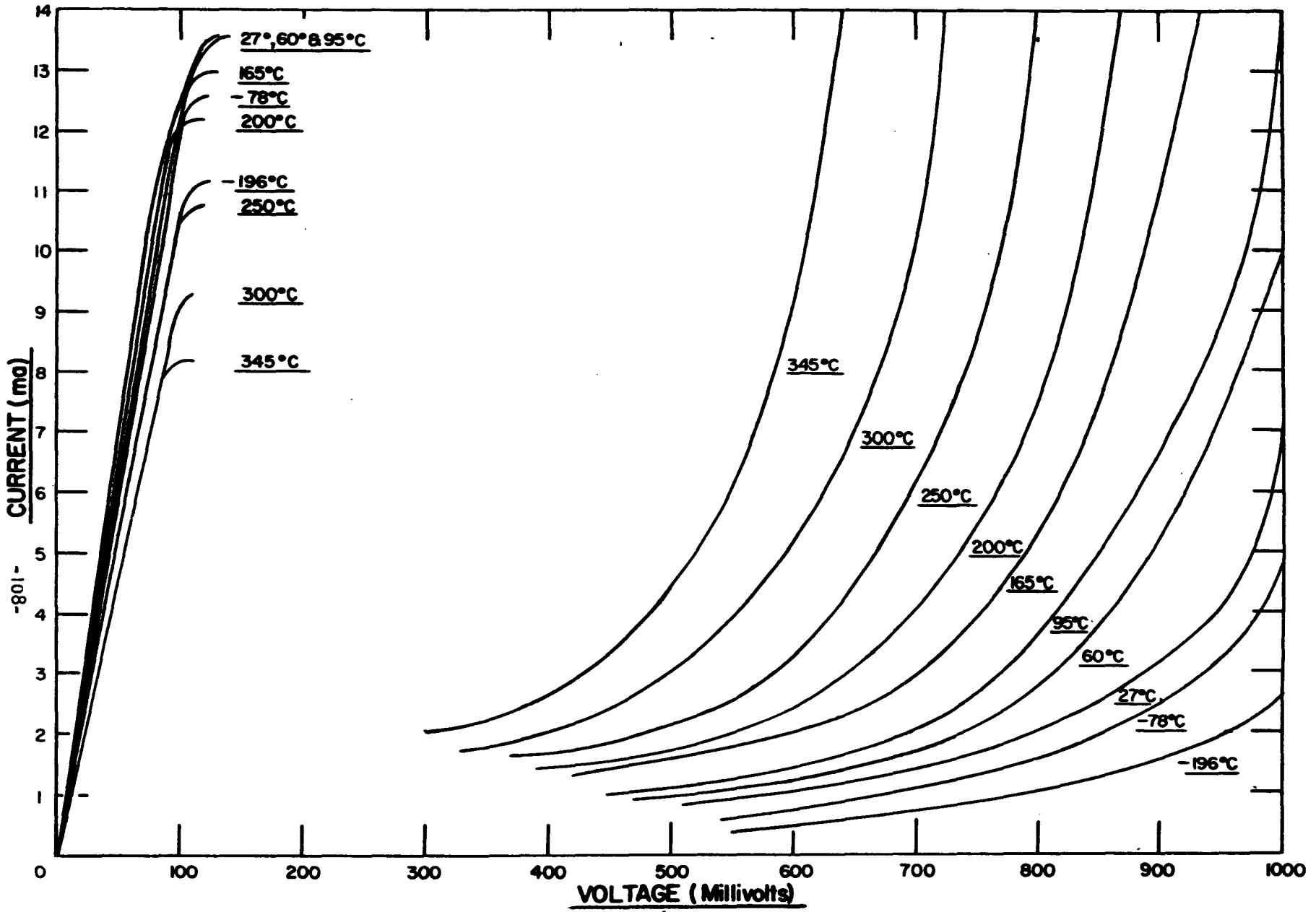

Fig. 49 Temperature behavior of the V-I characteristics of a gallium arsenide tunnel diode

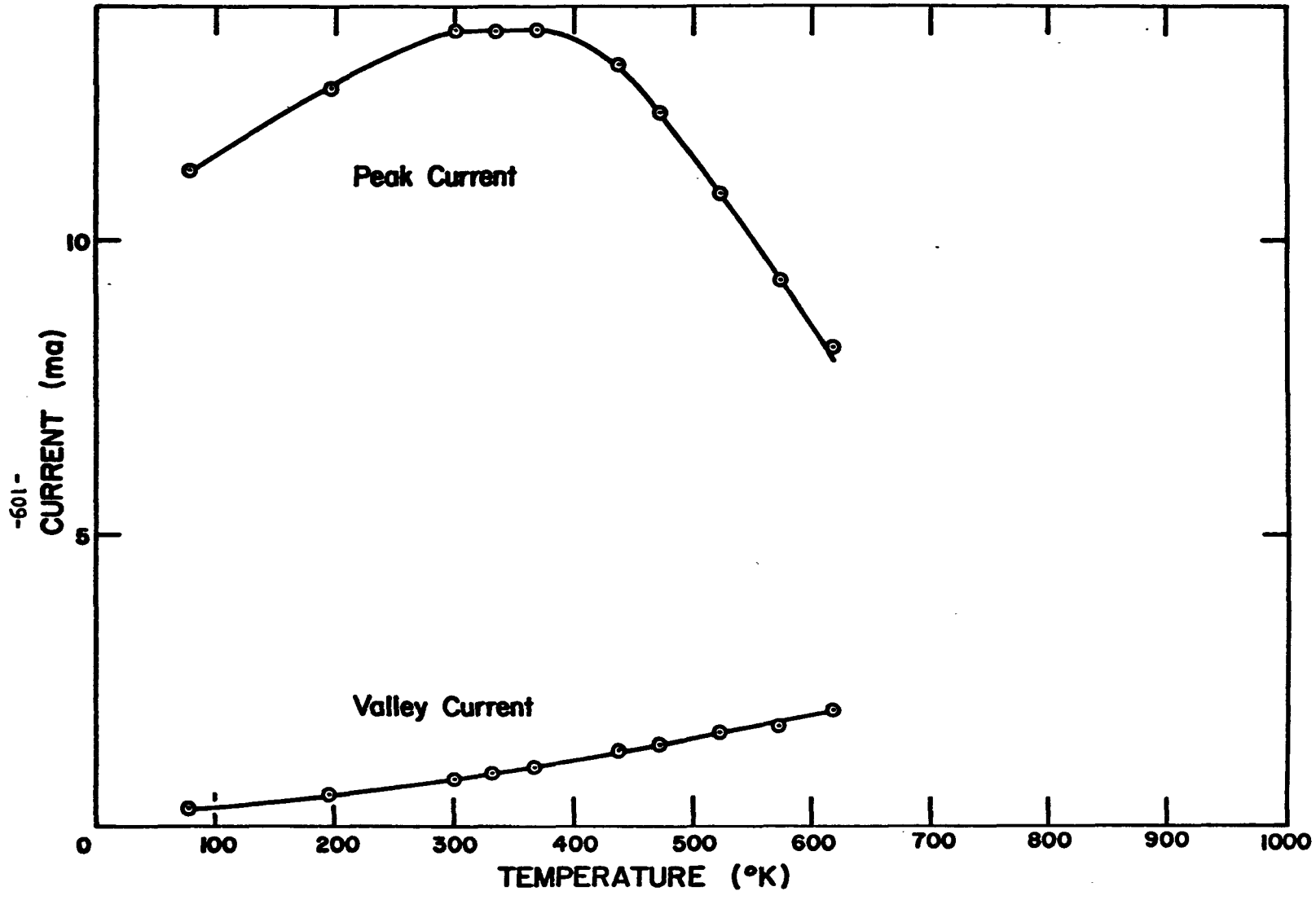

Fig. 50 GaAs tunnel diode - peak and valley current temperature dependence

temperatures. The decrease in peak current at lower temperatures is expected, since the energy gap increases and hence tunneling decreases. The peak current decreases at higher temperatures, which is expected, because of the Fermi function smearing out at elevated temperatures. The degradation problem was not noted in this unit, probably because this unit was not kept at elevated temperatures for any prolonged period.

VII. TRANSISTORS

A. General

The ultimate goal of this program was to prove feasibility of and develop a gallium arsenide transistor. In particular, feasibility samples of a high temperature, low power transistor and a high temperature, medium power transistor were to be fabricated.

This interest in gallium arsenide transistors was generated by some of the superior basic electrical properties of gallium arsenide compared with germanium or silicon. Some important transistor parameters are limited by these basic electrical properties of the specific semiconductor used for a device. The maximum operating temperature depends primarily on the concentration of thermally excited carriers, a function of the forbidden energy gap. Germanium and silicon transistors, with energy gaps of 0.7 and 1.1 eV, respectively, are operable to temperatures of 85°C and 150°C, respectively. For gallium arsenide the energy gap is 1.35 eV or a maximum device operating temperature of approximately 400°C. The power handling capability of a transistor depends on the temperature at which the collector-base junctions can operate and is also influenced by the energy gap. Again, based on electrical properties, gallium arsenide transistors should be superior. The ability of a transistor to amplify at high frequencies depends on material properties in a more complex manner; however, one important factor is the time required for minority carriers injected from the emitter to diffuse across the base region. This carrier diffusion is related to the mobility of carriers in the semiconductor. Germanium, with electron (μ_n) and hole (μ_p) mobilities of 3900 and 1900 cm^2/Volt-sec has yielded transistors operable to frequencies in excess of 1 kMc. Silicon, with μ_n = 1500 cm^2/Volt-sec and μ_p = 500 cm^2/Volt-sec, is limited to a few hundred Mc. Again gallium arsenide with $\mu_n \approx$ 10,000 cm^2/Volt-sec and $\mu_p \approx$ 450 cm^2/Volt-sec, should be superior to either germanium or silicon.

B. Fabrication Techniques

A primary difficulty in constructing transistors from compound semiconductors such as gallium arsenide results from the need of extremely thin base regions because of the very low carrier lifetimes. Diffusion techniques were chosen to form the base region because of their proven usefulness for forming such thin regions. Alloy techniques were chosen to form the emitter region. Also, an n-p-n structure was selected to take advantage of the higher electron mobility.

Figure 51 shows a sketch of the gallium arsenide transistor structure that yielded feasibility units. The starting material was Se, Te, S, or Sn doped n-type single crystals to a level of $0.5 - 1 \times 10^{17}$ atoms/cm^3 grown by the Teal-Little technique. Wafers from these crystals were then diffused in an evacuated ampoule with Mn, Mg or Zn. All slices were either mechanically or chemically polished on the As surface prior to diffusion. This yielded junction depths of approximately 0.3 mils and a surface concentration of $1 - 5 \times 10^{18}$ atoms/cm^3. The p-type layer on the unpolished surface was completely removed by lapping. A small mesa was formed on the p-type surface by masking, using the Kodak photo-resist technique, and then etching in CP-4. These mesas were either of 4 x 4 or 3 x 5 mil geometry. The n-type emitter region was then formed by alloying a 2 mil Sn pellet to within 2-3 microns of the collector-base junction. Simultaneously, a 99.8% gold - 0.2% selenium foil on a platinum tab was alloyed to the n-type surface of the wafer to form the collector contact. This operation was carried out at about 550°C in a small resistance heated furnace. A 2 mil diameter wire containing 99% gold - 1% zinc was then alloyed to the p-layer to form the ohmic base contact. The units were then given a brief CP-4 etch to clean the surfaces.

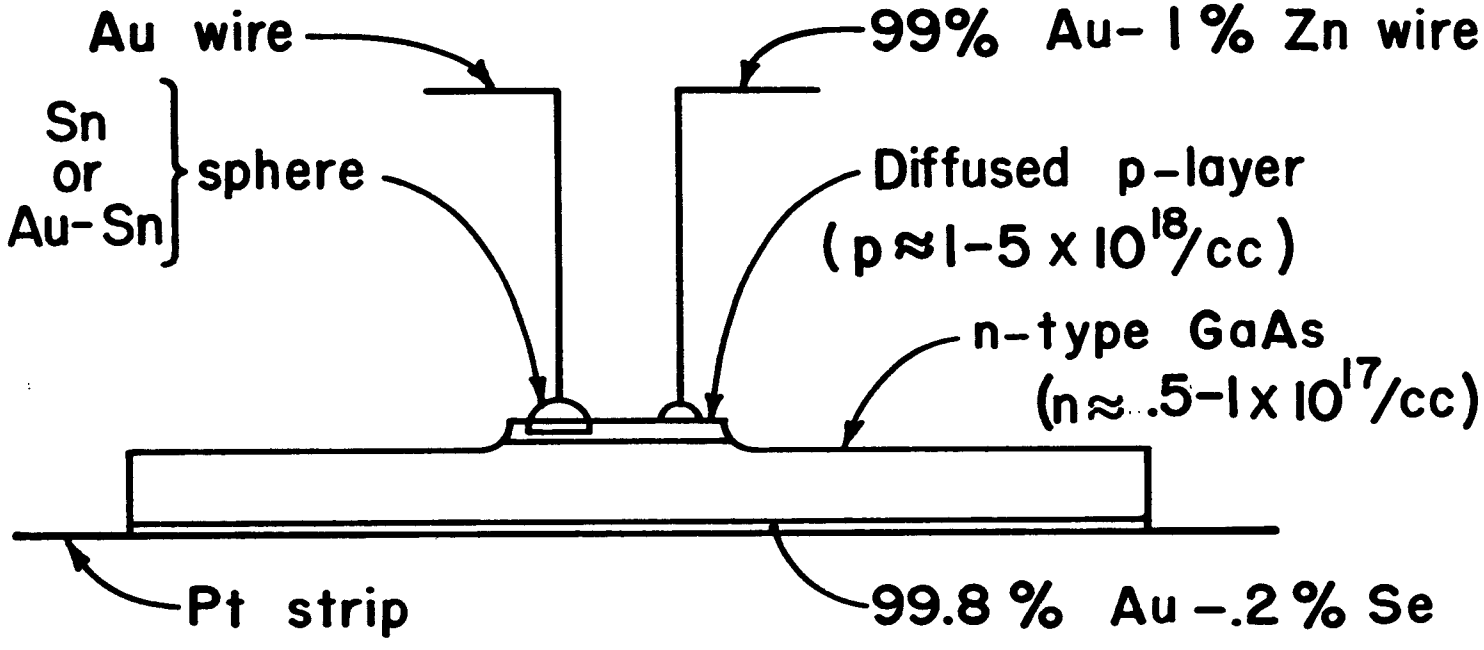

Fig. 5| Structural view of gallium arsenide npn mesa transistor

C. Transistor Characterization

Using the above process, many transistors were fabricated and their electrical parameters measured. Figure 52 shows the common base output characteristics of a gallium arsenide transistor. The collector current is 1 ma/div and the emitter current is 1 ma/step. The current gain, α, is 0.985 at a collector current of 5 ma and collector voltage of 5 Volts. The common emitter characteristics of the same transistor are shown in Fig. 53. Again, the collector current is 1 ma/div, and the base current is 20 μa/step. This yields a current gain, β, of 60 at 5 ma collector current and 5 Volts collector Voltage. Gains as high as 3000 have been observed when units were given the surface "passivation" etch described earlier in this report.

Table VII shows values for the common base "h" parameters, at a collector base voltage, V_{CB} = 5 Volts and emitter current, I_E = 1 ma, for several state-of-the-art gallium arsenide transistors with a small signal of 1000 cycles. The current gain, h_{fb}, shown in the first column is as high as 0.99. Input impedances, h_{ib}, of 50 ohms and output admittances, h_{ob}, of 0.5 micromhos were generally obtained. The last two columns show values of matched power gain calculated from the measured "h" parameters. Common emitter gains as high as 43.6 db were obtained.

Table VIII shows complete measurements on a typical gallium arsenide transistor. The leakage current, I_{CBO}, was 2×10^{-8} amperes. This value of I_{CBO} is somewhat higher than generally realized for a 15 mil^2 collector area, where currents of 10^{-9} to 10^{-10} amperes were more commonly observed. The collector-base breakdown voltage, BV_{CBO}, was 15 volts and collector-emitter breakdown voltages, BV_{CEO}, 15 volts. Collector and emitter transistion capacitances were 3.2 pf and 1.8 pf, respectively. The saturation voltage, V_{CE}, is seen to be 0.6 volts at I_C = 10 ma, I_B = 1 ma. Generally the better state-of-the-art units

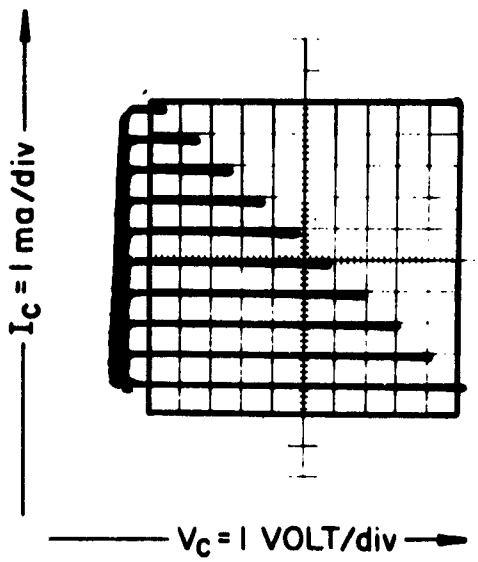

Fig. 52 Common base output characteristics of a GaAs transistor I_E = ma/step

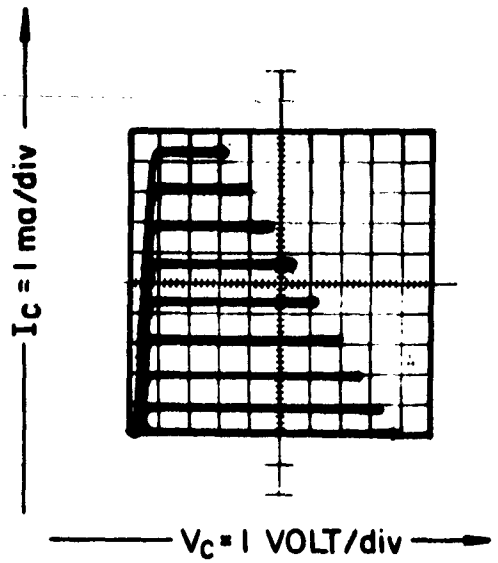

Fig. 53 Common emitter output characteristics of a GaAs transistor I_B = 0.02 ma/step

TABLE VII

h parameters and power gain of several gallium arsenide transistors at $V_{CB} = 5v$ & $I_E = -1ma$

unit	$-h_{fb}$	h_{ob} (μmhos)	h_{ib} (ohms)	$h_{rb} \times 10^6$	G* (db) common base	G* (db) common emitter
1	0.99	0.57	46	1700	26.5	41.7
2	0.99	0.285	50	720	30.1	43.6
3	0.99	0.85	44	3400	23.7	38.3
4	0.97	0.40	53	660	30.0	42.3
5	0.93	0.28	130	340	31.4	38.5

$$*G = \frac{h_{21}^2}{h_{11} h_{22}} X \frac{1}{\left(1 + \sqrt{1 - \frac{h_{12} h_{21}}{h_{11} h_{22}}}\right)^2}$$

TABLE VIII

Parameter measurements on a gallium arsenide transistor.

parameter	test conditions	value
I_{CBO}	V_{CB} = 10 Volts, I_E = 0	2×10^{-8} Amp
I_{EBO}	V_{EB} = 5 Volts, I_C = 0	0.25 ma
BV_{CBO}	I_C = 10 ma I_E = 0	15 Volts
BV_{CEO}	I_C = 10 ma I_B = 0	15 Volts
BV_{EBO}	I_E = 10 ma I_C = 0	11 Volts
C_{TC}	V_{CB} = 5 Volts, I_E = 0, f = 1mc	3.2 pf
C_{Te}	V_{EB} = 1 Volts, I_C = 0, f = 1mc	1.8 pf
V_{BE}	I_C = 10 ma I_B = 1ma	1.6 Volts
V_{CE}(Sat)	I_C = 10 ma I_B = 1ma	0.6 Volts
h_{FE}	V_{CE} = 5 Volts, I_E = 5 ma	10

exhibited V_{CE} = 0.5 to 1.0 Volt at the above mentioned conditions. This particular unit showed an h_{FE} value of 10 at I_C = 5 ma and V_{CE} = 5 Volts.

D. "h" Parameters vs Frequency Characterization

To adjust transistor fabrication it is necessary to know which parameters are limiting transistor performance. This type information can be obtained readily from electrical measurements of the transistor impedance, voltage transfer ratio, and current transfer ratio which are related to the physical parameters of the device. For example, from a plot of h_{ie} vs frequency an accurate value of base resistance, r_b' is obtained.

Figures 54 and 55 show plots of the real and imaginary parts of h_{ie} vs frequency for two state-of-the-art gallium arsenide transistors. The result of such plots should yield a simicircular graph, as seen in the figures. In these plots the lower real resistance, the point at which the imaginary component becomes zero, is a good measure of $r_b' + r_e$. Since r_e is the emitter series resistance and is usually less than a few ohms, the measured value closely approximates r_b'. Consequently, values of r_b' shown in the graphs are approximately 20 and 30 ohms, respectively. These were not unusual units; many other units that were measured exhibited values in the range of 20 to 60 ohms. These measurements were made on a Transfer Function Bridge for the high frequency end and on an RX meter in the low frequency range.

These values differ by almost an order of magnitude from the numbers obtained from $r_b' C_c$ measurements, in which $r_b' \approx$ 100 to 1000 ohms. The measurements obtained from h_{ie} vs frequency are believed to be more realistic. Assuming that the component of r_b' under the emitter is low, then certainly the surface resistance between the emitter and base should be low because of the high surface concentrations, C_o, of 1 to 5 x 10^{18}/cc. The discrepancy between the two r_b' values is not understood and hence has not been resolved yet.

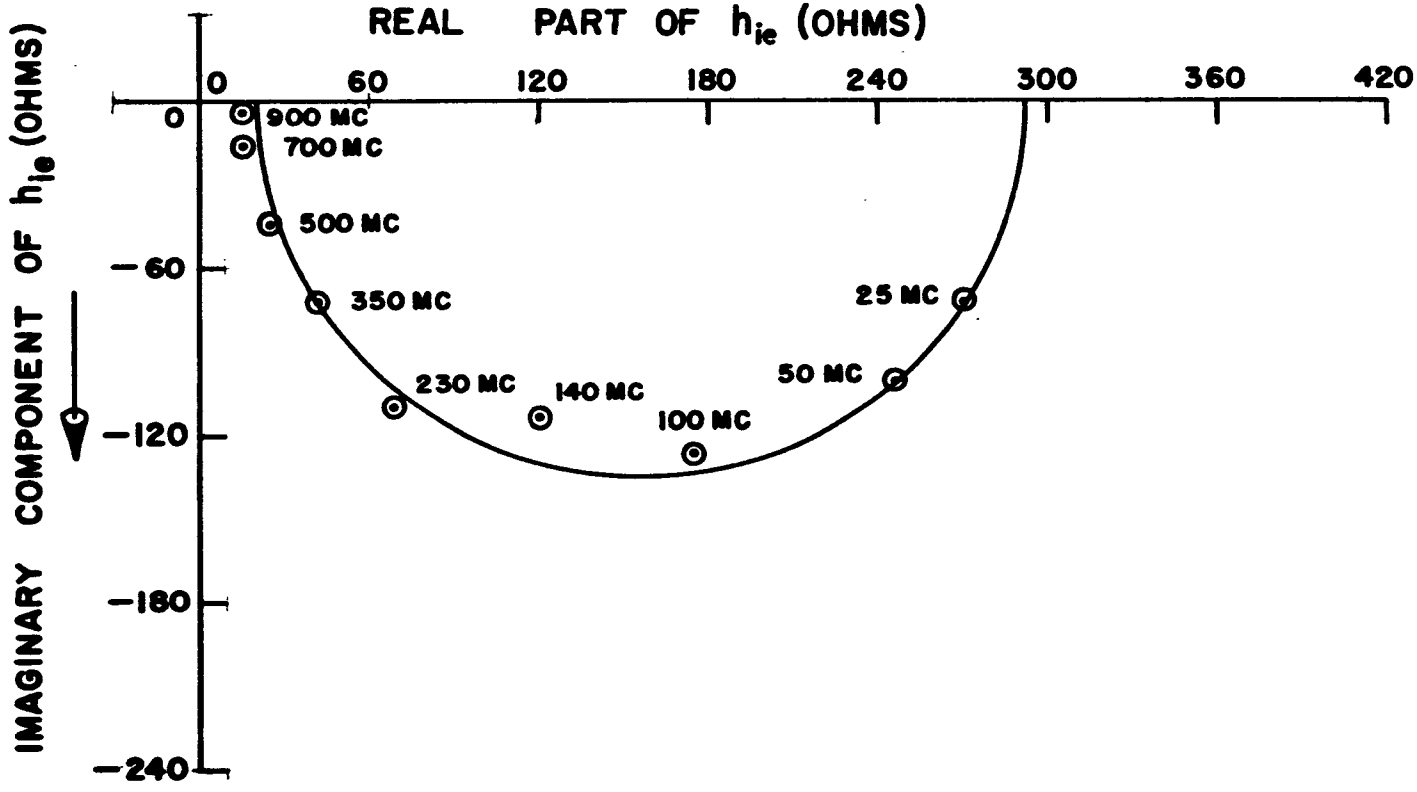

Fig. 54 Frequency dependence of grounded emitter input impedance for an experimental gallium arsenide transistor $V_{ce} = 3V$, I_c 5 ma.

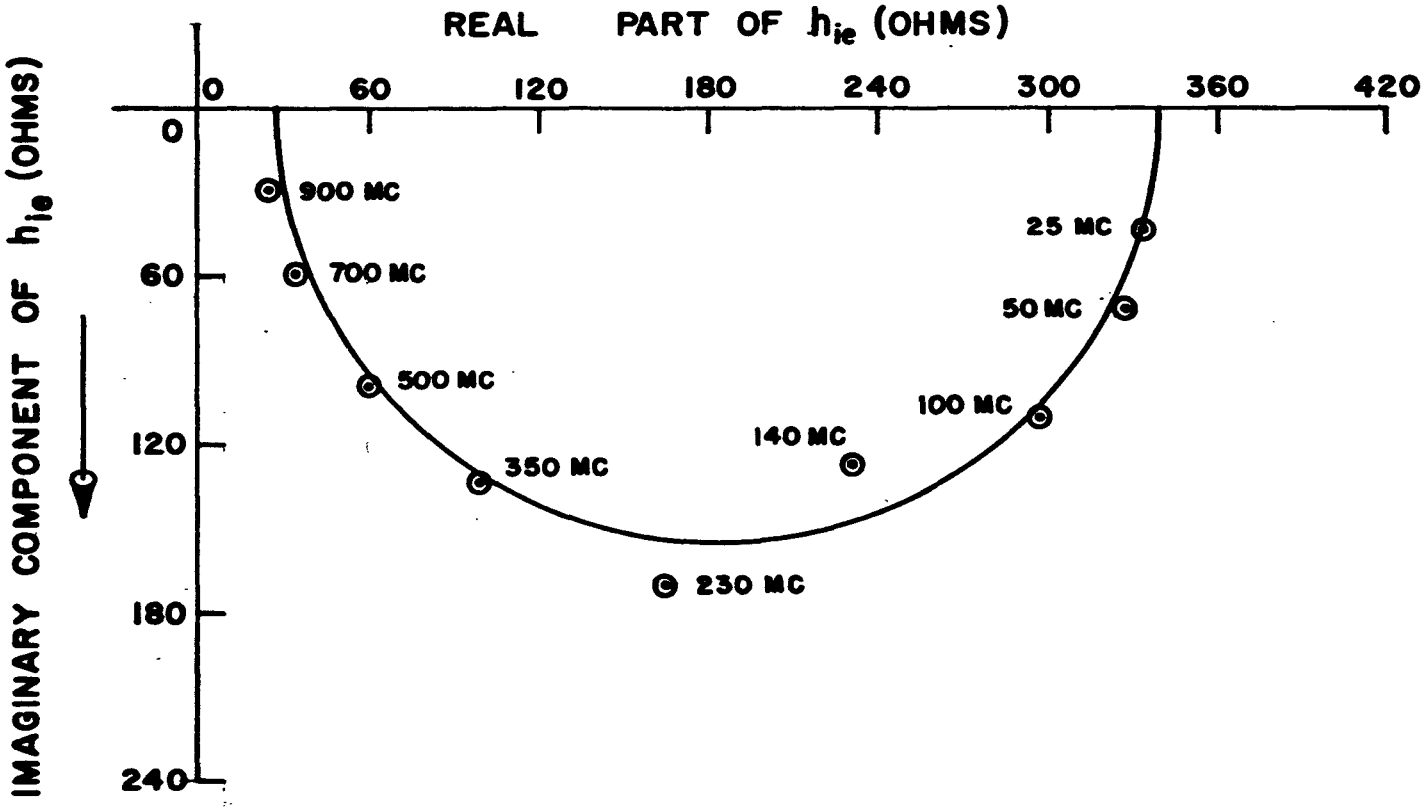

Fig.55 Frequency dependence of grounded emitter input impedance for an experimental gallium arsenide transistor $V_{ce} = 3V$, I_c 5ma .

Figure 56 shows a plot of common emitter current gain, h_{fe}, vs frequency for a state-of-the-art gallium arsenide transistor. If such a curve falls off at the rate of 6 db per octave over a given frequency range, it yields a value for the gain-bandwidth-product, f_t. f_t is the frequency at which the value of h_{fe} = 0 db, or $\beta = 1$. As seen from Fig. 56, the low frequency value, 20 db, corresponds to a β of 10. Beyond 100 Mc the gain does fall off with the expected 6 db/octave slope, thus resulting in an f_t value of approximately 730 Mc. In turn it can be safely stated that the α-cutoff frequency for this transistor is $f\alpha \geq 1$ kMc. f_α is the frequency at which the common base current gain is 0.707 of its low frequency value when $\alpha \approx 1$. A number of units have been measured that exhibited f_t values ranging from 600 to 800 Mc as shown in Table IX. These are the highest values of f_t known to have been observed on gallium arsenide transistors to this date.

The f_α of a graded base transistor is related to the carrier diffusion constant and the transistor base width by the approximate expression

$$f_\alpha = 2 \times \frac{0.39\ D_n}{W^2} \quad , \tag{32}$$

where the factor of 2 is an enhancement factor due to the graded base. Substituting values obtained on experimental transistors, f_α = 1000 Mc and W = 3μ, which were obtained by delineation techniques, gives D_n = 115 cm^2/sec. This yields an average electron mobility in the p-type base region of

$$\mu_n = \frac{q}{kT} D_n = 4600\ cm^2/\text{Volt-sec}, \tag{33}$$

which is approximately the value obtained from Hall measurements on some crystals used in fabricating the higher frequency units. These observed electrical and physical parameters, along with common base current gain, α, allow an estimate of the electron lifetime in the base region. If we assume that the current gain is limited by base transport, it is given by

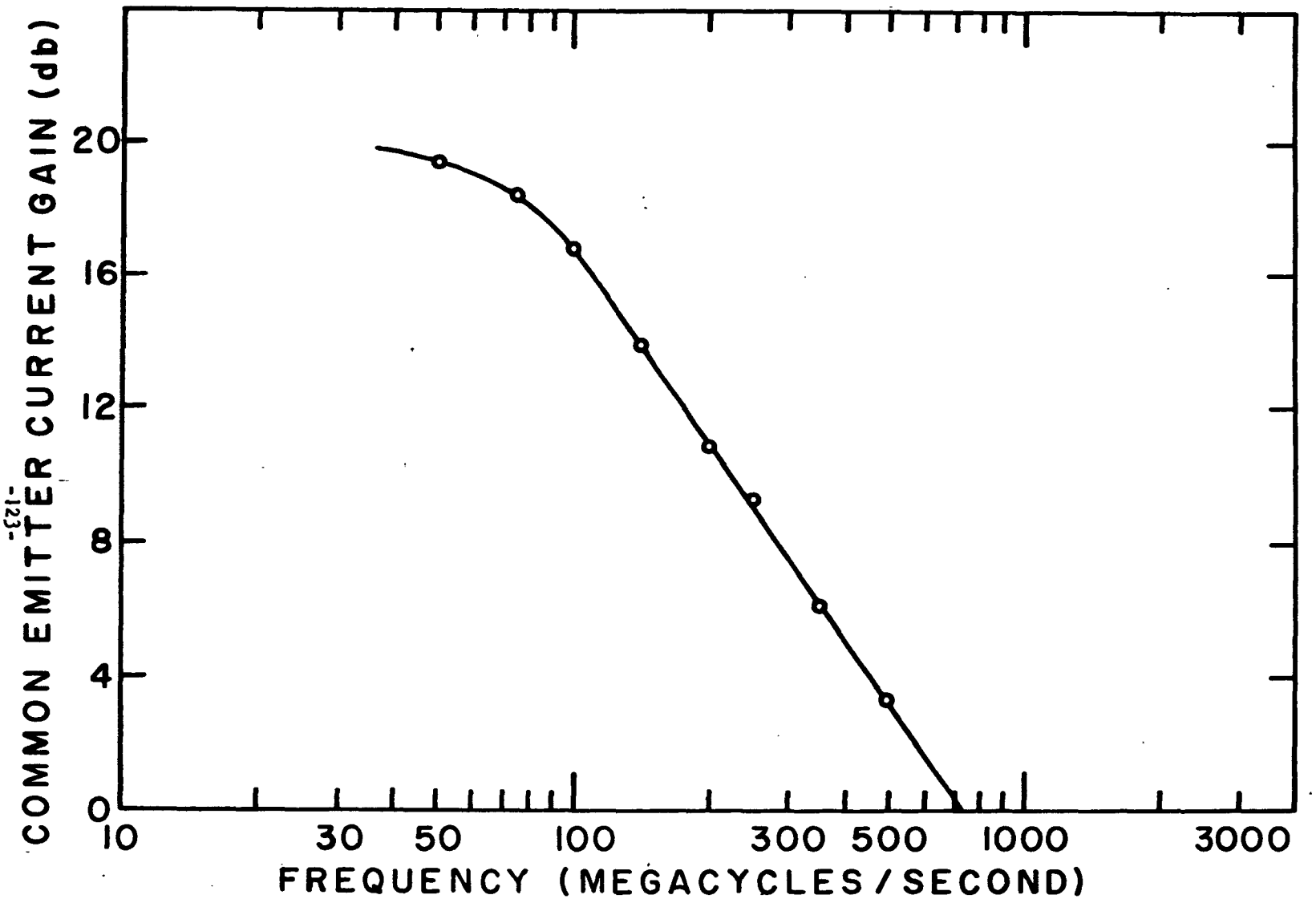

Fig.56 Frequency dependence of common emitter current gain for an experimental gallium arsenide transistor. $V_{CB} = 3v$, $I_E = 5ma$.

TABLE IX

GAIN BANDWIDTH PRODUCT FOR SOME GALLIUM ARSENIDE TRANSISTORS

UNIT NO.	f_T
Ga As 97	730 Mc
Ga As 98	800
Ga As 102	700
Ga As 104	755
Ga As 105	620
Ga As 106	620

$$\alpha = 1 - \frac{W^2}{L^2} , \tag{34}$$

where L is the diffusion length of electrons in the base region. For $\alpha = 0.9$ and $W = 3\mu$, $L = 6.7 \times 10^{-4}$ cm is obtained. The diffusion length may be expressed as

$$L = \sqrt{D\tau} . \tag{35}$$

Substituting the calculated values for L and D_n yields a lifetime $\tau \approx 5 \times 10^{-9}$ sec. This value of τ is about an order of magnitude lower than what has been calculated by the same technique on some earlier units with an $f_\alpha \approx 300$ mc. Nevertheless, it is consistent with what is generally believed to be the range of carrier lifetime in III-V compound materials. However, this difference in values of τ may not be truly realistic in that emitter efficiencies of the two units could be vastly different. It has not been determined what the emitter efficiencies are in gallium arsenide transistors and the assumption that $\gamma \approx 1$ may be erronous, where

$$\alpha = \alpha^* \beta \gamma , \tag{36}$$

$$\alpha^* = \left(1 + \frac{p_c \mu_p}{2n_c \mu_n}\right) \text{ in the collector efficiency,}$$

$$\beta = \left(1 - \frac{W^2}{L_{nb}^2}\right) \text{ the base transport factor,}$$

and

$$\gamma = \left(1 + \frac{\rho_e W}{\rho_b L_{pe}}\right)^{-1} \text{ the emitter injection efficiency.}$$

If γ does not really approach unity very closely, as assumed, then the original assumption that

$$\alpha = \beta$$

is in error and the value of τ calculated is meaningless. Questions have been raised regarding emitter injection efficiency on alloyed junctions in gallium arsenide transistors. This could explain the discrepancy in the values of τ calculated from two different transistors.

It would be very desirable to be able to determine τ in gallium arsenide by some other technique. To date carrier lifetime has not been measured meaningfully by any of the commonly known techniques. Photoconductive and photomagnetoelectric methods have been attempted, but neither can measure the apparent short lifetime of gallium arsenide ($\leq 10^{-8}$ sec). The PME approach, however, appears more promising. Earlier difficulties with this method were caused by the inhomogeneity of gallium arsenide and the extremely high surface recombination velocity thought to be present. Recently, both problems are believed to have been reduced and the PME method will be tried again. As pointed out, transistor current gain on some gallium arsenide units would seem to indicate $\tau \approx 10^{-8}$ sec; however, carrier lifetime is probably much less in the majority of the crystals, since good β units are generally not realized. Oxygen content of the material is known to introduce traps in the center of the forbidden energy gaps of gallium arsenide and could be a lifetime killer. This impurity could vary greatly from crystal to crystal. Attempts are now being made to resolve this lifetime problem and/or emitter injection efficiency in gallium arsenide.

The previously calculated value of carrier mobility, $\mu_n = 4600$ cm^2/volt-sec, in the diffused p-layer is of interest, since it points up the potential frequency capabilities of gallium arsenide as a transistor material. This value is a factor of three greater than calculated for the earlier unit that exhibited an $f_\alpha = 300$ Mc. This is not surprising in that the later unit also is a factor of three better in f_α for approximately the same base width value, W, of 3 microns. Consequently, if it were possible to attain the theoretical limit of μ_n at 10,000 cm^2/volt-sec in the p-layers and W at 0.25 - 0.50 microns, as in the presently highest frequency germanium units, gallium arsenide transistors would far surpass any presently available transistors in frequency. The problem remains in technology, which on gallium arsenide has not progressed far enough to allow the fullest exploitation of GaAs capability.

E. Switching Time Characterization

Because of the extremely low minority carrier lifetime, τ, exhibited by gallium arsenide, generally two orders of magnitude lower than in germanium or silicon ($\lesssim 10^{-8}$ sec compared to $\approx 10^{-6}$ sec), considerable interest existed in the switching capabilities of the state-of-the-art transistors. Primarily, considerable reduction in the storage time, t_s, which is dependent on τ in the collector region, should have been realized in the gallium arsenide transistor vs non-epitaxial germanium or silicon transistors. This reduction was realized, as will be shown in the data to follow; however, the advantage was short-lived with the advent of epitaxial germanium and silicon transistors.

Table X compares the switching characteristics of some state-of-the-art units with those of five 2N706 silicon mesa transistors, which were designed specifically for high speed switching applications at that time. These values were measured in the saturated mode using the circuit shown in Fig. 57. The gallium arsenide units were significantly faster than the 2N706's. Most gain was in the storage time, where the gallium arsenide units had values between 1 and 10 nanoseconds compared with 28 to 34 nanoseconds for the silicon transistors. The delay time, t_d, and fall time, t_f, for gallium arsenide were also somewhat shorter; while the rise time, t_r, was comparable to the other two materials. When the switching conditions in the circuit were optimized, a further reduction in total switching time, t_{total}, was realized in Table XI.

As the geometry of the state-of-the-art gallium arsenide transistors was reduced, a further reduction in t_{total} was realized. Several of these units were measured in the saturated mode on a new switching time set assembled under Contract NOrd 18902 and shown in Fig. 58. This circuit was built on a silver-plated chassis, with highest quality components and the best high frequency wiring techniques; pure silver tab leads were used throughout. This circuit was used with the sampling oscilloscope and a fast rise time pulse generator, shown in the block diagram of Fig. 59. With considerable effort to achieve proper resistive terminations and to eliminate strong capacitances, the circuit response

TABLE X

SWITCHING CHARACTERISTICS OF SOME EXPERIMENTAL GALLIUM ARSENIDE AND SILICON (2N706) TRANSISTORS

UNIT No.	t_d	t_r	t_{on}	t_s	t_f	t_{off}	t_{total}
GaAs 90	5	13	18	6	24	30	48
GaAs 91	5	12	17	10	22	32	49
GaAs 104	3	12	15	1	13	14	29
GaAs 105	3	13	16	1	19	20	36
GaAs 106	3	13	16	1	13	14	30
Si 5	8	13	21	28	22	50	71
Si 6	7	13	20	34	26	60	80
Si 10	8	12	20	34	26	60	80
Si 12	7	13	20	30	28	58	78
Si 13	7	13	20	32	24	56	76

TIMES IN NANOSECONDS

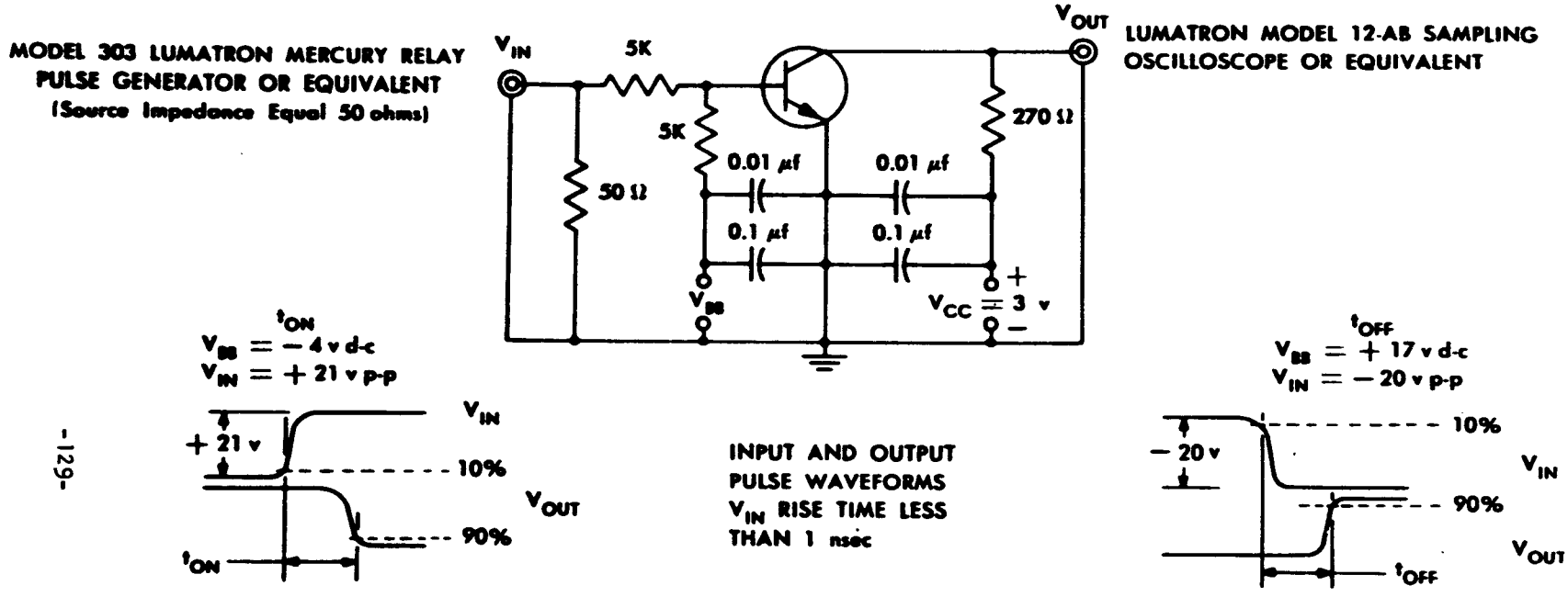

Fig. 57 Test circuit for switching transistors in the saturated mode.

TABLE XI

SWITCHING CHARACTERISTICS OF SOME EXPERIMENTAL GALLIUM ARSENIDE TRANSISTORS UNDER OPTIMIZED CONDITIONS

UNIT NO.	t_d	t_r	t_{on}	t_s	t_f	t_{off}	t_{total}
GaAs 92	4	10	14	3	9	12	26
GaAs 97	5	6	11	<1	7	<8	<19
GaAs 104	6	4	10	<1	9	<10	<20
GaAs 105	5	8	13	<1	19	<20	<33
GaAs 106	6	7	13	<1	10	<11	<24

TIMES IN NANOSECONDS

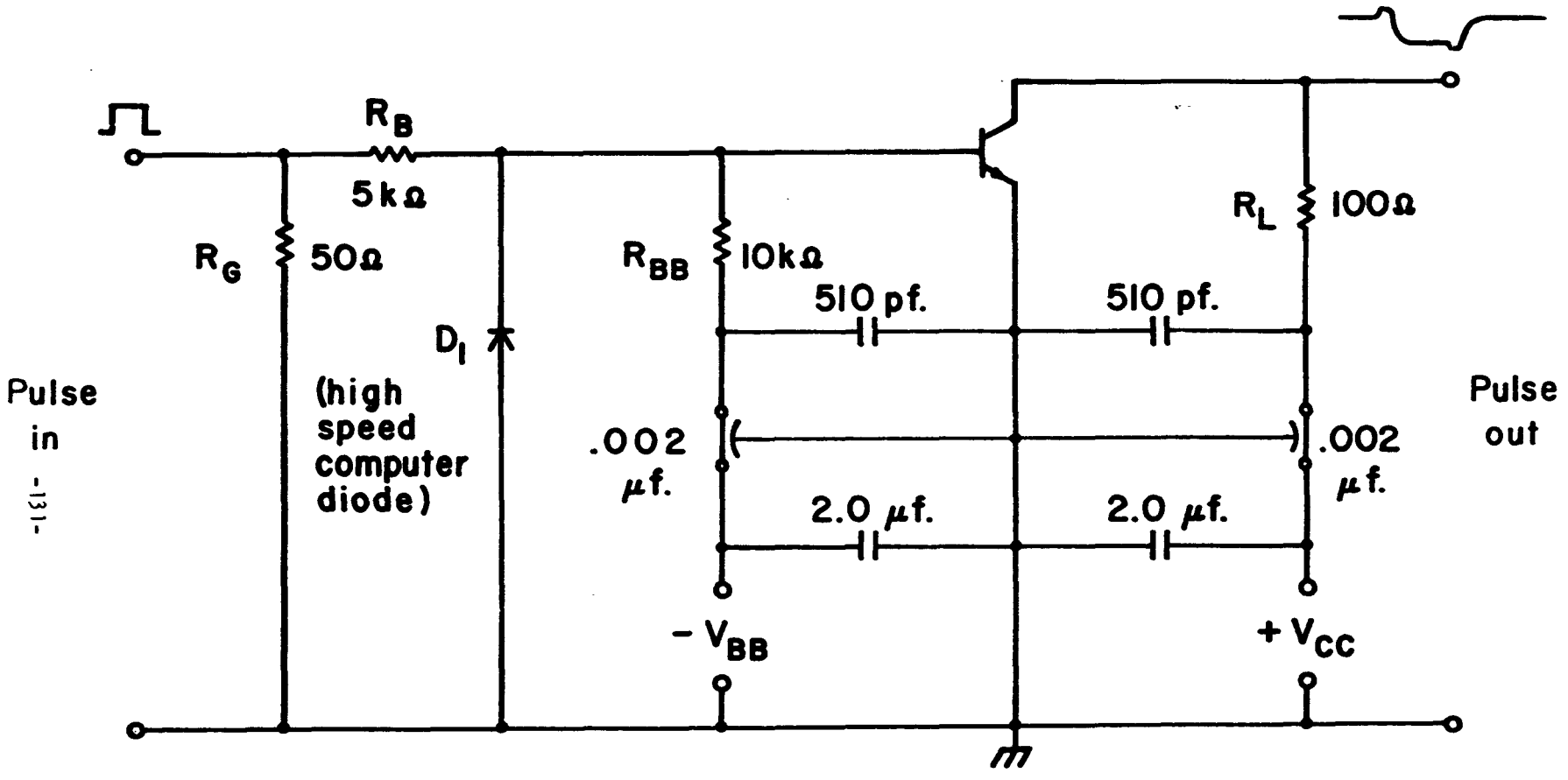

Fig. 58 Circuit for determining GaAs common emitter saturated switching times

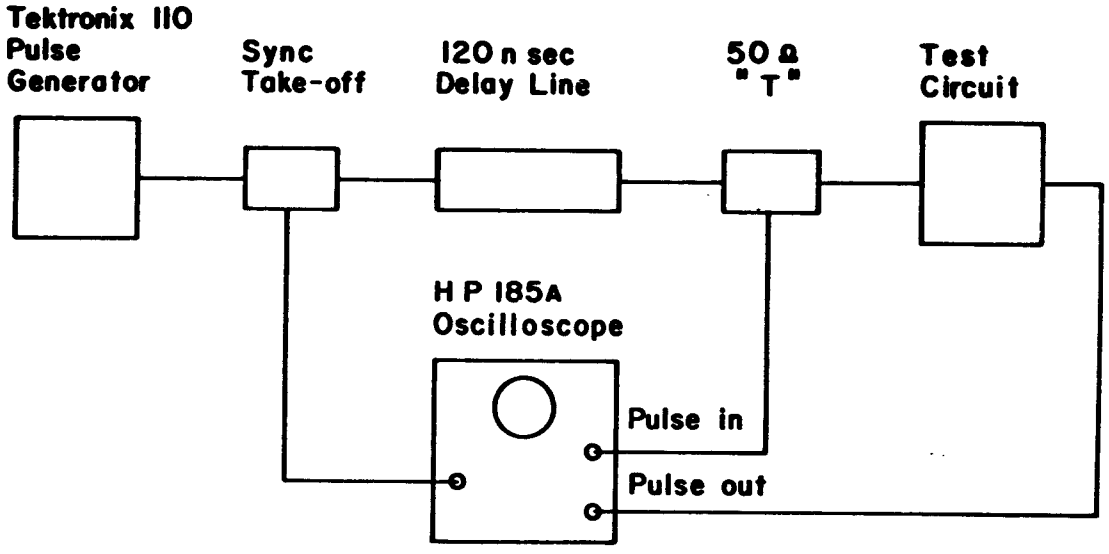

Fig. 59 Block diagram of the test equipment used to observe GaAs transistor switching characteristics

was brought within the rise time capability of the oscilloscope (0.8 nsec or 8×10^{-10} sec). One gallium arsenide unit, measured in this test, set, showed a total switching time of 10.3 nanoseconds. Figure 60 shows the collector current turn on response for this unit to be t_{on} = 6.5 nsec; Fig. 61 shows the turn-off response as t_{off} = 3.8 nsec, giving the t_{total} quoted above. The current, I_{CS}, switched was 10 ma with a turn-on current, I_{B1}, of 6.1 ma and a turn-off current, I_{B2}, of 9.3 ma. The turn-on and off currents were optimized to produce the best rise and fall times for the unit - t_r = 5.2 nsec and t_f = 2.4 nsec. This value of t_{total} was the best realized on any gallium arsenide units.

As was expected the values of storage time, t_s, were very low, on the order of 1 nanosecond or less. Further improvement of t_r and t_f could have probably been realized with further refinement of geometry. However, the t_{total} would still have been of about the same order of t_{total}, 2-5 nsecs, which is now being realized on good germanium epitaxial transistors. Consequently, the switching advantage that was believed to be gained from gallium arsenide transistors vanished and work on this facet of the transistor program was discontinued.

F. High Temperature Characterization

One of the most important advantages to be gained from gallium arsenide as a transistor material is its high temperature capability to operate at temperatures up to 400°C. All these units were built with tin alloyed emitters, which limited the upper limit of operation to about 200°C, just slightly below the melting point of tin. Consequently, an alloy-bearing tin was sought that would allow higher temperature operation. It was believed that the 62% Au- 38% Sn by weight alloy (melting point 418°C) would resolve this problem. However, it was found that upon alloying this Au-Sn compound with gallium arsenide the remaining Au-Sn became liquid at about 300°C. Only with considerable care in handling of units made with this alloy was it possible to obtain some data on transistors at temperatures up to 350°C.

Beta vs temperature data up to 350°C was obtained on a number of state-of-the-art gallium arsenide units made with the Au-Sn alloyed

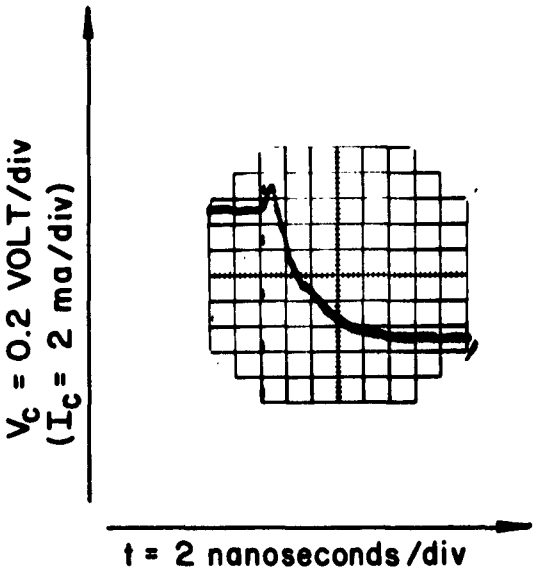

Fig. 60 A gallium arsenide transistor collector current turn on response, t_{on} = 6.5 nsec.

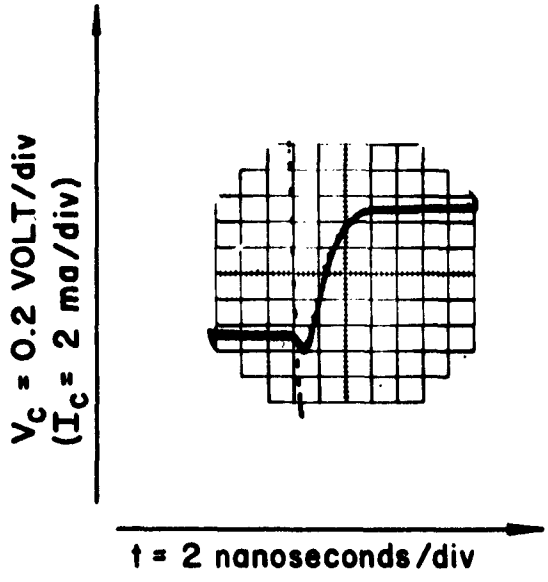

Fig. 61 A gallium arsenide transistor collector current turn off response, t_{off} = 3.8 nsec.

emitter. An initial determination on a canned transistor at temperatures up to 350°C showed considerable beta degradation after returning to room temperature. It was impossible to determine whether the source of degradation was a bulk or surface phenomenon, since the unit could not be opened for study. Hence, further investigations were carried out in vacuum. Again the degradation was noted; however, each time the beta could be returned to its original value by etching (5 parts NaOH-1 part H_2O_2). This condusively showed that the degradation phenomenon was not in the bulk material and was not permanent, as observed in the gallium arsenide tunnel diode. Figure 62 shows the temperature effect on the common emitter output characteristics for one unit while cycling from 25°C to 350°C and back to 35°C. As noted, very little change took place. Figure 63 shows an actual plot of the dc beta vs temperature for the same transistor at temperatures up to 350°C (v_{ce} = 5 volts and I_c = 2 ma). As noted, beta changed very little over this temperature range, with a change from a β = 14 to β = 11. This probably indicates that the minority carrier lifetime over this temperature range is relatively unchanged. Also an interesting conclusion is that the frequency over this range will be relatively unchanged. Independent measurements of μ_n over this temperature range in bulk material showed decreases by a factor of two. Hence, since in Eq. (32) $f_\alpha \propto D_n$, and in Eq. (33) $D_n \propto T\mu_n$ it is apparent that D_n would be unchanged from 25°C to 350°C; therefore, the value of f_α should not change. An interesting experiment to substantiate this would be a frequency vs temperature study. This and other parameters vs temperature are planned for gallium arsenide transistors.

G. Reliability

Twenty-one state-of-the-art gallium arsenide units were placed on life evaluation tests to determine the kind of failure that may be expected. They were subjected to a storage test at 150°C and were checked at 250 and 1000 hrs. The parameters evaluated were I_{CBO} at V_{CB} = 5.0 volts; beta at I_E = 5 ma, V_{CE} = 5 Volts; BV_{CBO} at I_C = 100 μa and BV_{EBO} at I_E = 100 μa. Storage was limited to 150°C because the tin alloyed emitters on the units would melt at 232°C. These units were arbitrarily chosen for the test; no special precautions, such as canning in drying agents or inert atmospheres were taken in their preparation.

Scale:

Horizontal, V_C = 1v/div.

Vertical, I_C = 1 ma/div.

I_B = 0.1 ma/step

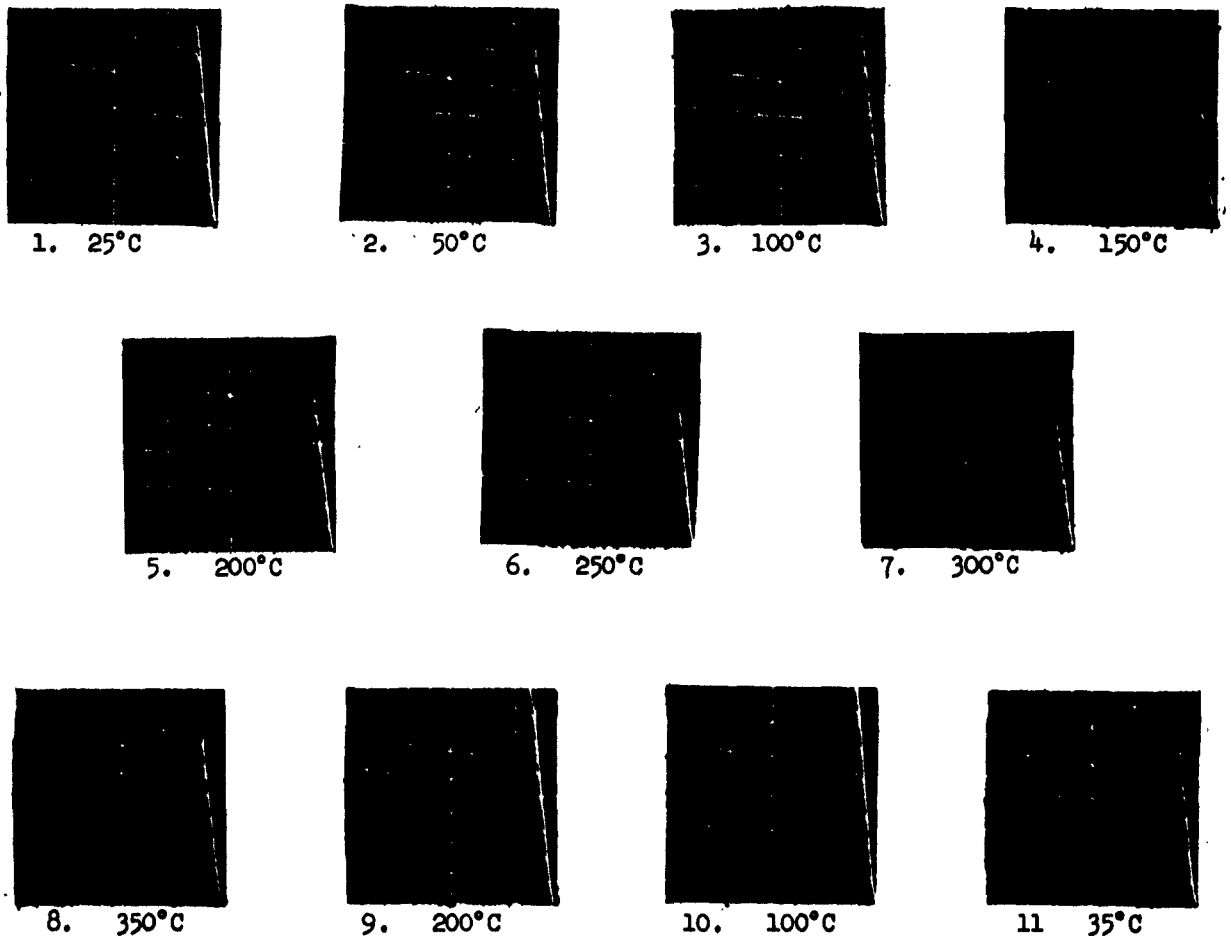

Fig. 62 Temperature effects on common emitter output characteristics of a GaAs transistor

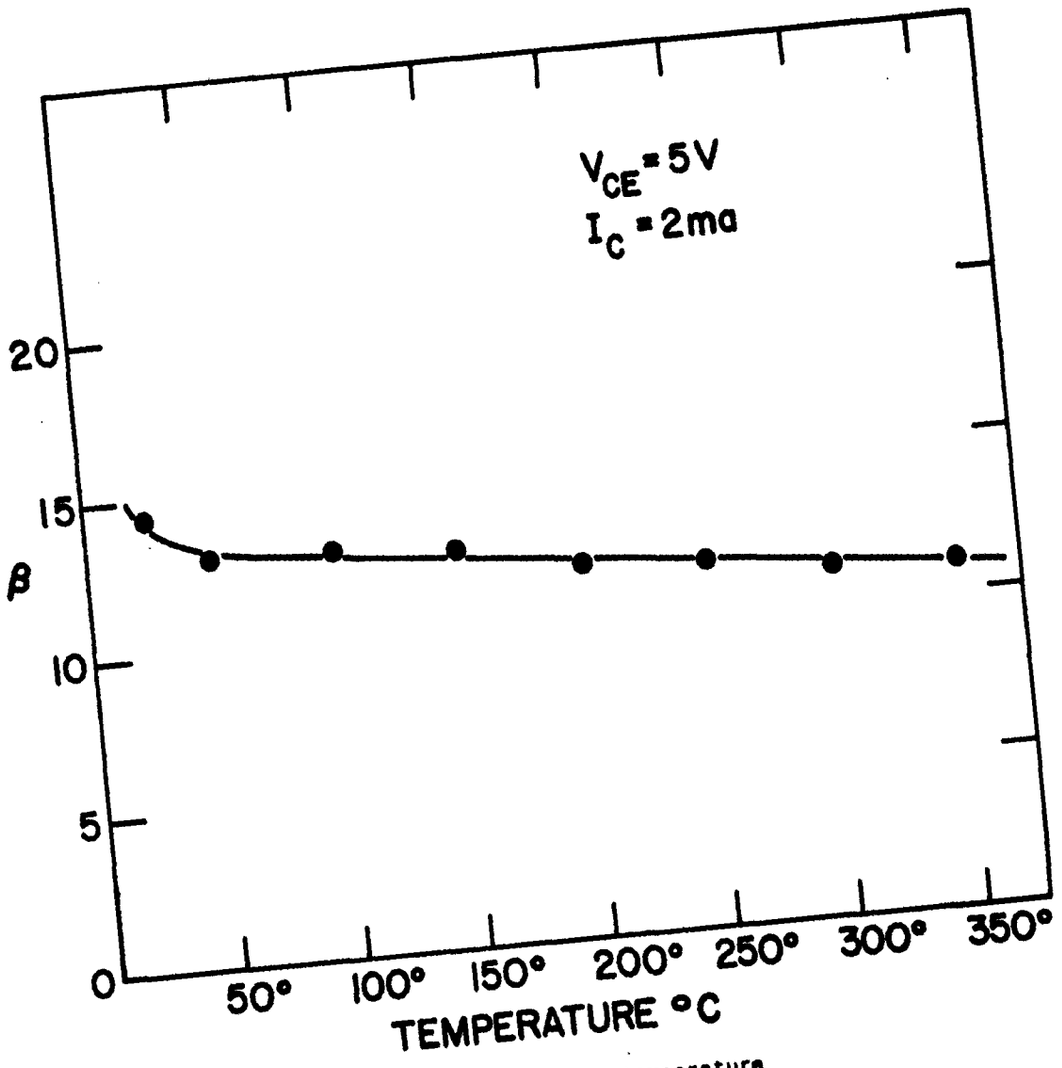

Fig. 63 DC beta vs temperature

Tables XII, XIII, XIV, and XV show the effect of this temperature storage on I_{CBO}, beta, BV_{CBO}, and BV_{EBO}, respectively. Three units failed catastrophically in respect to β and BV_{EBO} after 1000 hrs, with emitter-base shorts. Table 12 shows that the I_{CBO} values in general decreased after 1000 hrs storage. This might be from drying. However, in many cases the units showed no further decrease beyond 250 hours, but rather a slight increase. Perhaps a drying agent in the cans would prevent this. Only three units showed a very large change in beta with the bake-out. Each time the beta decreased, probably because of some contaminant on the device. BV_{CBO} and BV_{EBO} exhibited very little change during the drying process.

The primary conclusion to be drawn from these results in that 150°C storage has no drastic effect on gallium arsenide transistors. Again, certainly no real degradation was observed at this temperature, in contrast to the case of the gallium arsenide tunnel diode. Not much degradation was observed in beta at this temperature, as at 350°C. However, in either case the changes noted were conclusively shown to be surface phenomena.

TABLE XII

150°C LIFE STORAGE EFFECT ON I_{CBO}

	I_{CBO} in Microamps at V_{CB} = 5.0 Volts		
Unit	0 Hours	250 Hours	1,000 Hours
1	0.028	0.023	0.019
2	0.006	0.019	0.041
3	0.011	0.00042	0.0048
4	0.020	0.010	0.021
5	0.030	0.0006	0.012
6	0.045	0.0015	0.612
7	0.004	0.00073	0.0034
8	5.20	4.21	4.29
9	3.70	1.05	1.00
10	0.240	0.200	0.239
11	0.002	0.004	0.0075
12	152.00	115.00	129.00
13	36.30	154.00	153.00
14	0.001	0.00067	0.00079
15	0.01	0.01	0.0093
16	0.00076	0.00063	0.00034
17	0.00083	0.00043	0.00038
18	0.0036	0.0020	0.00145
19	0.0006	0.00023	0.00043
20	0.040	0.0043	0.0061
21	0.030	0.020	0.025

TABLE XIII

150°C LIFE STORAGE EFFECT ON BETA

	Beta at I_C = 5 ma, V_{CE} = 5.0 volts		
Unit	0 Hours	250 Hours	1,000 Hours
1	1.3	1.4	1.3
2	4.1	2.6	2.6
3	1.8	1.8	1.7
4	7.1	6.2	6.2
5	2.0	2.0	2.0
6	38.0	41.0	45.0
7	3.8	3.6	3.6
8	7.1	6.2	6.2
9	1.8	1.4	1.4
10	2.0	1.8	2.0
11	7.7	6.7	7.1
12	1.3	1.3	0
13	4.6	.9	.7
14	3.8	3.3	3.1
15	71.0	71.0	71.0
16	28.0	31.0	31.0
17	2.0	4.1	0
18	4.5	1.8	1.9
19	50 .0	50.0	50.0
20	17.0	13.0	0
21	46.0	18.0	18.0

TABLE XIV

150°C LIFE STORAGE EFFECT ON BV_{CBO}

BV_{CBO} in Volts at I_C = 100 μa			
Unit	0 Hours	250 Hours	1,000 Hours
1	14.0	14.5	14.4
2	11.2	11.2	11.2
3	14.2	14.6	14.5
4	13.2	13.6	13.4
5	13.8	14.0	13.7
6	10.8	11.2	11.0
7	10.6	10.5	10.5
8	15.2	15.9	15.9
9	12.0	11.0	11.0
10	13.2	13.1	13.1
11	12.0	12.5	12.4
12	3.6	4.0	3.7
13	6.2	4.4	3.6
14	12.4	12.8	12.7
15	11.9	12.0	11.8
16	12.5	13.2	13.1
17	14.0	14.6	14.5
18	12.0	12.5	12.3
19	11.8	12.2	12.0
20	12.3	12.5	12.4
21	22.2	22.1	22.2

TABLE XV

150°C LIFE STORAGE EFFECT ON BV_{EBO}

	BV_{EBO} in Volts at I_E = 100 μa		
Unit	0 Hours	250 Hours	1,000 Hours
1	3.3	4.0	4.0
2	3.0	1.1	2.0
3	4.1	3.9	3.9
4	6.4	6.4	6.4
5	5.3	4.5	5.4
6	3.4	3.2	3.4
7	2.1	3.0	3.1
8	5.0	4.5	4.9
9	4.5	3.6	3.3
10	3.8	4.8	5.2
11	4.4	4.1	4.5
12	1.9	2.5	0
13	4.3	2.3	2.2
14	3.9	3.5	3.7
15	6.5	6.6	6.7
16	5.5	5.8	6.0
17	6.1	6.2	0
18	6.3	6.4	6.4
19	6.3	6.3	6.4
20	5.0	4.4	5.7
21	4.9	5.1	5.2

VIII. CONCLUSION

Texas Instruments successfully executed Part I of the program as outlined in the Foreword. Alloy contact studies for both ohmic and rectifying contacts, diffusion studies of primarily acceptors, and etching studies were carried out. They permitted the fabrication of feasibility transistors. Some typical parameters realized on these transistors were those show in Table VIII.

The requirements of Parts 2 and 3 of the program were only partially fulfilled because no satisfactory high temperature and high injection efficiency emitter alloy has been found. Primarily both tin and gold-tin make good high injection efficiency emitter junctions, but neither allow operation of the devices up to the 400°C. However, other program requirements such as frequency, switching times, and power gain were met and measurements of the feasibility units were made. h_{fe} vs frequency measurements at V_{CB} of 3 Volts and I_E of 5 ma yielded gain bandwidths products, f_T, as great as 800 Mc. This value is the highest known to have been observed on gallium arsenide transistors and is believed limited only by geometry. h parameter measurements at f of 1000 cps, V_{CB} of 5 volts and I_E of 1 ma yielded common emitter power gains, G, ranging from 30-43.6 db. The switching characteristics of a number of these units were also investigated. In the saturated mode, with no speed-up capacitor, a number of GaAs transistors yielded total switching times, t_{total}, from 10-30 nanoseconds. Most of this time was in the rise time, t_r, and fall time, t_f, and not in storage time, t_s, which was typically less than one. Several units with gold-tin alloyed emitters were heated to 350°C with very careful handling. The betas of these transistors were found to change negligibly over the temperature range of 25-350°C. However, frequency vs temperature over this same range could be expected to decrease by a factor of two.

In essence, this program has demonstrated the feasibility of gallium arsenide transistors. It has shown the tremendous potential of GaAs devices to surpass either silicon or germanium devices for higher temperature operation, higher power capabilities, and increased frequency

response. However, before this potential can be realized, advances in GaAs materials and device technology comparable with those in silicon and germanium device technology will be necessary.

REFERENCES

1. F. A. Cunnell and C. H. Gooch, J. Phys. Chem. Solids 15, 127 (1960).
2. D. L. Kendall and M. E. Jones, Talks presented at Electrochem. Soc. Meet., May 1960, and at the Device Res. Conf., Stanford, July 1961.
3. B. Goldstein, Phys. Rev. 121, 1305 (1961).
4. J. W. Allen, J. Phys. Chem. Solids 15, 134 (1960).
5. H. Reiss, C. S. Fuller and F. J. Morin, Bell System Tech. 35, 535 (1956).
6. H. Ehrenreich, Phys. Rev. 120, 1951 (1960).
7. J. Crank, The Mathematics of Diffusion, p. 232, The Oxford University Press, 1957.
8. R. L. Longini, Solid State Electronics 5, 127 (1962).
9. W. Shockley and J. Moll, Phys. Rev. 119, 1480 (1960).
10. G. L. Pearson, W. Chambers, R. Mehta, and M. Benhler, Stanford Electronics Laboratory, Consolidated Quarterly Status Report for period ending June 30, 1962.
11. C. S. Fuller and J. A. Ditzenberger, J. Appl. Phys 27, 544 (1956).
12. R. Haisty and C. Kellett, Texas Instruments Incorporated, Unpublished data.
13. J. Kanz, Texas Instruments Incorporated, data elsewhere in this report.
14. L. A. D'Asoro, Bell Laboratories, personal communication.
15. J. J. Lander (p. 71) or D. G. Thomas (p. 284), Semiconductors, Norman B. Hannay, Ed., Reinhold, N. Y., 1959.
16. H. Reiss, J. Chem. Phys. 21, 1209 (1953).
17. J. M. Whelan, Properties of Elemental and Compared Semiconductors, Interscience Publishers, N. Y., 1960.
18. C. D. Thurmond and J. D. Struthers, J. Phys. Chem. 57, 831 (1953).
19. B. Goldstein, Phys. Rev. 113, 1024 (1960).
20. F. A. Cunnell and C. H. Gooch, Nature 188, 1096 (1960).

APPENDIX A

ESTIMATING STATISTICAL ERRORS IN DETERMINING NUCLEAR DISINTEGRATION RATE

ESTIMATING STATISTICAL ERRORS IN DETERMINING NUCLEAR DISINTEGRATION RATE

In studying diffusion in solids using radioactive elements, a measure of the rate of nuclear disintegrations in samples of known sizes is obtained to determine the concentration of the tracer element. Since the decay of radioactive elements takes place in a random manner, errors are introduced in counting rate determinations by the random variations. Consideration of the uncertainty in the counting rate from random fluctuations is particularly important for low activity samples, because the likely statistical errors may far exceed the errors due to other causes. The information gained can be used in planning an experiment; i.e., in determining specific activity a radioisotope must yield a desired detection limit for a specified counting time; the information may also be used to determine the statistical reliability of experimental data. Established methods of statistical analysis can be applied in the estimation of the error due to random variations in a disintegration rate determination (R-1, 2, 3). Only a brief summary of the most basic considerations is presented here.

Use of Standard Deviation

It can be shown that the probability of occurrence of various counts which differ from the true average rate can be predicted by either a Poisson or a Gaussian distribution (by the use of approximations which are normally valid in counting radioactive disintegrations). The standard deviation, σ, of a single measured value of a total number of counts, N, may be expressed as $\sigma = (N)^{1/2}$. This is valid for either a Poisson or Gaussian distribution when N is large. The standard deviation is an important statistical quantity and possible errors corresponding to various probabilities may be estimated by factors of it. Thus, the uncertainty of a counting determination which is associated with a particular probability of occurrence can be expressed as $\pm K\sqrt{N}$. As K assumes larger values, the probability that an error will exceed $\pm K\sqrt{N}$ diminishes. The values of K which correspond to a number of commonly used errors are shown in the following table.

Table

Statistical Errors in Counting Determinations

Name of Error	K	Probability of Observing Error within $\pm K\sqrt{N}$
Probable error	0.674	0.500
Standard deviation	1.000	0.683
Nine-tenths error	1.645	0.900
Ninety-five hundredths error	1.960	0.950

For example, if 100 counts are recorded in a given time, the results may be expressed as $N \pm 0.674\sqrt{N}$ or 100 ± 6.7 counts. There are fifty chances out of a hundred that the error in the number of counts would fall within a ± 6.7 counts since a $K = 0.674$ corresponds to a 0.50 probability level. It is emphasized that the uncertainty refers only to that which might be present because of random fluctuations in the decay rate.

Estimation of Error in Counting Rate

Usually the result of a counting determination is expressed as a certain number of net counts per minute. This value can in turn be related to the number of disintegrations per minute and ultimately to a concentration value for the element in question. The net counting rate is simply the difference between the total count rate and the background count rate.

The background has its origin in various natural sources of radiation including cosmic-radiation and the naturally-occurring radioactive elements present in the experimental apparatus. Since a low background rate is desirable, shielding and other methods are used to minimize it.

The standard deviation of a net counting rate, which is a difference, is equal to the square root of the sum of the squares of the standard deviations of the total rate and the background rate (R-3):

$$\sigma_{R_S} = (\sigma^2_{R_T} + \sigma^2_{R_B})^{1/2} \qquad (1)$$

Since the expression for the standard deviation of the number of counts is $\sigma_N \simeq (N)^{1/2}$

and $\sigma_R = \frac{\sigma N}{t}$ (where t is counting time),

then $\sigma_R = \frac{\sqrt{N}}{t} = \sqrt{\frac{R}{t}}$ (where R is counting rate).

Thus, Equation (1) may be written as follows

$$\sigma_{R_S} = \left(\frac{R_T}{t_T} + \frac{R_B}{t_T} \right)^{1/2} . \qquad (2)$$

Typical Problem

A common problem which arises in the measurement of a disintegration rate is the following:

The count of a sample (including the background) for 10 minutes yielded a total of 426 counts. The background was counted alone for 10 minutes and yielded 334 counts. What uncertainty should be assigned to the net counting rate of the sample due to random variations?

Solution:

The net counting rate of the sample is

$$R_S = \frac{426}{10} - \frac{334}{10} = 9.2 \text{ counts/minute.}$$

The standard deviation of the net counting rate is given by Equation 2.

$$\sigma_{R_S} = \left(\frac{42.6}{10} \quad \frac{33.4}{10} \right)^{1/2} = 2.8 \text{ counts/minute.}$$

Thus the results of the determination may be expressed as 9.2 ± 2.8 counts per minute with a confidence level of 68.3 per cent. If a higher confidence level is desired, the standard deviation should be multiplied by the appropriate K as shown in the Table.

Jarrett (R-2) presents an analysis designed to minimize the error introduced by the background by use of an efficient distribution between the total counting time and the background counting time. Also, Jarrett presents a number of curves and nomographs which are convenient to use in estimating the statistical error inherent in the measurement of radioactivity.

REFERENCES

R-1 Friedlander, G. and Kennedy, J. W., Introduction to Radiochemistry, 199-215, John Wiley, New York, 1949.

R-2 Jarrett, A. A., AECU-262, Oak Ridge National Laboratory, Oak Ridge, Tennessee, 1946.

R-3 Overman, R. T. and Clark, H. M., Radioisotope Techniques, 98-130, McGraw-Hill, New York, 1960.

APPENDIX B

Mg DIFFUSION THROUGH SiO_2 FILM - ANALYTIC SOLUTION

APPENDIX B

Mg Diffusion through SiO_2 Film - Analytic Solution

The diffusion of magnesium in gallium arsenide through the silicon dioxide film presents the problem of finding the concentration at the interface of SiO_2 and GaAs. This problem has been solved analytically.

Consider the SiO_2 - GaAs semi-infinite system as shown in Fig. 1.

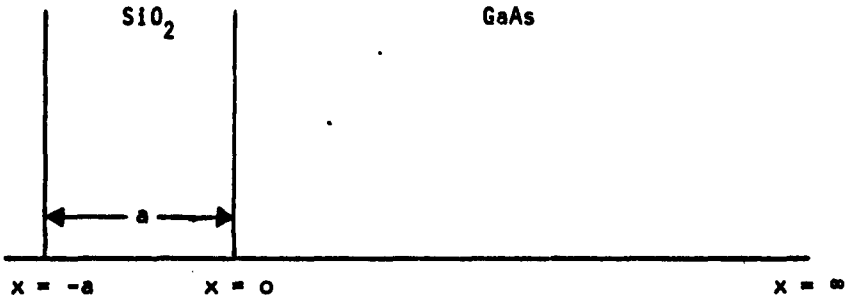

Fig. 1

We know magnesium diffusion follows the complementary error function distribution in gallium arsenide and therefore concentration - independent diffusion coefficient in GaAs has been assumed.

Thus, suppose in the semi-infinite region $-a < x < \infty$, the diffusion coefficient is D_1 in the region $-a < x < o$ and D_2 in the region $o < x < \infty$. During diffusion, two operations take place:

(1) Inward diffusion in the region $-a < x < \infty$ starting from the surface $x = -a$, the surface of silicon diode, and

(2) Out-diffusion from the region $o < x < \infty$ through the interface $x = o$.

The solution of these two cases should then be added electrically to give the concentration at the interface SiO_2 - GaAs.

The boundary conditions for these two cares follow:

Case 1

$$C_t(x,t) = D_1 C_{xx}(x,t) \qquad (-a \leq x < o,\ t > o) \qquad (1a)$$

$$C_t(x,t) = D_2 C_{xx}(x,t) \qquad (x > o,\ t > o) \qquad (1b)$$

$$C(x,o) = 0 \qquad (-a \leq x < o) \qquad (1c)$$

$$C(x,o) = 0 \qquad (x > o) \qquad (1d)$$

$$C(-a,t) = C_s \qquad (t > o) \qquad (1e)$$

$$\lim_{x \to \infty} C(x,t) = 0 \qquad (1f)$$

$$D_1 C_x(-o,t) = D_2 C_x(+o,t) \qquad (1g)$$

$$C(-o,t) = (1-H)\, C(+o,t) + HC_{GaAs} \qquad (1h)$$

Note: Boundary condition (1h) takes into account the difference of solid solubilities of the diffusant in SiO_2 and GaAs, the concentration in GaAs may approach a maximum solid solubility, which it cannot exceed. H is the step function.*

Case 2

$$C_t(x,t) = D_1 C_{xx}(x,t) \qquad (-a \leq x < o, t > o) \qquad (2a)$$

$$C_t(x,t) = D_2 C_{xx}(x,t) \qquad (x > o,\ t > o) \qquad (2b)$$

$$C(x,o) = 0 \qquad (-a \leq x < o) \qquad (2c)$$

$$C(x,o) = C_x \qquad (x > o) \qquad (2d)$$

---

*R. C. Wackwitz, "Analytic Solution of the Multiple Diffusion Problems" Journal Applied Physics, Vol. 33, #9, Sept. 1962.

where C_x is the concentration of donors in GaAs.

$$\lim_{x \to \infty} C(x,t) = C_x \qquad (t > o) \tag{2e}$$

$$C_x(-a, t) = o \tag{2f}$$

$$D_1 C_x(-o,t) = D_2 C_x(+o,t) \tag{2g}$$

$$D_2 C_x(+o,t) = K\left[C(+o,t) - C(-o,t)\right] \tag{2h}$$

Note: Boundary condition (2h) assumes that the out-diffusion from GaAs to SiO_2 is proportional to the difference between GaAs and SiO_2 instantaneous surface concentrations.

For small values of t, the solution of equation (1) is

$$C_{SiO_2}(x,t) = C_s \operatorname{erfc}\left(\frac{a+x}{2y}\right) - C_s \alpha \operatorname{erfc}\left(\frac{a-x}{2y}\right) + C_s \alpha \operatorname{erfc}\left(\frac{3a+x}{2y}\right)$$

$$- C_s\alpha^2 \operatorname{erfc}\left(\frac{3a-x}{2y}\right) - \frac{\alpha HC_{GaAs}}{\alpha'} \operatorname{erfc}\left(\frac{x}{2y}\right) - \frac{\alpha HC_{GaAs}}{\alpha'} \operatorname{erfc}\left(\frac{2a+x}{2y}\right)$$

$$+ \frac{\alpha^2 HC_{GaAs}}{\alpha'} \operatorname{erfc}\left(\frac{2a-x}{2y}\right) - \frac{\alpha^2 HC_{GaAs}}{\alpha'} \operatorname{erfc}\left(\frac{4a+x}{2y}\right)$$

$$C_{GaAs}(x,t) = \frac{\mu\alpha}{\alpha'}\left[2 C_s \operatorname{erfc}\left(\frac{a+x}{2y}\right) - HC_{GaAs} \operatorname{erfc}\left(\frac{x}{2y}\right) + HC_{GaAs} \operatorname{erfc}\left(\frac{2a+x}{2y}\right)\right.$$

$$\left. + 2 C_x \alpha \operatorname{erfc}\left(\frac{3a+x}{2y}\right) - HC_{GaAs}\alpha \operatorname{erfc}\left(\frac{4a+x}{2y}\right)\right]$$

and the solution of equation (2) is

$$C_{SiO_2}(x,t) = \frac{K^2 C_x}{\mu\beta}\left[\frac{d}{h^2} \operatorname{erfc}\left(\frac{4a+x}{2y}\right) - \frac{d}{h^2}\left(1-hx-2h^2y^2\right) e^{4ah} e^{hx} e^{h^2y^2}\right.$$

$$\operatorname{erfc}\left(\frac{4a+x}{2y} + hy\right) + \frac{d}{h^2}\ \operatorname{erfc}\left(\frac{2a-x}{2y}\right) - \frac{d}{h^2}\ (1-hx-2h^2y^2)\ e^{2ah}\ e^{-hx}\ e^{h^2y^2}$$

$$\cdot \operatorname{erfc}\left(\frac{2a-x}{2y} + hy\right) - \left(\frac{2yd}{h\sqrt{\pi}} + \frac{1}{h^2y\sqrt{\pi}}\right)\left\{e^{-\left(\frac{2a-x}{2y}\right)^2} + e^{-\left(\frac{4a+x}{2y}\right)^2}\right\}$$

$$+ \frac{1}{h^3y^3\sqrt{\pi}}\left\{(2a-x)\ e^{-\left(\frac{2a-x}{2y}\right)^2} + (4a+x)\ e^{-\left(\frac{4a+x}{2y}\right)^2}\right\} + \frac{1}{h}\left\{\operatorname{erfc}\left(\frac{2a+x}{2y}\right)\right.$$

$$\left. - e^{2ah}\ e^{hx}\ e^{h^2y^2} \operatorname{erfc}\left(\frac{2a+x}{2y} + hy\right)\right\}\Bigg] \cdots$$

$$C_{GaAs}\ (x,t) = C_x\left[1 + \frac{2d}{h}\ \operatorname{erfc}\left(\frac{a}{2y}\right) - 2\left(1+\frac{d}{h}\right) e^{ah}\ e^{h^2y^2} \operatorname{erfc}\left(\frac{a}{2y} + hy\right)\right.$$

$$- \frac{K^2}{\beta h}\left\{\operatorname{erfc}\left(\frac{\mu x-a}{2y}\right) - \left(1 - \frac{d}{h}\right) \operatorname{erfc}\left(\frac{\mu x+a}{2y}\right) - \frac{d}{h}\ \operatorname{erfc}\left(\frac{\mu x+3a}{2y}\right)\right\}$$

$$+ \frac{K^2}{\beta h}\ e^{h\mu x}\ e^{h^2y^2}\left\{e^{-ah} \operatorname{erfc}\left(\frac{\mu x-a}{2y} + hy\right) + \frac{d}{h}\ e^{ah}\left(1 + \frac{h}{d} - h\mu x - ah - 2h^2y^2\right)\right\} +$$

$$\cdot \operatorname{erfc}\left(\frac{\mu x+a}{2y} + hy\right) - \frac{2yh}{\sqrt{\pi}}\left\{e^{-\left(\frac{\mu x+a}{2y}\right)^2} + e^{-\left(\frac{\mu x+3a}{2y}\right)^2}\right\} - (1-h\mu x-3ah-2h^2y^2)$$

$$\left. \cdot e^{h\mu x}\ e^{3ah}\ e^{h^2y^2} \operatorname{erfc}\left(\frac{\mu x+3a}{2y} + hy\right)\right]$$

Final solution, therefore, looks as follows:

$$C_{SiO_2}\ (x,t) = C_s \operatorname{erfc}\left(\frac{a+x}{2y}\right) - C_s\alpha \operatorname{erfc}\left(\frac{a-x}{2y}\right) + C_s\alpha \operatorname{erfc}\left(\frac{3a+x}{2y}\right) - C_s\alpha^2 \operatorname{erfc}\left(\frac{3a-x}{2y}\right)$$

$$- \frac{\alpha HC_{GaAs}}{\alpha'}\ \operatorname{erfc}\left(\frac{x}{2y}\right) - \left[\frac{K^2C_x}{\mu\beta h} + \frac{\alpha HC_{GaAs}}{\alpha'}\right] \operatorname{erfc}\left(\frac{2a+x}{2y}\right) - \left[\frac{K^2dC_x}{\mu\beta h^2} - \frac{\alpha^2HC_{GaAs}}{\alpha'}\right]$$

$$\cdot \operatorname{erfc}\left(\frac{2a-x}{2y}\right) - \left[\frac{K^2dC_x}{\mu\beta h^2} + \frac{\alpha^2HC_{GaAs}}{\alpha'}\right] \operatorname{erfc}\left(\frac{4a+x}{2y}\right) + \frac{K^2C_x}{\mu\beta}\left[\frac{d}{h^2}\ (1-hx-2h^2y^2)\right.$$

$$\left. \cdot e^{4ah}\ e^{hx}\ e^{h^2y^2} \operatorname{erfc}\left(\frac{4a+x}{2y} + hy\right) + \frac{d}{h^2}\ (1-hx-2h^2y^2)\ e^{2ah}\ e^{-hx}\ e^{h^2y^2} \operatorname{erfc}\left(\frac{2a-x}{2y} + hy\right)\right.$$

$$+\left(\frac{2yd}{h\sqrt{\pi}}+\frac{1}{h^2y\sqrt{\pi}}\right)\left\{e^{-\left(\frac{2a-x}{2y}\right)^2}+e^{-\left(\frac{4a+x}{2y}\right)^2}\right\}-\frac{1}{h^3y^3\sqrt{\pi}}\left\{(2a-x)\,e^{-\left(\frac{2a-x}{2y}\right)^2}\right.$$

$$\left.+(4a+x)\,e^{-\left(\frac{4a+x}{2y}\right)^2}\right\}-\frac{1}{h}e^{2ah}\,e^{hx}\,e^{h^2y^2}\,\operatorname{erfc}\left(\frac{2a+x}{2y}+hy\right)\Bigg] \qquad (3a)$$

$$C_{GaAs}(x,t)=\frac{\mu\alpha}{\alpha'}\Bigg[2C_s\operatorname{erfc}\left(\frac{a+x}{2y}\right)-HC_{GaAs}\operatorname{erfc}\left(\frac{x}{2y}\right)+HC_{GaAs}\operatorname{erfc}\left(\frac{2a+x}{2y}\right)$$

$$+2C_s\alpha\operatorname{erfc}\left(\frac{3a+x}{2y}\right)-HC_{GaAs}\alpha\operatorname{erfc}\left(\frac{4a+x}{2y}\right)\Bigg]-C_x\Bigg[1+\frac{2d}{h}\operatorname{erfc}\left(\frac{a}{2y}\right)$$

$$-2\left(1+\frac{d}{h}\right)e^{ah}\,e^{h^2y^2}\operatorname{erfc}\left(\frac{a}{2y}+hy\right)-\frac{K^2}{\beta h}\left\{\operatorname{erfc}\left(\frac{\mu x-a}{2y}\right)-\left(1-\frac{d}{h}\right)\operatorname{erfc}\left(\frac{\mu x+a}{2y}\right)\right.$$

$$-\frac{d}{h}e^{ah}\left(1+\frac{h}{d}-h\mu x-ah-2h^2y^2\right)\operatorname{erfc}\left(\frac{\mu x+a}{2y}+hy\right)-\frac{2yh}{\sqrt{\pi}}\left\{e^{-\left(\frac{\mu x+a}{2y}\right)^2}\right.$$

$$\left.\left.+e^{-\left(\frac{\mu x+3a}{2y}\right)^2}\right\}-(1-h\mu x-3ah-2h^2y^2)\,e^{h\mu x}\,e^{3ah}\,e^{h^2y^2}\operatorname{erfc}\left(\frac{\mu x+3a}{2y}+hy\right)\Bigg] \qquad (3b)$$

where $\mu=\sqrt{\frac{D_1}{D_2}}$, $\beta=\sqrt{D_1D_2}$, $\alpha=\frac{1-\mu\bar{H}}{1+\mu\bar{H}}$, $\bar{H}=1-H$,

$$\alpha'=1-\mu\bar{H},\quad d=\frac{K}{D_1}(1-\mu),\quad h=\frac{K}{D_1}(1+\mu)\quad\text{and}\quad y=\sqrt{D_1t}.$$

Knowing D_1 and D_2, this solution will give the concentration value at the interface SiO_2 - GaAs.

This solution is very general in that it can be applied to any semi-infinite composite system which has a skin or surface layer of finite thickness. Both media should have concentration-independent diffusion coefficient.

Further, the solution given by expressions (3a) and 3b) can be proven to be the unique solution to this boundary value problem.

It is interesting to note that the values of f (y,z) where

$$f(y,z) = \operatorname{erfc} y \pm e^{2yz}\, e^{z^2} \operatorname{erfc}(y+z)$$

for different values of y and z are available in literature*.

The above solutions are given for small values of t. The general solutions are, however, desired when the diffusion is carried for greater lengths of time.

For all values of t, the solutions can be written as follows:

$$C_{SiO_2}(x,t) = C_s \sum_m \alpha^m \operatorname{erfc}\left(\frac{2ma + x + a}{2y}\right) - C_s \sum_m \alpha^{m+1} \operatorname{erfc}\left(\frac{2ma - x + a}{2y}\right)$$

$$+ \frac{\alpha HC_{GaAs}}{\alpha'} \sum_m \alpha^m \operatorname{erfc}\left(\frac{2ma - x}{2y}\right) - \frac{\alpha HC_{GaAs}}{\alpha'} \sum_m \alpha^m \operatorname{erfc}\left(\frac{2ma + x + 2a}{2y}\right)$$

$$- KC_x\left[1 + \sum_n \frac{e^{Z_n(x+a)} + e^{-Z_n(x+a)}}{be^{Z_n a} + ge^{-Z_n a}}\right]$$

and,

$$C_{GaAs}(x,t) = \frac{\mu\alpha}{\alpha'}\left[2C_s \sum_m \alpha^m \operatorname{erfc}\left(\frac{2ma + x + a}{2y}\right) - HC_{GaAs} \sum_m \alpha^m \operatorname{erfc}\left(\frac{2ma + x}{2y}\right)\right.$$

$$\left. + HC_{GaAs} \sum_m \alpha^m \operatorname{erfc}\left(\frac{2ma + x + 2a}{2y}\right)\right] -$$

$$-C_x\left[1 + \sum_n \frac{D_1}{2K}\left\{\frac{(h+Z_n)e^{Z_n a} + (d-Z_n)e^{-Z_n a} - K^2/\beta\, e^{-Z_n(\mu x - a)} + K^2/\beta\, e^{-Z_n(\mu x + a)}}{b\, e^{Z_n a} + g\, e^{-Z_n a}}\right\}\right]$$

where,

$$b = \frac{D_1 Z_n}{2K}(Z_n a + 3)\left[1 + \frac{K(\mu+1)(Z_n a+2)}{D_1 Z_n (Z_n a+3)}\right]$$

$$g = \frac{D_1 Z_n}{2K}(Z_n a - 3)\left[1 + \frac{K(\mu-1)(Z_n a-2)}{D_1 Z_n (Z_n a-3)}\right]$$

---

* Smits and Miller, "Rate Limitation at the Surface for Impurity Diffusion in Semiconductors", Bell Telephone System Technical Publications Monograph 3119.

and, Z_n ($n = 1, 2, 3, \ldots.$) are the roots of the equation

$$1 + \left(\mu + \frac{D_1 Z}{K}\right) \tanh (Za) = 0.$$

FINAL REPORT DISTRIBUTION FOR

CONTRACT NObsr 77532 AND CONTRACT NObsr 85424

Addressee	Number of Copies
Commander U.S. Naval Ordnance Laboratory White Oak, Maryland Attention: W. W. Scanlon	1
Commanding Officer U. S. Army Signal Research and Development Laboratory Solid State Division Attention: SIGRA/SL-PF (H. Jacobs)	1
Commander Aeronautical Systems Division Attention: R. D. Alberts ASRNEM, AFSC Wright-Patterson Air Force Base Dayton, Ohio	1
Commander, ESD (AFCRL) Attention: R. P. Dolan, CRR-CSA L. G. Hanscom Field Bedford, Massachusetts	1
Ordnance Corps, Department of the Army Diamond Ordnance and Fuze Laboratories Connecticut Avenue & Van Ness Street, N.W. Washington 25, D. C. Attention: T. M. Liimatainen	1
Director National Bureau of Standards Electronics and Electricity Division Electronic Engineering Section Washington 25, D. C. Attention: Gustave Shapiro	1
Advisory Group on Electron Devices 346 Broadway, 8th Floor New York 13, New York Attention: H. J. Sullivan	3
Commander Armed Services Technical Information Agency Attention: TIAI Arlington Hall Station Arlington 12, Virginia	10
Armour Research Foundation Technology Center Chicago 16, Illinois Attention: J. W. Buttrey	1

FINAL REPORT DISTRIBUTION FOR

CONTRACT NObsr 77532 AND CONTRACT NObsr 85424

Addressee	Number of Copies
Department of the Navy Bureau of Ships Semiconductor Group, Code 681A1A Washington 25, D. C. Attention: Mr. A. H. Young	3
Department of the Navy Bureau of Ships, Code 210L Washington 25, D. C.	2
Department of the Navy Bureau of Naval Weapons, Code RREN-4 Washington 25, D. C.	1
Department of the Navy Bureau of Naval Weapons, Code RAAV-333 Washington 25, D. C.	1
Department of the Navy Office of Naval Research Chief of Naval Research, Code 427 Washington 25, D. C. Attention: A. A. Shostak	1
Director U.S. Naval Research Laboratory Washington 25, D. C. Attention: Code 2020	1
Director U.S. Naval Research Laboratory Washington 25, D. C. Attention: A. Brodzinsky, Code 5210	1
Director U.S. Naval Research Laboratory Washington 25, D. C. Attention: G. Abraham, Code 5266	1
Commander New York Naval Shipyard Material Laboratory, Code 923 Naval Base Brooklyn 1, New York	1

Addressee	Number of Copies
Batelle Memorial Institute 505 King Avenue Columbus, Ohio Attention: Mr. Peet	1
Bell Telephone Laboratories Murray Hill, New Jersey Attention: R. M. Ryder	1
CBS Laboratories High Ridge Road Stamford, Connecticut Attention: W. W. Gaertner	1
Fairchild Semiconductor Corporation 545 Whisman Road Mountain View, California Attention: H. S. Bobb	1
General Electric Company Semiconductor Product Department Electronics Park Syracuse, New York Attention: H. M. Sullivan	1
Hughes Products Semiconductor Division 500 Superior Avenue Newport Beach, California Attention: E. L. Steele	1
Massachusetts Institute of Technology Lincoln Laboratory Lexington 73, Massachusetts Attention: R. H. Rediker	1
Motorola, Incorporated Semiconductor Division 5005 East McDowell Road Phoenix, Arizona	1
Pacific Semiconductors, Incorporated 10451 West Jefferson Boulevard Culver City, California Attention: H. Q. North	1
Philco Corporation Lansdale Division Lansdale, Pennsylvania Attention: C. C. Thornton	1

Addressee	Number of Copies
Radio Corporation of America RCA Laboratories Princeton, New Jersey Attention: W. W. Webster	1
Radio Corporation of America Semiconductor & Materials Division Route 202 Somerville, New Jersey Attention: E. O. Johnson	1
Raytheon Company Research Division Library 28 Seyon Street Waltham 54, Massachusetts	1
Sylvania Electric Products, Incorporated Semiconductor Division 100 Sylvan Road Woburn, Massachusetts Attention: T. A. Longo	1
Tapco Group Thompson Ramo Wooldridge, Incorporated New Devices Laboratory 7209 Platt Avenue Cleveland 4, Ohio	1
Transitron Electronic Corporation 168 Albion Street Wakefield, Massachusetts	1
Westinghouse Electric Corporation Youngwood, Pennsylvania	1

Bureau of Ships, Department of the Navy, Washington 25, D. C. RESEARCH AND DEVELOPMENT OF HIGH TEMPERATURE SEMICONDUCTOR DEVICES. Final Report, March, 1963, 175 p., illus.

Unclassified Report

Objectives: To study and investigate methods and techniques for developing GaAs transistors. Alloyed materials for both ohmic and rectifying contacts were developed, and diffusion studies of acceptors and etching studies were made, permitting fabrication of feasibility transistors. No high temperature and high injection efficiency emitter alloy was found. Both tin and gold-tin make good high injection efficiency emitter junctions, but neither allows operation of the devices up to 350°C. Typical parameters realized were: β = 10-20, with some up to 3000; I_{CBO} = 2 x 10^{-8} amp; BV_{CBO} = 15 V; $V_{CE}(Sat)$ = 0.6 V; C_{TC} = 3.2 pf; C_{Te} = 1.8 pf. Feasibility units were made and characteristics such as frequency, switching times and power gain

1. Gallium Arsenide Transistors
2. High Temperature Devices
I. Contract Nos. NObsr-77532 and NObsr-85424
II. Texas Instruments Incorporated, Dallas, Texas
III. Wurst, E. C.

Bureau of Ships, Department of the Navy, Washington 25, D. C. RESEARCH AND DEVELOPMENT OF HIGH TEMPERATURE SEMICONDUCTOR DEVICES. Final Report, March, 1963, 175 p., illus.

Unclassified Report

Objectives: To study and investigate methods and techniques for developing GaAs transistors. Alloyed materials for both ohmic and rectifying contacts were developed, and diffusion studies of acceptors and etching studies were made, permitting fabrication of feasibility transistors. No high temperature and high injection efficiency emitter alloy was found. Both tin and gold-tin make good high injection efficiency emitter junctions, but neither allows operation of the devices up to 350°C. Typical parameters realized were: β = 10-20, with some up to 3000; I_{CBO} = 2 x 10^{-8} amp; BV_{CBO} = 15 V; $V_{CE}(Sat)$ = 0.6 V; C_{TC} = 3.2 pf; C_{Te} = 1.8 pf. Feasibility units were made and characteristics such as frequency, switching times and power gain

1. Gallium Arsenide Transistors
2. High Temperature Devices
I. Contract Nos. NObsr-77532 and NObsr-85424
II. Texas Instruments Incorporated, Dallas, Texas
III. Wurst, E. C.

Bureau of Ships, Department of the Navy, Washington 25, D. C. RESEARCH AND DEVELOPMENT OF HIGH TEMPERATURE SEMICONDUCTOR DEVICES. Final Report, March, 1963, 175 p., illus.

Unclassified Report

Objectives. To study and investigate methods and techniques for developing GaAs transistors. Alloyed materials for both ohmic and rectifying contacts were developed, and diffusion studies of acceptors and etching studies were made, permitting fabrication of feasibility transistors. No high temperature and high injection efficiency emitter alloy was found. Both tin and gold-tin make good high injection efficiency emitter junctions, but neither allows operation of the devices up to 350°C. Typical parameters realized were: β = 10-20, with some up to 3000; I_{CBO} = 2 x 10^{-8} amp; BV_{CBO} = 15 V; $V_{CE}(Sat)$ = 0.6 V; C_{TC} = 3.2 pf; C_{Te} = 1.8 pf. Feasibility units were made and characteristics such as frequency, switching times and power gain

1. Gallium Arsenide Transistors
2. High Temperature Devices
I. Contract Nos. NObsr-77532 and NObsr-85424
II. Texas Instruments Incorporated, Dallas, Texas
III. Wurst, E. C.

Bureau of Ships, Department of the Navy, Washington 25, D. C. RESEARCH AND DEVELOPMENT OF HIGH TEMPERATURE SEMICONDUCTOR DEVICES. Final Report, March, 1963, 175 p., illus.

Unclassified Report

Objectives: To study and investigate methods and techniques for developing GaAs transistors. Alloyed materials for both ohmic and rectifying contacts were developed, and diffusion studies of acceptors and etching studies were made, permitting fabrication of feasibility transistors. No high temperature and high injection efficiency emitter alloy was found. Both tin and gold-tin make good high injection efficiency emitter junctions, but neither allows operation of the devices up to 350°C. Typical parameters realized were: β = 10-20, with some up to 3000, I_{CBO} = 2 x 10^{-8} amp; BV_{CBO} = 15 V; $V_{CE}(Sat)$ = 0.6 V; C_{TC} = 3.2 pf; C_{Te} = 1.8 pf. Feasibility units were made and characteristics such as frequency, switching times and power gain

1. Gallium Arsenide Transistors
2. High Temperature Devices
I. Contract Nos. NObsr-77532 and NObsr-85424
II. Texas Instruments Incorporated, Dallas, Texas
III. Wurst, E. C.

were evaluated. h_{FE} vs frequency measurements at V_{CB} = 3 V, I_E = 5 ma yielded gain bandwidth products, f_T, as great as 800 Mc. This value is the highest known observed on GaAs transistors and is believed limited only by geometry control. h parameter measurements at f = 1000 cps, V_{CB} = 5 V, and I_E = 1 ma yielded common emitter power gains, G, ranging from 30-43.6 db. Switching characteristics of several units were also investigated. In the saturated mode, with no speedup capacitor, some units yielded total switching time from 10-30 nsec with only moderate overdrive. Most of this time was in rise and fall and not in storage time, which was typically less than one. Feasibility tunnel diodes were fabricated and evaluated.

were evaluated. h_{FE} vs frequency measurements at V_{CB} = 3 V, I_E = 5 ma yielded gain bandwidth products, f_T, as great as 800 Mc. This value is the highest known observed on GaAs transistors and is believed limited only by geometry control. h parameter measurements at f = 1000 cps, V_{CB} = 5 V, and I_E = 1 ma yielded common emitter power gains, G, ranging from 30-43.6 db. Switching characteristics of several units were also investigated. In the saturated mode, with no speedup capacitor, some units yielded total switching time from 10-30 nsec with only moderate overdrive. Most of this time was in rise and fall and not in storage time, which was typically less than one. Feasibility tunnel diodes were fabricated and evaluated.

were evaluated. h_{FE} vs frequency measurements at V_{CB} = 3 V, I_E = 5 ma yielded gain bandwidth products, f_T, as great as 800 Mc. This value is the highest known observed on GaAs transistors and is believed limited only by geometry control. h parameter measurements at f = 1000 cps, V_{CB} = 5 V, and I_E = 1 ma yielded common emitter power gains, G, ranging from 30-43.6 db. Switching characteristics of several units were also investigated. In the saturated mode, with no speedup capacitor, some units yielded total switching time from 10-30 nsec with only moderate overdrive. Most of this time was in rise and fall and not in storage time, which was typically less than one. Feasibility tunnel diodes were fabricated and evaluated.

were evaluated. h_{FE} vs frequency measurements at V_{CB} = 3 V, I_E = 5 ma yielded gain bandwidth products, f_T, as great as 800 Mc. This value is the highest known observed on GaAs transistors and is believed limited only by geometry control. h parameter measurements at f = 1000 cps, V_{CB} = 5 V, and I_E = 1 ma yielded common emitter power gains, G, ranging from 30-43.6 db. Switching characteristics of several units were also investigated. In the saturated mode, with no speedup capacitor, some units yielded total switching time from 10-30 nsec with only moderate overdrive. Most of this time was in rise and fall and not in storage time, which was typically less than one. Feasibility tunnel diodes were fabricated and evaluated.